

Differential Protection Modeling of the Randstad 380 kV South Ring High Voltage Cable in ATP - EMTP

Master of Science Thesis

K. S. Velitsikakis
[Student Number: 4183673]

June 2013

Department of Electrical Sustainable Energy
Faculty of Electrical Engineering, Mathematics and Computer Science
Electrical Power Systems
Delft University of Technology

Differential Protection Modeling of the Randstad 380 kV South Ring High Voltage Cable in ATP - EMTP

K. S. Velitsikakis

Thesis Committee:

Prof. Mart van der Meijden
Dr. dipl – ing. Marjan Popov
Dr. Olindo Isabella
Ir. Ernst Wierenga

*The Thesis project was carried out in collaboration with TenneT TSO B.V.,
headquartered in Arnhem*

Department of Electrical Sustainable Energy
Faculty of Electrical Engineering, Mathematics and Computer Science
Electrical Power Systems
Delft University of Technology

*"When the going gets tough,
The tough gets going"*

Joseph P. Kennedy

To my beloved parents and brothers

Abstract

Modern transmission power networks consist mainly of High Voltage overhead lines, since the later have proven their high operational reliability. However, technological developments have made it possible to use High Voltage cables, not only in the distribution grids, but also at higher transmission voltage levels. Thus, more mixed configurations, consisting of overhead lines and underground cables will take place in the near future. The Dutch transmission system operator, TenneT TSO, is a pioneer at this field, since it will install the longest 380 kV cable through the “Randstad 380 kV” project. On the other hand, mixed transmission systems bring new challenges at the field of the Power System protection because of their complexity. Consequently, the protection schemes need to be developed in order to retain their fast and reliable performance. Modern numerical protective relays are used, which can combine various operations within the same device, i.e. differential protection, distance protection etc. Before installing the protective relays, firstly their correct operation needs to be verified. For that reason, specific testing setups and programs are used to simulate possible transient fault conditions that can occur in a power system.

This Thesis Project focuses on the differential protection of the 380 kV XLPE cable, which is installed at the South Transmission Ring of the Randstad area in the Netherlands. A number of simulations were carried out to verify the correct operation of the protection scheme, when faults occur within the High Voltage cable and at other points of the system. Important conclusions were reached, with respect to the correct response of the developed differential relay model and its operating time, when the protection current transformers are not driven into saturation. Moreover, recommendations for future research are given regarding the implementation of the differential protection model to the other parts of the studied configuration together with the distance protection scheme. The electromagnetic transient program ATP has been used to model the mixed configuration between the Maasvlakte and Westerlee substations of the Randstad’s South Ring.

Acknowledgements

The Master Thesis Project would not have been successfully completed without the help of my supervisors. First of all, I would like to thank dr. dipl - ing. Marjan Popov for introducing me to TenneT TSO and for guiding me during my Thesis project. Mr. Popov significantly helped me to overcome any obstacles I met with his important inputs and advice regarding the ATP – EMTP software. My special thanks go to my supervisor at TenneT TSO, ir. Ernst Wierenga, for his assistance and support during all the months of my work. Moreover, I would like to thank Mr. Frank Wester, who gave me the chance to carry out my project at the “Asset Strategy” department of TenneT TSO and each and every of my colleagues, who welcomed me as a part of their team. For that reason, I would like to thank Mrs. Miriam Engelen and Mr. Henk Sanders for helping me adapt in a Dutch working environment.

Furthermore, I would like to thank my best friends Vasileios (Bill), Katerina, Ranjan (Ron) and George, my friend and roommate Vangelis and all my friends for their support and nice memories they filled me with during the two years I spent in Delft.

Last but not least, I would like to gratefully thank my beloved family for the unique and endless support they provide me every single day of my life. Without the help of my parents and brothers, nothing would have been possible for me.

Table of Contents

Abstract	5
Acknowledgements.....	6
Abbreviations.....	9
List of Figures.....	10
List of Tables	13
Chapter 1.....	14
Introduction.....	14
1.1 The Randstad 380 kV Project	14
1.2 Research Objectives	16
1.3 Thesis Outline	17
Chapter 2.....	18
Modeling of the Maasvlakte – Westerlee - Wateringen 380 kV connection in ATP–EMTP.....	18
2.1 Introduction	18
2.2 High Voltage Overhead Line model.....	18
2.2.1 Specification Data of the 380 kV Overhead Transmission Lines	19
2.2.2 Modeling of the Line Constants Routine	22
2.3 High Voltage Underground XLPE Cable model	22
2.3.1 Geometrical Specifications of the 380 kV XLPE Cable	24
2.3.2 Material Properties of the 380 kV XLPE Cable	25
2.3.3 Modeling of the Cable Constants Routine	26
2.4 Series Reactor model.....	27
2.4.1 Series Reactor model in ATP – EMTP.....	28
2.5 380 kV Power Source model.....	29
2.5.1 Power Source model in ATP - EMTP	30
Chapter 3.....	32
Current Transformers (CTs).....	32
3.1 Introduction	32
3.2 Basic Principles of the CTs	32
3.2.1 Technical Specifications for Protection CTs	34
3.3 CT Saturation	36
3.3.1 CT Saturation due to pure AC fault current	37
3.3.2 CT Saturation due to DC offset fault current component.....	38
3.3.3 Classes of Protection CTs	39

3.4 Protection CT model in ATP – EMTP	41
3.4.1 CT Equivalent per Phase Circuit in ATP - EMTP	41
3.4.2 Magnetization Curve and SATURA routine in ATP – EMTP	42
3.4.3 Transient Response of the Protection CT model in ATP – EMTP	44
Chapter 4.....	50
Line Differential Protection (DP)	50
4.1 Introduction	50
4.2 Basic Principles of Differential Protection	50
4.3 Numerical Measuring Technique – Discrete Fourier Transform (DFT).....	52
4.3.1 Discrete Fourier Transform (DFT).....	53
4.4 SIEMENS Numerical Line Differential Relay 7SD52	55
4.4.1 SIEMENS Differential Relay Model in ATP – EMTP	57
Chapter 5.....	62
Differential Protection of the Randstad 380 kV South Ring HV Cable – Results and Conclusions	62
5.1 Introduction	62
5.2 Protection Scheme of the Maasvlakte – Calandkanaal – Hoek van Holland – Westerlee 380 kV mixed connection	62
5.2.1 Description of the General Protection Scheme	62
5.2.2 Settings of the SIEMENS Differential Relays 7SD52	63
5.3 Fault Simulation Results	66
5.3.1 Single Phase to Ground Fault within the Protected Zone.....	66
5.3.2 Two Phase Fault within the Protected Zone	72
5.3.3 Three – Phase to Ground Fault within the Protected Zone	76
5.3.4 Three – Phase to Ground Fault outside the Protected Zone	80
5.4 Conclusions.....	87
5.5 Recommendations	87
Appendix A	90
Data of the OHL Phase and Ground Wires	90
Appendix B	92
Data of the XLPE HV Cable	92
Appendix C	94
Data of the Protection CTs	94
Bibliography.....	96

Abbreviations

ATP – EMTP: Alternative Transient Program – Electromagnetic Transient Program

HV: High Voltage

OHL: Overhead Line

HVC: High Voltage Cable

TSO: Transmission System Operator

MVL: Maasvlakte substation

WTL: Westerlee substation

WTR: Wateringen substation

LCC: Line/Cable Constant

XLPE: Cross Linked Polyethylene

RMS: Root Mean Square

CT: Current Transformer

ALF: Accuracy Limit Factor

SF: Safety Factor

VT: Voltage Transformer

EMF: Electromagnetic Force

DC: Direct Current

TP: Transient Performance

AR: Auto – Reclosing

DP: Differential Protection

DFT: Discrete Fourier Transformation

CB: Circuit Breaker

List of Figures

Figure 1-1. Dutch transmission grid map

Figure 1-2. Geographic overview of the Randstad 380 kV South Ring substations

Figure 1-3. Simplified configuration of the transmission system studied, represented in ATP – EMTP

Figure 2-1. HV tower of the FD/T type

Figure 2-2. HV tower of the DK/T type

Figure 2-3. Bending of a transmission line wire at mid-span

Figure 2-4. Bundling of the phase conductors in the 380 kV overhead transmission lines

Figure 2-5. Current loops in a single core cable

Figure 2-6. (Left) Typical layout of a 380 kV XLPE single core cable – (Right) Cross section of a 380 kV 1200 mm² XLPE single core cable

Figure 2-7. Triangle configuration of the under-water 380 kV XLPE cable system

Figure 2-8. Typical configuration of a series reactor

Figure 2-9. Cross section of a series reactor

Figure 2-10. Magnetization curve of the iron core in the ATP – EMTP series reactor model

Figure 2-11. Per phase equivalent of the saturable series reactor in ATP – EMTP

Figure 2-12. Power source model in ATP – EMTP

Figure 3-1. Typical current transformer used in HV applications

Figure 3-2. Per phase equivalent of a current transformer

Figure 3-3. Vectorial representation of the CT currents

Figure 3-4. Data specifications of the protection CTs installed in the MVL – WTL mixed configuration

Figure 3-5. Typical magnetization curve of the applied CT in the mixed transmission configuration

Figure 3-6. Operating point of a CT when the accuracy limit current flows in the primary side

Figure 3-7. Graphic representation of I_2 , $I_{2,sat}$, I_e

Figure 3-8. Total flux in the CT magnetic core under offset fault current conditions

Figure 3-9. Graphic representation of I_2 and $I_{2,sat}$

Figure 3-10. Secondary current, flux and magnetization current under CT saturation

Figure 3-11. Magnetization curves for the different CT classes

Figure 3-12. Transient magnetization of the TPX and TPY CTs during an AR operation

Figure 3-13. Equivalent per phase circuit of a protection CT as modeled in ATP – EMTP

Figure 3-14. Simplified equivalent per phase CT circuit as modeled in ATP – EMTP

Figure 3-15. Magnetization curve of the 4000/1 protection CTs used in the mixed transmission system

Figure 3-16. Magnetization curve ($i_e - V_2$) of the protection CTs

Figure 3-17. Magnetization curve ($i_e - \Phi$) of the protection CTs

Figure 3-18. Test circuit of the protection CT in ATP – EMTP

Figure 3-19. Primary, secondary and excitation currents of the protection CT with nominal current flowing in the primary winding

Figure 3-20. Primary, secondary and excitation currents of the protection CT with current 71.69 times the nominal one flowing in the primary winding

Figure 3-21. Primary, secondary and excitation currents of the protection CT with current 84.3 times the nominal one flowing in the primary winding

Figure 3-22. Secondary and excitation currents under extreme saturation conditions of the protection CT

Figure 4-1. Differential protection under an external fault

Figure 4-2. Differential protection under an internal fault

Figure 4-3. Stabilized pick – up characteristic of the differential relay

Figure 4-4. Block diagram of a numerical differential relay
 Figure 4-5. Basic principle of the Discreet Fourier Transform
 Figure 4-6. SIEMENS 7SD52 differential protection scheme
 Figure 4-7. Adaptive pick – up characteristic of the SIEMENS differential relay 7SD52
 Figure 4-8. Tripping logic of the SIEMENS differential relay 7SD52
 Figure 4-9. Logic flowchart of the differential relay’s model implemented in ATP – EMTP
 Figure 4-10. Test circuit of the differential relay model in ATP – EMTP
 Figure 4-11. Tripping signal of the differential relay under normal operating conditions
 Figure 4-12. Tripping signal of the differential relay under external fault conditions
 Figure 4-13. Tripping signal generated for the faulty phase under internal fault conditions
 Figure 4-14. Tripping signals generated for the healthy phases under internal fault conditions

Figure 5-1. Basic protection scheme of the MVL – WTL mixed transmission connection
 Figure 5-2. Schematic diagram of the mixed transmission configuration in ATP – EMTP
 Figure 5-3. Phase currents flowing at the primary side of the protection CTs
 Figure 5-4. Current to ground of the cable’s faulty phase A
 Figure 5-5. Phase currents flowing at the secondary side of the protection CTs
 Figure 5-6. Comparison between the CTs secondary phase currents at the sending and remote end of the HV cable respectively
 Figure 5-7. I_{Diff} and I_{Res} as calculated for each phase
 Figure 5-8. $I_{Diff} - I_{Res}$ trajectory and adaptive pick – up characteristic of the differential relay
 Figure 5-9. $I_{Diff} - I_{Res}$ trajectory and adaptive pick – up characteristic of the differential relay, when the single phase to ground fault is cleared
 Figure 5-10. Tripping signals generated at the output of the differential relay for each phase separately
 Figure 5-11. Phase currents flowing at the primary side of the protection CTs
 Figure 5-12. Comparison between the CTs secondary phase currents at the sending and remote end of the HV cable respectively
 Figure 5-13. I_{Diff} and I_{Res} as calculated for each phase
 Figure 5-14. $I_{Diff} - I_{Res}$ trajectory of faulty Phase A and adaptive pick – up characteristic of the differential relay
 Figure 5-15. $I_{Diff} - I_{Res}$ trajectory of faulty Phase B and adaptive pick – up characteristic of the differential relay
 Figure 5-16. $I_{Diff} - I_{Res}$ trajectory of healthy Phase C and adaptive pick – up characteristic of the differential relay
 Figure 5-17. Tripping signals generated at the output of the differential relay for each phase separately
 Figure 5-18. Phase currents flowing at the primary side of the protection CTs
 Figure 5-19. Comparison between the CTs secondary phase currents at the sending and remote end of the HV cable respectively
 Figure 5-20. I_{Diff} and I_{Res} as calculated for each phase
 Figure 5-21. $I_{Diff} - I_{Res}$ trajectory of faulty Phase A and adaptive pick – up characteristic of the differential relay
 Figure 5-22. $I_{Diff} - I_{Res}$ trajectory of faulty Phase B and adaptive pick – up characteristic of the differential relay
 Figure 5-23. $I_{Diff} - I_{Res}$ trajectory of faulty Phase C and adaptive pick – up characteristic of the differential relay
 Figure 5-24. Tripping signals generated at the output of the differential relay for each phase separately
 Figure 5-25. Currents to ground of the faulty phases A, B and C
 Figure 5-26. Phase currents flowing at the primary side of the protection CTs

Figure 5-27. Comparison between the CTs secondary phase currents at the sending and remote end of the HV cable respectively

Figure 5-28. I_{Diff} and I_{Res} as calculated for each phase

Figure 5-29. $I_{Diff} - I_{Res}$ trajectory of faulty Phase A and adaptive pick – up characteristic of the differential relay

Figure 5-30. $I_{Diff} - I_{Res}$ trajectory of faulty Phase B and adaptive pick – up characteristic of the differential relay

Figure 5-31. $I_{Diff} - I_{Res}$ trajectory of faulty Phase C and adaptive pick – up characteristic of the differential relay

Figure 5-32. Tripping signals generated at the output of the differential relay for each phase separately

Figure 5-33. Comparison between the CTs secondary currents of Phase A at the sending and remote end of the HV cable respectively

Figure 5-34. I_{Diff} and I_{Res} as calculated for each phase

Figure 5-35. $I_{Diff} - I_{Res}$ trajectory of faulty Phase A and adaptive pick – up characteristic of the differential relay

Figure 5-36. $I_{Diff} - I_{Res}$ trajectory of healthy Phase C and adaptive pick – up characteristic of the differential relay

Figure 5-37. Tripping signals generated at the output of the differential relay for the faulty Phase A

Figure Appendix C. Magnetization curve of the protection CTs 4000/1

List of Tables

Table 2-1. OHL phase and ground wires specifications

Table 2-2. Data for the conductors used in the MVL – WTL connection

Table 2-3. Data for the conductors used in the WTL – WTR connection

Table 2-4. Geometrical specifications for a 380 kV XLPE single core cable

Table 2-5. ϵ_r and μ_r of the XLPE insulator in a 380 kV single core cable

Table 2-6. Technical specifications of the series reactors

Table 2-7. Saturation characteristics of the series reactor non-linear inductance

Table 2-8. Three-phase to ground and single-phase to ground fault currents in the MVL and WTL substations

Table 2-9. Positive and zero sequence resistances and inductances in the MVL and WTL substations

Table 3-1. Definitions of the basic data of a protection CT

Table 3-2. Transient performance classes of the protection CTs

Table 3-3. Pairs of $i_e - V_2$ RMS values

Table 3-4. Pairs of $i_e - \Phi$ peak values

Table 3-5. Saturation analysis results of the protection CT model in ATP – EMTP ($R_B=10\Omega$)

Table 3-6. Saturation analysis results of the protection CT model in ATP – EMTP ($R_B=3\Omega$)

Table Appendix A. Data of the phase wires provided by TenneT TSO

Table Appendix A. Data of the ground wires provided by TenneT TSO

Table Appendix B. Electrical and mechanical data of the 380 kV XLPE cable provided by TenneT TSO

Table Appendix B. Geometrical data of the 380 kV XLPE cable provided by TenneT TSO

Table Appendix C. Data of the protection CTs provided by TenneT TSO

Chapter 1

Introduction

1.1 The Randstad 380 kV Project

The Dutch Transmission System Operator, TenneT TSO, is responsible for the 380 kV and 220 kV High Voltage grid throughout the Netherlands. TenneT TSO monitors the balance between the electricity demand and supply, ensuring by this way a reliable and uninterrupted transmission of electric energy to its users. The major part of the transmission grid consists of HV overhead lines, because of simplicity and efficiency reasons. Only a few kilometers of HV cables are installed underground because of some specific demands, for instance, when the transmission route is close to residential areas and the installation of overhead lines is not possible. In the figure below, the red lines represent the 380 kV transmission grid in the Netherlands.



Figure 1-1. Dutch transmission grid map [Source: www.tennet.eu]

Due to its innovative expansion strategies and due to limitations because of landscape and densely populated areas, TenneT TSO is working on the “Randstad 380 kV” project. The latter regards the expansion of the Dutch transmission grid in the Randstad region because of the significantly increasing electricity demand. The new HV connections, together with the existing ones will form two ring structures, namely the North and the South Ring. More specifically, the North Ring will include the HV substations of Beverwijk, Diemen and Bleiswijk, whereas the South Ring will include the Maasvlakte, Westerlee, Wateringen, Bleiswijk, Krimpen and Crayestein substations. However, the expanded grid will be a mixed 380kV transmission system, consisting of overhead lines and XLPE underground cables. The total length of the HV cable will be more than 20 kilometers, covering a big portion of the entire route in the region. This will be the longest underground 380 kV connection installed in the world, making TenneT TSO a pioneer in the HV innovative constructions and installations.

This project focuses on the South Ring and more precisely on the mixed transmission connection between the substations Maasvlakte and Westerlee. The configuration consists of two overhead transmission line parts of 12.5 km and 5.1 km long respectively, while a HV underground cable of 2.1 km of length is installed between them. It has to be noticed that the length of this part of the ring structure is lower than the length of the Bleiswijk – Crayenstein – Maasvlakte route, as it is shown in Figure 1-2. Thus, the impedance of the first part will be lower than the impedance of the second part and this would lead to a possible overloading of the Maasvlakte – Westerlee – Bleiswijk transmission route. In order to overcome this drawback, TenneT TSO has installed oil – filled series reactors between the HV cable and the overhead line connected to the Westerlee substation.

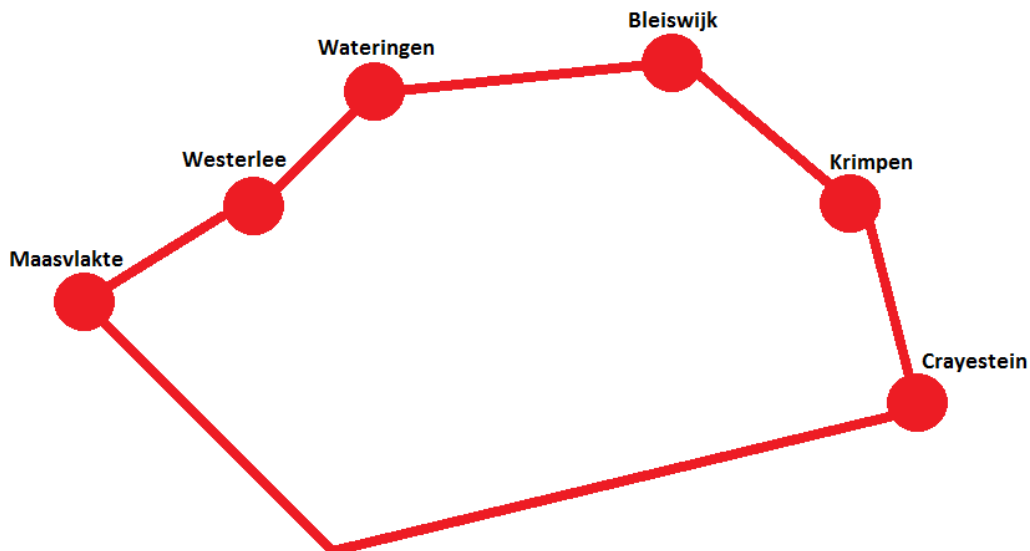


Figure 1-2. Geographic overview of the Randstad 380 kV South Ring substations

The transmission grid has to maintain its uninterrupted operation in order to reliably transmit the generated power throughout the country. Nonetheless, possible faults could disturb the normal operation of the network, leading to undesirable problems, i.e. blackouts. Moreover, the equipment installed in the system is characterized by its high production and maintenance costs. Hence, excessive fault conditions may damage the equipment. For these reasons, intelligent systems are adopted and implemented to every piece of the power network, in order to provide an appropriate protection against undesirable switching and lightning transient phenomena. Various protection schemes are being used, with the differential and distance protection being the most famous among them. These schemes combine the high reliability with the fast tripping operation, while the desired coordination and selectivity between them can be reached accordingly.

The principle of the current differential protection, which is studied in this project, is based on the comparison between the current flowing into and out of the protected zone. Under normal operating conditions, or in the case that a fault occurs outside the protected area, the two currents are equal in terms of magnitude and phase and the differential protection relay does not operate. On the other hand, in case of a fault within the protected zone, the differential current will have a non – zero value, leading to the tripping operation of the protective device. The distance protection is based on the protected line impedance measurement and can define various zones of protection, by distinguishing them with an appropriate time grading. When the impedance measured by the distance relay has a value lower than the setting value, a tripping command will be generated and sent to the corresponding circuit breakers, which will clear the fault. The two protection systems can be combined to form a full protection scheme for any configuration along the transmission grid.

1.2 Research Objectives

As it was mentioned above, the transmission part between the Maasvlakte and Westerlee substations of the Randstad 380 kV South Ring is of importance in this project. More specifically, the following constitute the research objectives of this report:

- A detailed model of the configuration studied, as shown in Figure 1-3, which will include the overhead transmission lines, the XLPE HV cable, the series reactors and the power sources in the two ends of the system. The models of the OHL and the HVC should take into account, not only their electrical characteristics, but also the geometrical characteristics of their structure.
- A detailed model of the current transformers, which are used in the differential protection scheme. This model should thoroughly describe the response of the devices under normal and saturated operating conditions.
- A detailed model of the protective relay, based on the SIEMENS 7SD52 differential relay. The developed algorithm should describe the relay's operating logic under normal and fault conditions, by taking into account some certain simplifications.
- The correct tripping and blocking operation of the differential protection implemented on the HV cable. More specifically, various faults should be simulated within the protected object, as well as outside the protected zone to confirm the correct operation of the relay model.

This project has been carried out at the "Asset Strategy" subdepartment of TenneT TSO. All the data used were provided by the Dutch operator and the totally free Electromagnetic Transient Program "ATP" was used for the configuration modeling.

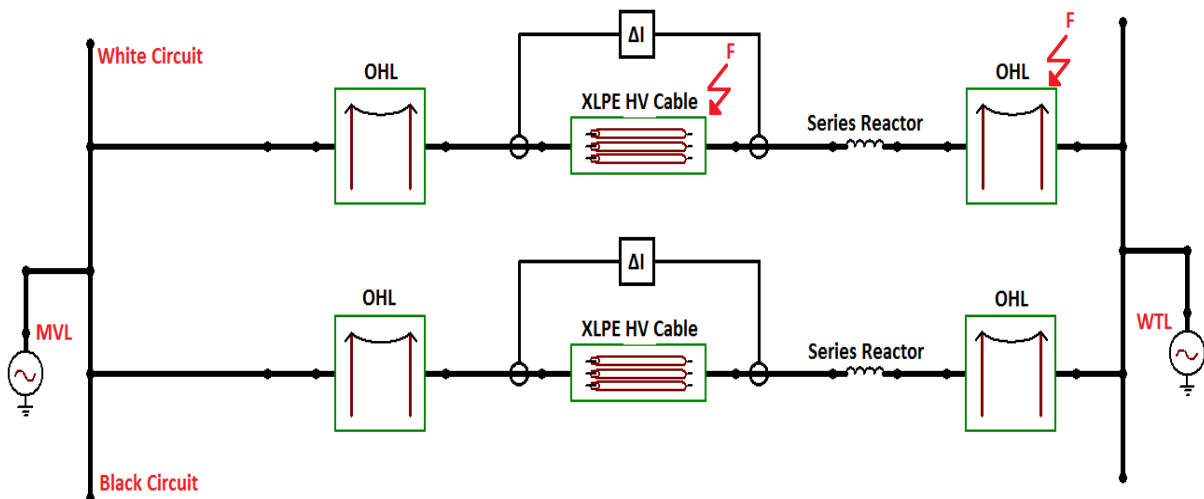


Figure 1-3. Simplified configuration of the transmission system studied, represented in ATP – EMTP

1.3 Thesis Outline

A brief description of the chapters' content is presented below:

- Chapter 2: Deals with the description of the various models implemented in ATP – EMTP. The models' description regards the power sources, the overhead transmission lines, the HV underground cable and the series reactors, which form the configuration between the Maasvlakte and Westerlee substations.
- Chapter 3: Thoroughly describes the operation and the main characteristics of the current transformers. Moreover, it focuses on the transient response of the protection current transformers, whereas it explains in details the CT model implemented in ATP – EMTP together with the results obtained by performing sensitivity analysis of the applied model.
- Chapter 4: Presents the basic principles of the differential protection. The main features of the SIEMENS 7SD52 differential relay are described together with the relay model built in ATP – EMTP. Additionally, some basic results of a test circuit, including the model of the protective device are also studied.
- Chapter 5: Presents the results obtained by the various simulations of fault conditions. Three possible faults within the HV cable (single phase to ground, two – phase and three - phase to ground) are simulated, while a three – phase to ground fault outside the protected zone of the cable is simulated too. Last but not least, the chapter discusses the conclusions reached by the obtained results and some recommendations for further research.

Chapter 2

Modeling of the Maasvlakte – Westerlee - Wateringen 380 kV connection in ATP–EMTP

2.1 Introduction

The basic configuration between the substations of Maasvlakte and Wateringen is a mixed connection, consisting of High Voltage OHL, HV Underground Cables and series reactors. More specifically, there are three sections of OHL, with the first one starting from the Maasvlakte substation and being connected to the HV cable, while the second section is connected between the remote end of the cable and the Westerlee substation. The third part is responsible for the 380 kV connection between the Westerlee and Wateringen substations. The total length of the XLPE cable is divided into two, approximately equal parts, due to its underwater installation in the area of Calandkanaal and Nieuwe Waterweg. In order to adequately estimate the behavior of the mixed system under fault conditions, the basic components mentioned above, along with the generators, should be accurately modeled in the Electromagnetic Transient Program.

In this chapter, the exact ATP – EMTP models for each component of the configuration studied are presented and analyzed.

2.2 High Voltage Overhead Line model

The basic differential equation, which describes the voltage at a certain distance along an OHL [1], is given below:

$$-\frac{\partial v}{\partial x} = R'i + L' \frac{\partial i}{\partial t} \quad (2-1)$$

where R' and L' are the constants of the line per unit length. However, in an n-conductor line the general vector equation (2-2) is used:

$$-\begin{bmatrix} \frac{dV_1}{dx} \\ \frac{dV_2}{dx} \\ \cdot \\ \cdot \\ \frac{dV_n}{dx} \end{bmatrix} = \begin{pmatrix} Z'_{11} & \dots & Z'_{1n} \\ \vdots & \ddots & \vdots \\ Z'_{n1} & \dots & Z'_{nn} \end{pmatrix} \begin{bmatrix} I_1 \\ I_2 \\ \cdot \\ \cdot \\ I_n \end{bmatrix} \quad (2-2)$$

where [V]: vector of the phase to ground voltages
 [I]: vector of the conductors' currents
 [Z]: series impedance matrix

The series impedance matrix consists of the series self-impedance (diagonal elements Z_{ii}) and the series mutual-impedance (off diagonal elements Z_{ij}). The self-impedance Z_{ii} is calculated according to the loop formed by the conductor i and the earth return path, while the mutual-impedance Z_{ij} represents the voltage induced in the conductor j , when a current flows through the conductor i . Carson's formula [2] is used for the Z_{ii} and Z_{ij} calculation, and this formula is also used in the ATP – EMTP software. More specifically, a transmission line can be modeled by using the Line/Cable Constant routine, which is based on Carson's equations, and this routine is chosen for the modeling of the OHL parts of this study too.

2.2.1 Specification Data of the 380 kV Overhead Transmission Lines

The 380 kV OHL is a double-circuit transmission line (Wit and Zwart), consisting of six phases and two ground wires. The transmission part between the MVL-WTL substations has phase wires of the steel/aluminum type, while the section connecting the WTL-WTR substations is of the Bobolink type. Moreover, both transmission lines have shield wires of the HAWK type, as it is shown in the table below.

Specifications of the 380 kV Transmission Overhead Lines			
Section	Phase Wire	Ground Wire	Line Length [km]
Maasvlakte – Westerlee (I)	St/Al 52/591	Hawk 39/242	12.5
Maasvlakte – Westerlee (II)	St/Al 52/591	Hawk 39/242	5.1
Westerlee - Wateringen	Bobolink 50/725	Hawk 39/242	6.8

Table 2-1. OHL phase and ground wires specifications

However, for the adequate modeling of the transmission lines through the LCC routine in ATP – EMTP, the exact geometrical characteristics of the HV towers, the phase and the ground wires should be specified [3]. In other words, the information listed is used as an input in the routine:

- Height of the phase/ground wires
- Horizontal distance of the phase/ground wires from the center of the tower
- Height of the phase wires/ground at the mid-span of the transmission line
- Number of bundles used in the phase wires
- Distance between the bundles
- Angle between the bundles
- Inner and outer radius of the phase/ground wires
- DC resistance of the phase/ground wires

The figures below represent the structure of the HV towers used for the connection between the three substations. Two different tower types are being used by TenneT TSO for this specific connection, the FD/T type between the MVL-WTL substations and the DK/T between the WTL-WTR substations.

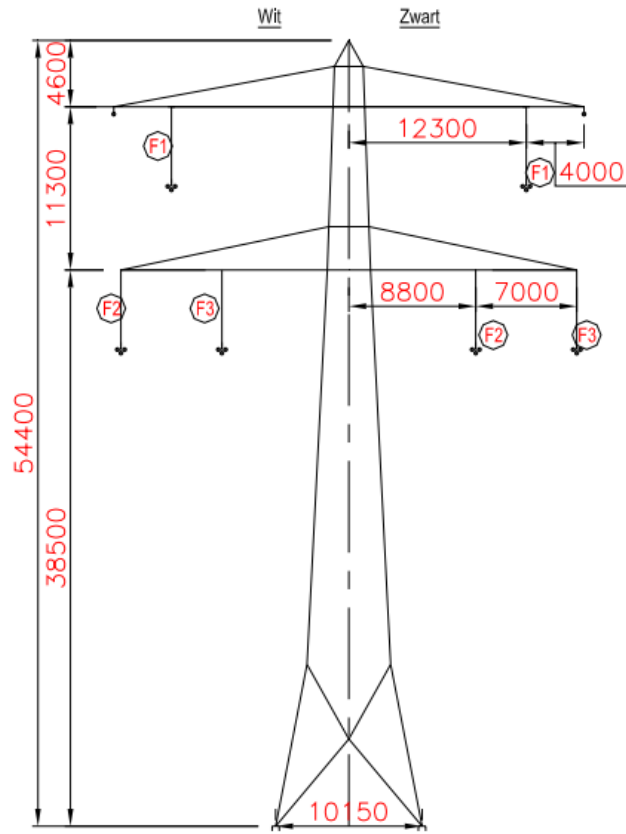


Figure 2-1. HV tower of the FD/T type

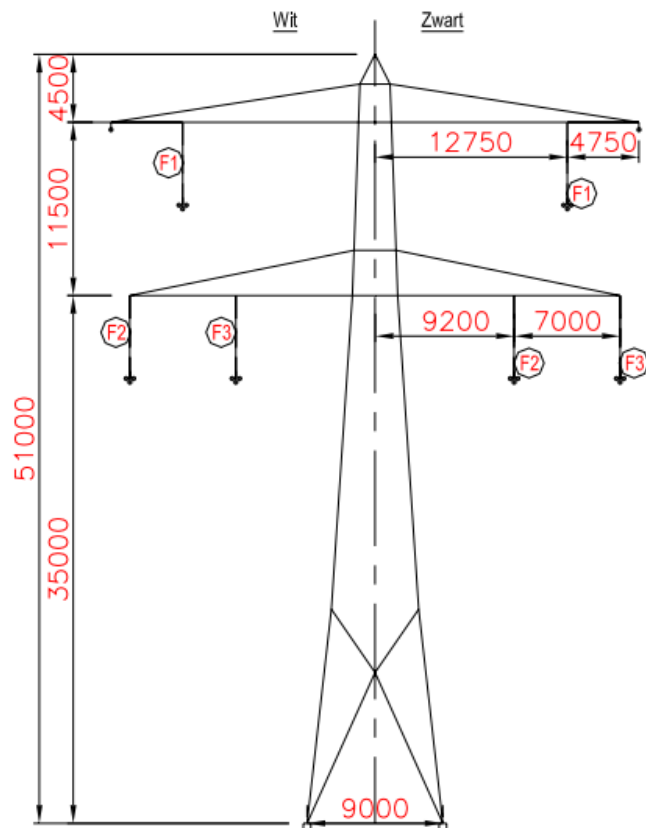


Figure 2-2. HV tower of the DK/T type

It has to be noticed that two assumptions were taken into consideration for the modeling of the OHL, regarding the exact height of the phase wires and the height of both the phase and ground wires at the mid-span of the line. More specifically, the phase wires are hanging approximately five meters below the steel construction, with a string insulator providing protection against a possible flashover. Besides, the minimum vertical distance of the phase wires from the ground at the mid-span of the line is taken to be equal to 13 meters. The latter is translated into a height difference of 20.5 meters from the theoretical no-bending wire, as it is shown in Figure 2-3.

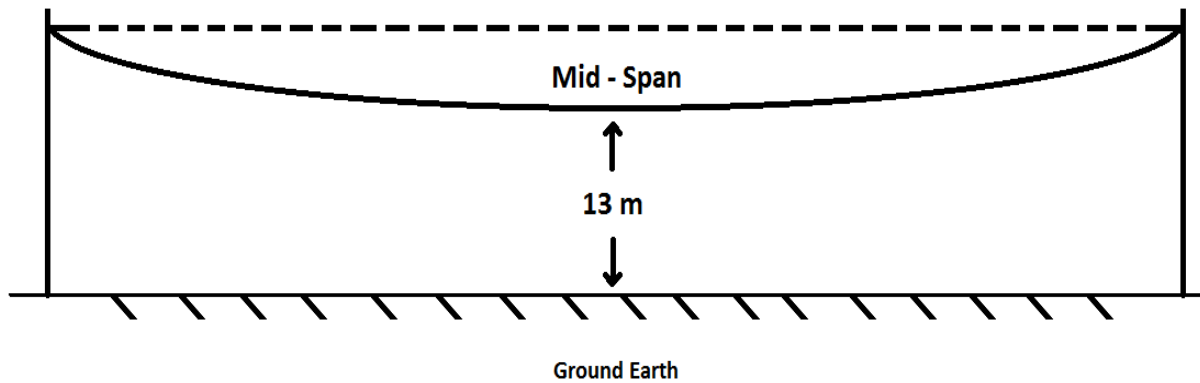


Figure 2-3. Bending of a transmission line wire at mid-span

The two tables below summarize the basic data of the phase and the shield wires, which are used as an input in the LCC routine of ATP – EMTP for two different types of OHL. The complete data sheets, provided by the manufacturer, are included in Appendix A.

Conductor Data for the transmission connection Maasvlakte - Westerlee					
	Outer Radius R_{out} [cm]	DC Resistance [Ω /km]	Number of Bundles	Bundling Distance [cm]	Bundling Angle [$^{\circ}$]
Phase Wire	1.62	0.0488	4	40	45
Ground Wire	1.09	0.1199	-	-	-

Table 2-2. Data for the conductors used in the MVL – WTL connection

Conductor Data for the transmission connection Westerlee - Wateringen					
	Outer Radius R_{out} [cm]	DC Resistance [Ω /km]	Number of Bundles	Bundling Distance [cm]	Bundling Angle [$^{\circ}$]
Phase Wire	1.812	0.0399	3	45	30
Ground Wire	1.09	0.1199	-	-	-

Table 2-3. Data for the conductors used in the WTL – WTR connection

Figure 2-4 shows the bundling of the phase conductors, in case of using three and four bundles respectively. On the left - hand side arrangement, the angle displacement between the bundles is 45° , while on the right - hand side arrangement the angle displacement is 30° .

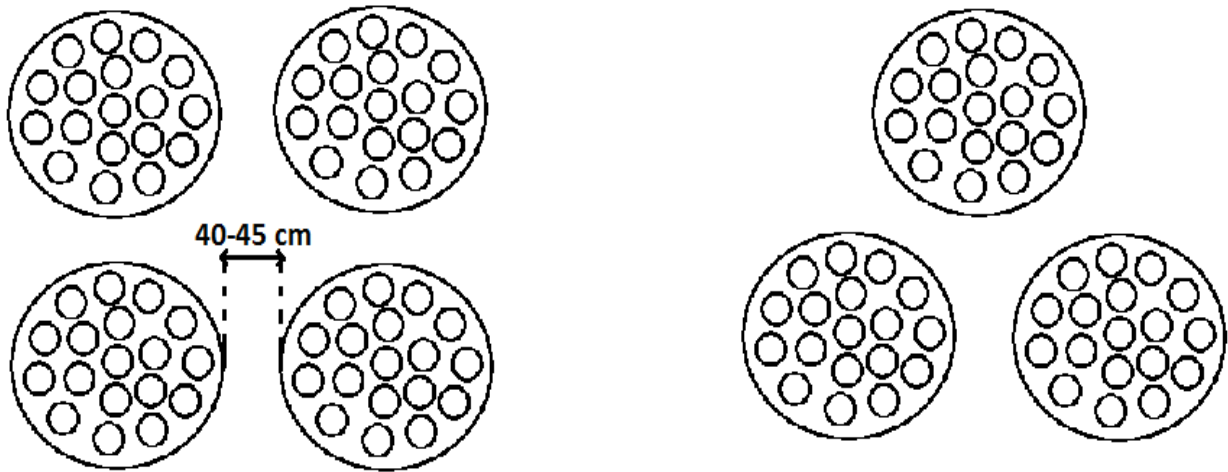


Figure 2-4. Bundling of the phase conductors in the 380 kV overhead transmission lines

2.2.2 Modeling of the Line Constants Routine

Apart from the geometrical characteristics of the phase and ground conductors and the structure of the HV towers, the LCC routine provides several types of modeling the electrical components (Bergeron, PI, JMarti, Noda, Semlyem). For the OHL of the mixed system, the Bergeron model is used, since it calculates the series impedance matrix at a desired frequency. The frequency selected here corresponds to the nominal frequency of the power system, 50 Hz. Based on [4], the Bergeron model leads to satisfying results, when compared with the JMarti model, while the time domain results cover the worst case scenario of a transient study, thus, being on the safe side.

In addition, the skin effect is also taken into account, and this is the reason why only the DC resistance of the conductors is specified in the routine's data. The skin effect depends on the frequency and it represents the tendency of an AC current to be distributed within a conductor, in such a way that the current density is largest near the surface of the conductor. Under fault conditions, frequencies involved may reach very high levels –tens or hundreds of kHz-, which are greater than the nominal operating frequency. As a result, the effective resistance of the conductor increases, causing the current to flow mainly at the “skin” of the wire.

2.3 High Voltage Underground XLPE Cable model

As in the case of an overhead transmission line, there is a basic vector equation, which describes the series impedances in a single core cable. This equation is given below:

$$-\begin{bmatrix} \frac{dV_1}{dx} \\ \frac{dV_2}{dx} \\ \frac{dV_3}{dx} \end{bmatrix} = \begin{pmatrix} Z'_{11} & Z'_{12} & Z'_{13} \\ Z'_{21} & Z'_{22} & Z'_{23} \\ Z'_{31} & Z'_{32} & Z'_{33} \end{pmatrix} \begin{bmatrix} I_1 \\ I_2 \\ I_3 \end{bmatrix} \quad (2-3)$$

These coupled equations provide the voltage per unit length at a certain distance along the three loops that are formed within the cable and between the latter and the earth (or water in case of a submarine cable). More specifically, as it can be seen in Figure 2-5, current paths are formed between the conductor and the metallic sheath, the sheath and the armor and finally between the metallic armor and the earth/water. The series impedance matrix consists of the series self-impedances, Z'_{ii} (diagonal elements) and the series mutual-impedances, Z'_{ij} (off-diagonal elements). For each loop, the self-impedance is defined as a sum of three other impedances:

$$Z'_{11} = Z'_{core-out} + Z'_{core/sheath-insulation} + Z'_{sheath-in} \quad (2-4)$$

$$Z'_{22} = Z'_{sheath-out} + Z'_{sheath/armor-insulation} + Z'_{armor-in} \quad (2-5)$$

$$Z'_{33} = Z'_{armor-out} + Z'_{armor/earth-insulation} + Z'_{earth} \quad (2-6)$$

where $Z'_{core-out}$: impedance per unit length between the conductor and the outside of the tube
 $Z'_{core/sheath-insulation}$: impedance per unit length of the insulation between the core and the sheath
 $Z'_{sheath-in}$: impedance per unit length between the sheath and the inside of the tube

Similar as, per unit length impedances are defined for the second and third loop respectively.

On the other hand, the mutual impedances represent the effect, one loop has over another, while sharing a common branch. Since there is no common branch between the first and the third loop, then $Z'_{13}=Z'_{31}=0$. The support routine LCC is responsible for generating the series impedance matrix, as it was also mentioned in paragraph 2.2.

For an adequate cable model, the Cable Constants routine requires the geometrical and material characteristics of the cable as an input. However, the model considers certain assumptions regarding the construction of the cable core. For that reason, re-calculations of the basic data are needed before defining the inputs of the LCC [5]. Paragraphs 2.3.1 and 2.3.2 explicitly analyze the procedure that is followed for the cable modeling.

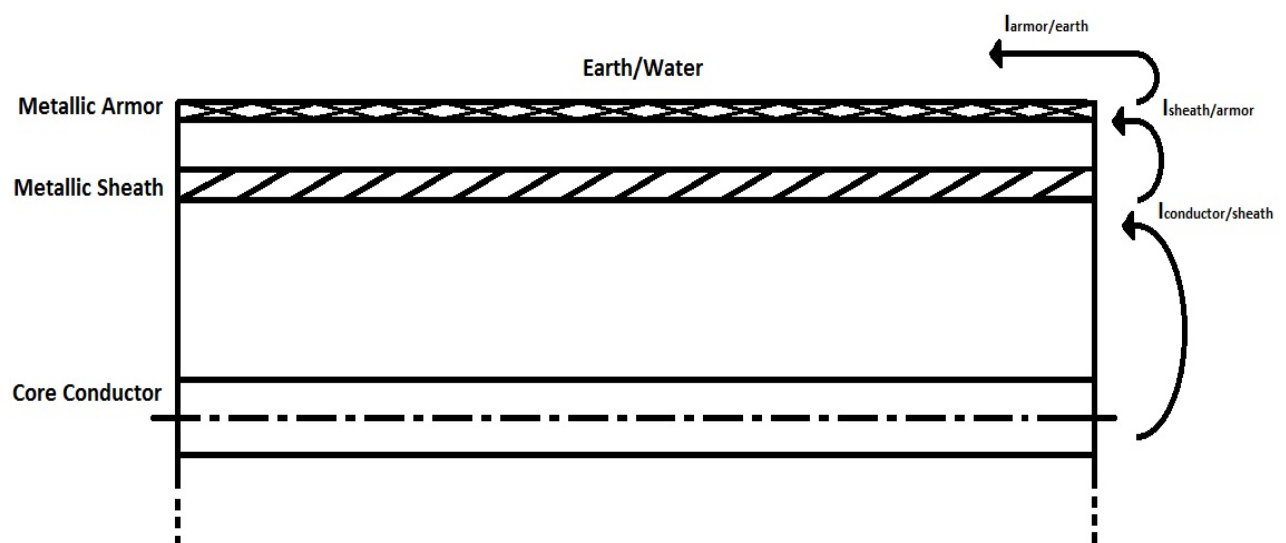


Figure 2-5. Current loops in a single core cable

2.3.1 Geometrical Specifications of the 380 kV XLPE Cable

For the water-crossing part in the Calandkanaal/Nieuwe Waterweg area of the Randstad 380 kV project, TenneT TSO has installed HV XLPE 2x1600 mm² (Cu) single core cables. There are two circuits in parallel (namely ‘Wit’ and ‘Zwart’), while for each phase two cables, 2.1 km long are needed. Thus, approximately 25 km of cable length is used for the water-crossing connection. Several layer parts form the complete single core cable, as it is shown in the figure below, and these are: conductor, semi-conducting layers, cross-linked polyethylene insulation, copper screen and lead sheath.

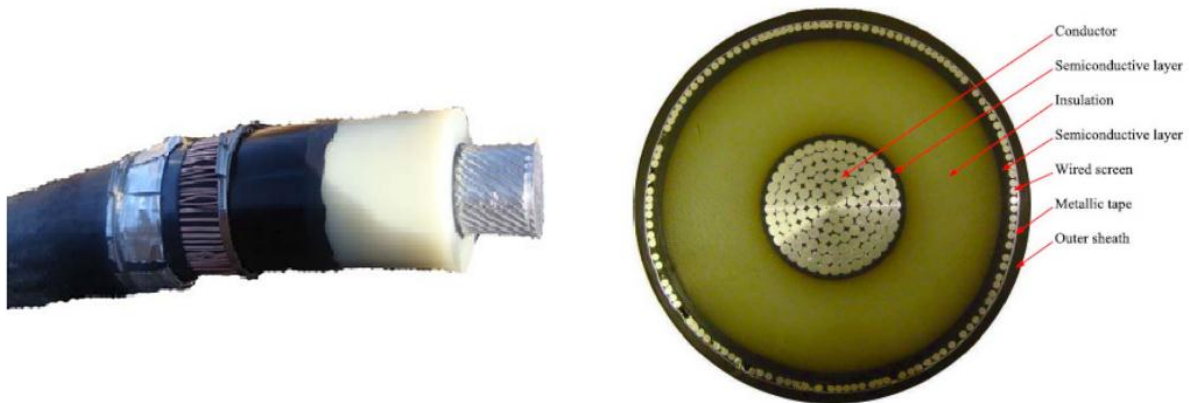


Figure 2-6. (Left) Typical layout of a 380 kV XLPE single core cable – (Right) Cross section of a 380 kV 1200 mm² XLPE single core cable

- **Core conductor:** is responsible for conducting the operating current with low losses [6]. It is made by copper (Cu), having a cross section of 1600 mm² and a diameter of 49.8 mm, while it is stranded and segmented. The stranding lowers the effective resistance of the conductor, especially when skin and proximity effects take place.
- **XLPE insulation:** its purpose is to prevent any electrical connection between the core conductor and the lead sheath, which both carry currents during the operation of the cable. The insulation thickness is 27 mm and two semi-conducting layers, of 2.2 mm and 1.5 mm thickness respectively, separate the latter from the core conductor and the copper screen.
- **Copper screen:** is responsible for lowering the electric field around the insulated conductor. A copper wire is wrapped around the XLPE insulation, while a contact tape is laid over the helically wrapped wires to ensure electrical contact between them. The thickness of this layer is 2.9 mm.
- **Lead sheath:** is used as a return path for the cable’s charging current as well as a conduction path for the current under fault conditions. It is made by tellurium (Te) alloy and it has a thickness of approximately 2 mm.

The table below summarizes the basic geometrical specifications of the single core cable. The exact cable data provided by the manufacturer are included in Appendix B.

Single Core Cable Data for the water – crossing connection in Calandkanaal/Nieuwe Waterweg				
Cross section [mm ²]	Core Conductor diameter [mm]	Insulation thickness [mm]	Diameter over Lead Sheath [mm]	Overall Diameter [mm]
1600	49.8	27	121	131

Table 2-4. Geometrical specifications for a 380 kV XLPE single core cable

Through the LCC routine in ATP – EMTP, it is not possible to model the core conductor as stranded and segmented, but only as a solid one [7]. As a result, a re-calculation for the conductor's resistivity is needed, because a higher value than the nominal one compensates for the lack of stranding in the model. The resistivity is re-calculated according to the equation (2-7):

$$\rho' = R_{DC} \frac{R_{out}^2 \cdot \pi}{l} \quad (2-7)$$

where ρ' : the re-calculated conductor resistivity [Ωm]
 R_{DC} : the DC resistance of the core conductor [Ω]
 R_{out} : the conductor's radius [m]
 l : length of 1km

The normal resistivity of the copper is $1.72 \times 10^{-8} \Omega m$, while the rated DC resistance and radius of the core conductor are $0.0154 \Omega/km$ and 24.9 mm respectively. By using these values in (2-7), the approximated resistivity used for the model is calculated:

$$\rho' = R_{DC} \frac{R_{out}^2 \cdot \pi}{l} = 0.0154 \frac{(0.0249)^2 \cdot \pi}{1000} = 2.99812 \times 10^{-8} \Omega m$$

Furthermore, the single core cables have been installed under water in the Calandkanaal/Nieuwe Waterweg area. The configuration of the installation is that of open triangle, as it is shown in Figure 2-7. The installation depth is approximately 26 m and the distance between the cables of the two circuits is assumed to be six meters.

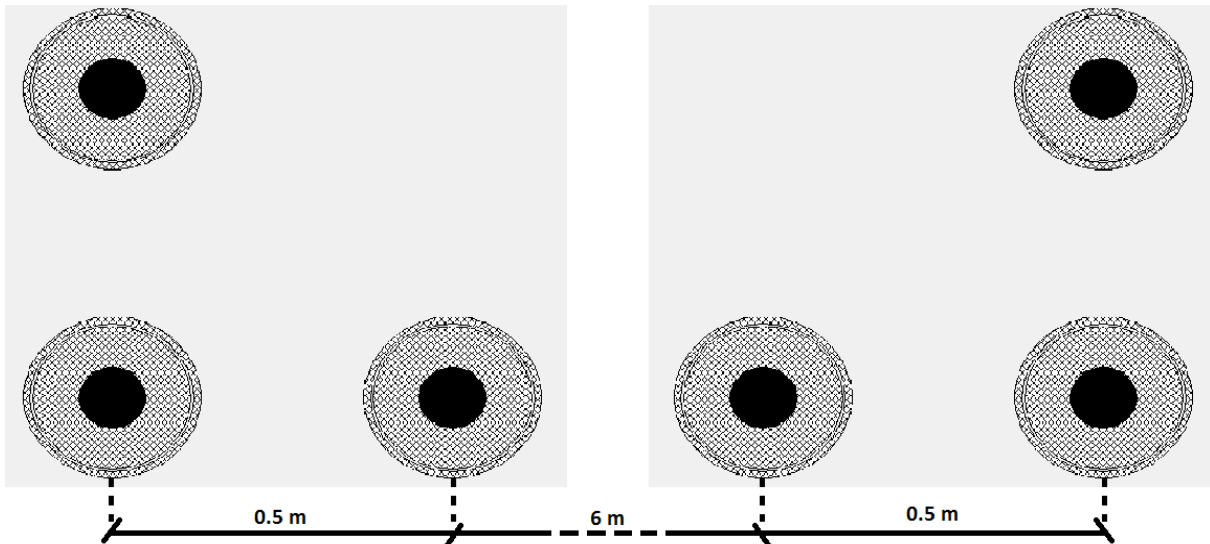


Figure 2-7. Triangle configuration of the under-water 380 kV XLPE cable system

2.3.2 Material Properties of the 380 kV XLPE Cable

Apart from the geometrical data of the single core cable, LCC requires material specifications too. More specifically, the relative permittivity (ϵ_r) and permeability (μ_r) of the insulating material and the lead sheath have to be determined as input data. Table 2-5 shows the values of ϵ_r and μ_r of the XLPE, which are used in the cable model.

Relative Permittivity and Permeability of the Cross-Linked Polyethylene (XLPE)	
ϵ_r	μ_r
2.4	1

Table 2-5. ϵ_r and μ_r of the XLPE insulator in a 380 kV single core cable

Although the LCC routine supports the modeling of the insulator, of the lead sheath and of the outer armor, it does not support the modeling of the semi-conducting layers. Thus, the effect of the latter cannot be taken into account, unless the relative permittivity of the insulating material is increased. For the re-calculation of the $\epsilon_{r,ins}$, the thickness of the XLPE insulation is increased, so that it is extended from the core conductor to the lead sheath. The equation below gives the re-calculated ϵ_r :

$$\epsilon = \epsilon_{ins} \frac{\ln\left(\frac{r_2}{r_1}\right)}{\ln\left(\frac{b}{a}\right)} \quad (2-8)$$

where ϵ_{ins} : the nominal relative permittivity of the XLPE insulator
 a : inner radius of the insulating material [mm]
 b : outer radius of the insulating material [mm]
 r_1 : outer radius of the core conductor [mm]
 r_2 : inner radius of the lead sheath [mm]

The inner and outer radius of the insulator are 27.1 mm and 54.1 mm respectively, by taking into account the semi-conducting layer, which exists between the core conductor and the XLPE insulation. The outer radius of the conductor is equal to 24.9 mm, while the inner radius of the lead sheath is 78.5 mm, including both the two semi-conducting layers and the copper screen. The re-calculation gives:

$$\epsilon = \epsilon_{ins} \frac{\ln\left(\frac{r_2}{r_1}\right)}{\ln\left(\frac{b}{a}\right)} = 2.4 \frac{\ln\left(\frac{78.5}{24.9}\right)}{\ln\left(\frac{54.1}{27.1}\right)} = 3.986$$

As for the lead sheath, it is assumed that the relative permittivity is taken equal to the one of XLPE, because the tellurium's alloy permittivity is not known.

On the other hand, the core conductor, the insulator and the lead sheath are assumed to have relative permeability equal to unity. By this way, the 'solenoid effect' caused by the copper screen is not taken into account and no re-calculations are required for the input data in the LCC routine.

2.3.3 Modeling of the Cable Constants Routine

Just like in the case of overhead transmission lines, the Bergeron type of model is chosen for the HV cable [8]. The power frequency, $f = 50$ Hz, is selected as the frequency that the series impedance matrix is calculated. Moreover, only the DC resistance of the core conductors is determined in the input data of the routine, since the option of the skin effect is enabled.

2.4 Series Reactor model

Between the Maasvlakte and Westerlee substations, TenneT TSO has installed series reactors in both parallel circuits –Wit and Zwart-, in the Hoek van Holland area. As it was mentioned in Chapter 1, the Randstad ring consists of two halves: the northern half, which includes the substations of Maasvlakte, Westerlee, Wateringen, Bleiswijk and Krimpen, and the southern half, which connects Maasvlakte and Krimpen through the Crayestein substation. The length of the southern part is longer than the one of the northern half and consequently the impedance of the first is higher too. The series reactors have been installed in the northern half, so that the two impedances become approximately equal. By this way, an equal division of the power is achieved between the two halves and the problem of overloading the northern section is surpassed.

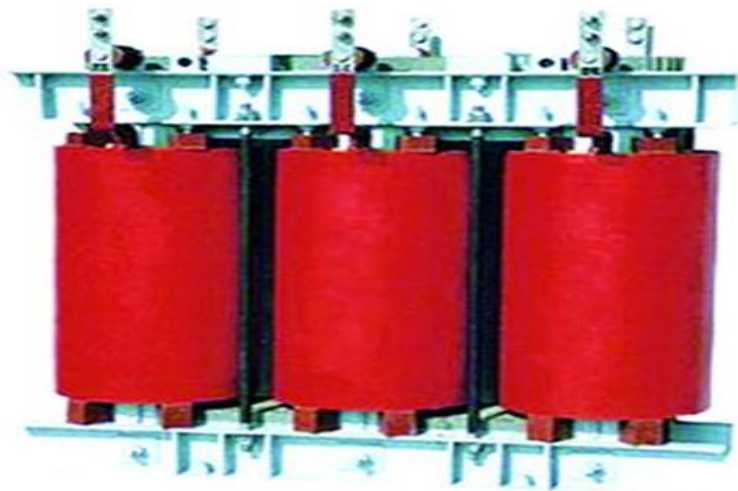


Figure 2-8. Typical configuration of a series reactor [Source: www.hslec.com/en/]

The series reactor is of iron core and oil is used as the cooling medium. Table 2-6 summarizes the main technical specifications of the reactor and Figure 2-9 shows its cross section.

Nominal Data of the Series Reactor installed in the Hoek van Holland area	
Operating Voltage [kV]	420
Through Current [A]	4000
Nominal Impedance [Ω]	10.1/ 8.5/ 6.5 **

Table 2-6. Technical specifications of the series reactors

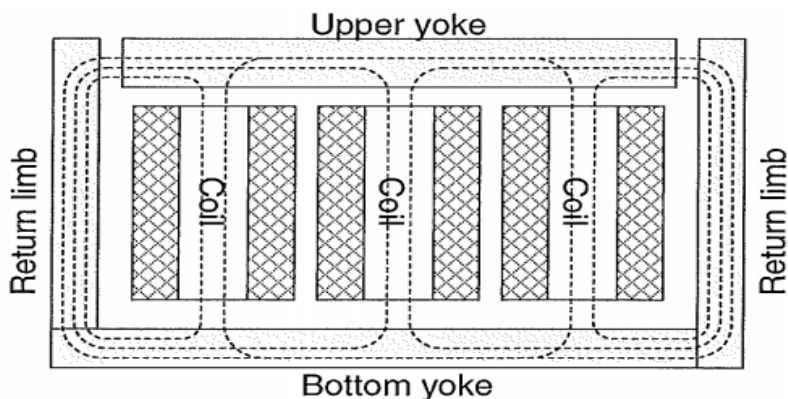


Figure 2-9. Cross section of a series reactor [Source: KEMA Consulting Report – 30813039 – 09 -1733]

** The nominal impedance of the series reactor is selectable by an off-load tap changer.

2.4.1 Series Reactor model in ATP – EMTP

For a complete model of the series reactor, all of its electrical characteristics have to be taken into consideration. More specifically, apart from the unsaturated inductance and the resistance of the magnetic path, which are calculated according to the nominal dimensions of the reactor, both the saturation and the parasitic capacitances are modeled too. Figure 2-9 above shows the path that the magnetic flux follows between the two yokes and the two return limbs. For the air and iron sections, the following can be stated:

- The air gaps are represented by a linear inductance (L) with 22.68 mH
- The iron core, which can be driven into saturation, is represented by a non-linear inductance (L_s) with 4.35 mH
- The series resistance (R_s) is 26.15 m Ω

For the non-linear inductance, the non-linear current depended inductor of Type-98 is used in ATP – EMTP. This component requires pairs of current-flux values as an input for defining the magnetization curve. These values are shown in Table 2-7 below, while Figure 2-10 shows the magnetization curve, as it is defined by ATP – EMTP itself:

Input Data for the Type-98 non-linear inductance of the Series Reactor		
	Current [A]	Flux [Wb-T]
Knee Point	10100	43.9673
Saturated Section	56568	68.291

Table 2-7. Saturation characteristics of the series reactor non-linear inductance

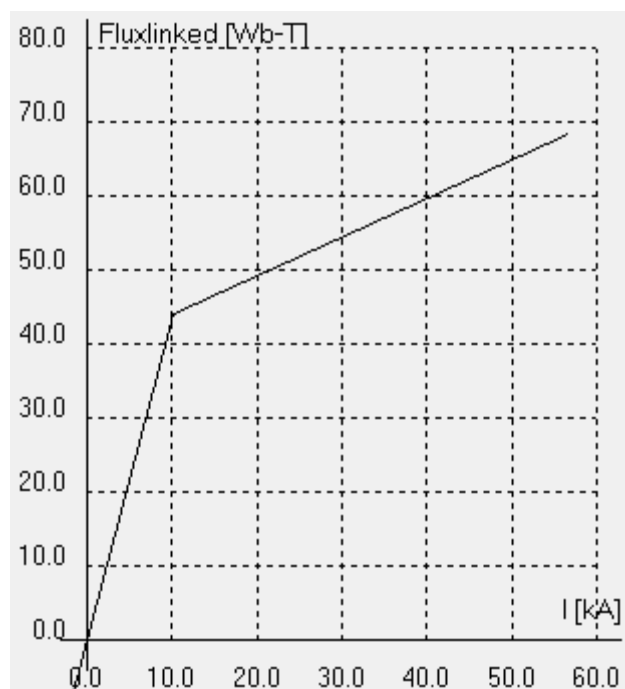


Figure 2-10. Magnetization curve of the iron core in the ATP – EMTP series reactor model

Furthermore, parasitic capacitances appear in the windings of the series reactor, as long as at its terminals and the bushings:

- Winding capacitance, C_s , of 500 pF
- Terminal capacitance, $C_t/2$, of 1830 pF

The figure below shows the equivalent per phase circuit of the series reactor, as it was modeled in ATP – EMTP.

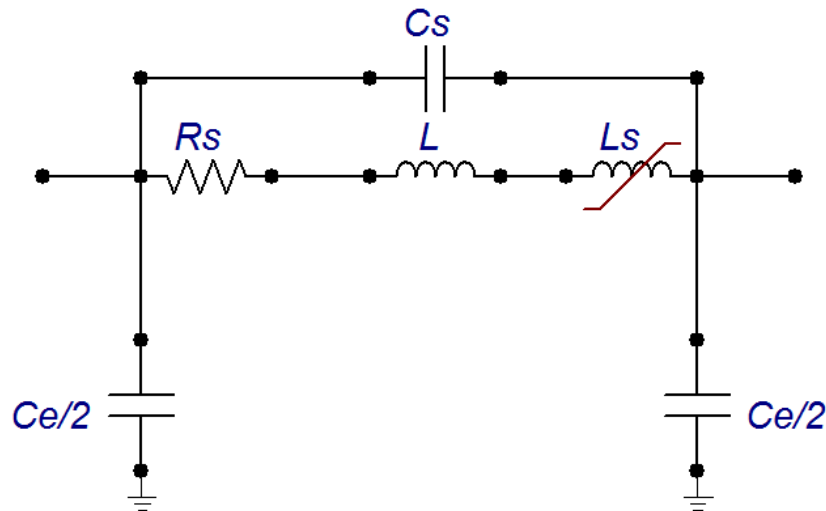


Figure 2-11. Per phase equivalent of the saturable series reactor in ATP – EMTP

2.5 380 kV Power Source model

The mixed transmission connection is supplied by the two substations, Maasvlakte and Westerlee. However, in order to study the configuration's behavior under fault conditions, the two power sources should be modeled accordingly. In other words, the correct short circuit current has to be determined to all kind of faults (single-phase to ground fault, double-phase to ground fault, double-phase fault, three-phase to ground fault). In the study [9], the current values for the three-phase to ground, $I''_{k,3-phase}$, and single-phase to ground, $I''_{k,1-phase}$, faults at the two substations are mentioned and re-presented in the table below:

Fault Currents in the Maasvlakte and Westerlee Substations		
Substation	$I''_{k,3-phase}$ [kA]	$I''_{k,1-phase}$ [kA]
Maasvlakte	62.97	73.67
Westerlee – Wit	36.6	34.12
Westerlee - Zwart	36.59	33.68

Table 2-8. Three-phase to ground and single-phase to ground fault currents in the MVL and WTL substations

Depending on these values, the positive and zero sequence impedances for the three locations can be calculated, according to the equations 2-9 and 2-10 [10]:

$$I''_{k,3-phase} = \frac{1,1 \cdot U_n}{\sqrt{3} |Z_1|} \quad (2-9)$$

$$I''_{k,1-phase} = \frac{\sqrt{3} \cdot 1,1 \cdot U_n}{|Z_1| + |Z_2| + |Z_0|} \quad (2-10)$$

where $I''_{k,3-phase}$: subtransient three-phase to ground fault current [kA]

- $I''_{k,1\text{-phase}}$: subtransient single-phase to ground fault current [kA]
 U_n : nominal RMS line-to-line voltage of the system [kV]
 Z_1 : positive sequence impedance [Ω]
 Z_2 : negative sequence impedance [Ω]
 Z_0 : zero sequence impedance [Ω]

It has to be noticed that the system's voltage is 380 kV, thus, the voltage factor, c_{\max} , for calculating the maximum short circuit current is equal to 1.1. Furthermore, the positive and negative sequence impedances are assumed to be equal ($Z_1 = Z_2$). Since there are no precise values available for the sequence resistances, R_1 and R_0 , and reactances, X_1 and X_0 , it is assumed that the equation (2-11) gives an analogy between these values:

$$R = 0.1X \quad (2-11)$$

Table 2-9 lists the calculated values for the positive and negative sequence resistances, reactances and inductances for both substations.

Positive and Negative Sequence Impedances in the Maasvlakte and Westerlee Substations								
Substations	Z_1 [Ω]	Z_0 [Ω]	R_1 [Ω]	X_1 [Ω]	L_1 [mH]	R_0 [Ω]	X_0 [Ω]	L_0 [mH]
Maasvlakte	3.8325	2.1625	0.381348	3.81348	12.145	0.215177	2.15177	6.8527
Westerlee – Wit	21.219	8.032	0.65609	6.5609	20.894	0.79921	7.9921	25.452
Westerlee - Zwart	6.5955	8.305	0.65627	6.5627	20.9	0.82637	8.2637	26.3175

Table 2-9. Positive and zero sequence resistances and inductances in the MVL and WTL substations

2.5.1 Power Source model in ATP - EMTP

For the model of the power source in ATP – EMTP, an ideal three-phase voltage source is used, in series with the subtransient values for the positive and zero sequence resistance and inductance. More specifically, the subtransient impedance is modeled by the symmetric coupled line element, Line_SY3, which requires the values of R_1 , L_1 , R_0 and L_0 as input data. Figure 2-12 shows the equivalent model of a power source in ATP - EMTP.

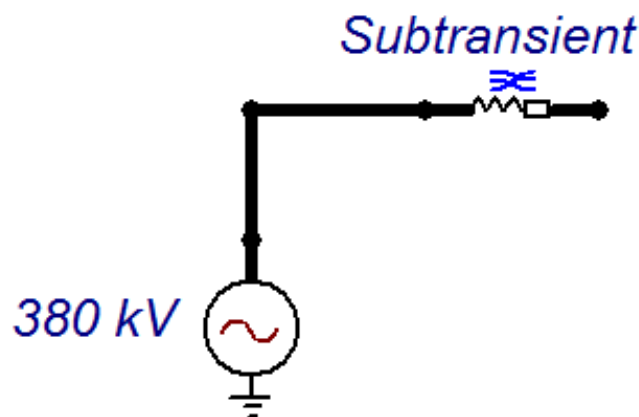


Figure 2-12. Power source model in ATP - EMTP

Chapter 3

Current Transformers (CTs)

3.1 Introduction

The complexity of the Electrical Power Systems requires an appropriate management of the data processing, not only for the monitoring of the equipment, but also for its control and protection. The current transformers, along with the voltage transformers (VTs) comprise the basis of the data processing and they are essential for the normal operation of the protection devices. For this purpose, CTs must supply the protective relays with currents, which are proportional to the ones flowing at their primary side with the correct polarity and high accuracy. CTs are also used in the mixed transmission connection between the Maasvlakte – Westerlee – Wateringen substations, since differential and distance protection schemes have been implemented.

This chapter presents the basic information regarding the operation, the classes and the possible saturation errors of the CTs; the ATP – EMTP model of the protection CTs installed in the mixed configuration is presented too. The figure below shows a typical CT that is used in HV power systems.



Figure 3-1. Typical current transformer used in HV applications [Source: www.directindustry.com]

3.2 Basic Principles of the CTs

The Current Transformers in practice correspond to a current driven transformer, which consists of a magnetic circuit. The primary winding of the circuit is made of N_1 turns, while the secondary of N_2 turns, producing by this way the CT's nominal ratio, N_1/N_2 . The latter is based on Ampere's law,

which states that the sum of the ampere-turns is equal to the closed integral of the magnetic field [11]:

$$N_1 i_1 + N_2 i_2 = \int \vec{H} \cdot \vec{n} \, dl \quad (3-1)$$

where i_1 : current flowing in the primary winding
 i_2 : current flowing in the secondary winding
 N_1 : number of turns of the primary winding
 N_2 : number of turns of the secondary winding
 \vec{H} : magnetic field vector
 \vec{n} : tangent unit vector

For an ideal transformer, the right part of (3-1) is equal to zero, while in a real transformer this term corresponds to the errors introduced by the magnetic circuit due to the excitations current, i_e :

$$N_1 i_1 + N_2 i_2 = N_2 i_e \quad (3-2)$$

Based on the above, a CT can be represented by two basic parts: an ideal transformer with turns ratio equal to N_1/N_2 and a magnetizing branch, through which the excitation current flows. Figure 3-2 shows the equivalent per phase circuit of a CT, where:

- R_1 and R_2 the primary and secondary winding resistances respectively
- L_1 and L_2 the primary and secondary leakage inductances
- N the ration of the ideal transformer
- \vec{i}_m the magnetizing current
- \vec{i}_a the current which represents the losses in the CT (hysteresis losses and eddy currents)

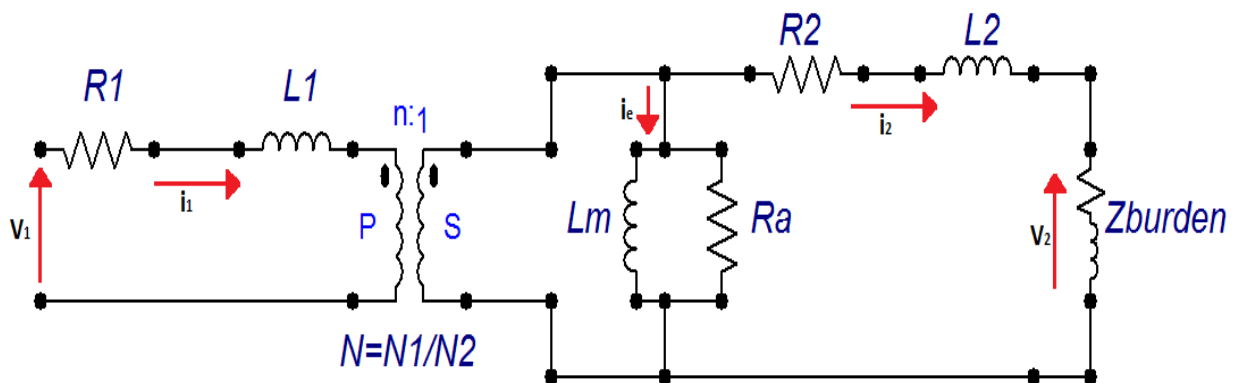


Figure 3-2. Per phase equivalent of a current transformer

As it was mentioned above, the excitation current is the one that introduces the errors in the CT. Due to i_e , there is a phase displacement, δ , between the primary current, i_1 , and the secondary current, i_2 . Larger values of the excitation current lead to larger values of the displacement angle, thus, the error ϵ is larger too. The latter is shown in the figure below:

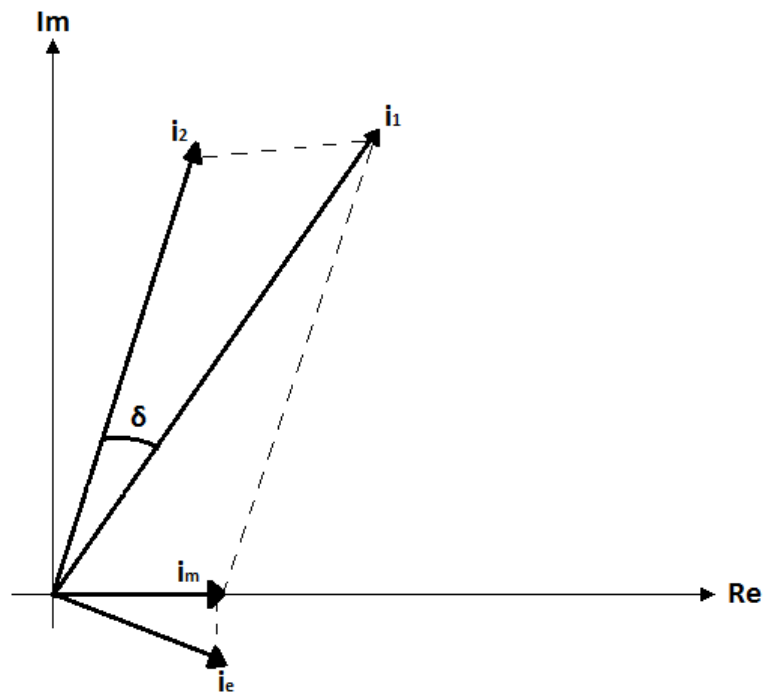


Figure 3-3. Vectorial representation of the CT currents

3.2.1 Technical Specifications for Protection CTs

The CTs are divided in two major categories, depending on their functionality: the protection CTs and the instrument CTs. The basic difference between the two categories is that the ‘protection type’ CTs are able to conduct currents much higher than the nominal one, while the ‘instrument type’ CTs are characterized by operating currents lower than the ones of the protection devices [12]. Accordingly, two different factors are defined for each CT type:

- the Accuracy Limit Factor (ALF) for the ‘protection type’
- the Safety Factor (SF) for the ‘instrument type’

A protection CT is able to provide a secondary current with certain accuracy, when current flows through its primary winding up to a threshold value [13]. This value is defined as the multiplication of the CT’s nominal primary current with the ALF:

$$I_{al} = ALF \cdot I_n \quad (3-3)$$

If the primary current exceeds the accuracy limit value, I_{al} , the current transformer will be driven into saturation and by this way errors will be introduced in the secondary current. CT errors are analytically discussed in paragraph 3.3. Apart from the accuracy limit factor, a protection CT is also defined by the accuracy class, the rated transformation ratio and the rated power, P_n . The table below summarizes the basic data specifications of a protection CT:

Technical Specifications of a Protection CT	
Rated transformation ratio	Ratio of nominal primary to nominal secondary current
Rated power, P_n [VA]	Rated power in the secondary side under nominal secondary current and nominal burden connected

Accuracy class [5P or 10P]	Composite error, ϵ_c , at $ALF \cdot I_n$ current
Accuracy Limit Factor [ALF]	Multiplication factor, which determines the maximum primary current that can be transformed to the secondary with the defined accuracy class
Secondary winding resistance, R_{CT} [Ω]	Nominal resistance of the secondary given by the manufacturer

Table 3-1. Definitions of the basic data of a protection CT

The current transformers being used in the mixed connection studied, have a nominal ratio of 4000/1, ALF is equal to 60, while they are of the 5P class. The complete data sheets, provided by the manufacturer, are included in Appendix C. Figure 3-4 gives a graphic representation of a protection CT's specifications:

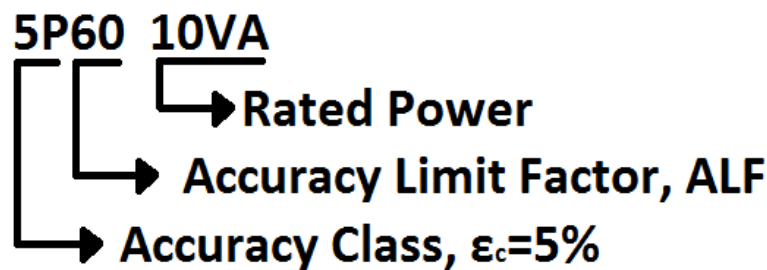


Figure 3-4. Data specifications of the protection CTs installed in the MVL – WTL mixed configuration

One important factor, which determines the operation of the CT, has to do with the burden connected at the secondary side of the latter. More precisely, the rated ALF is defined as the multiplication factor when the nominal burden, R_{Bn} , corresponds to the real load consumption of the current transformer. However, when the burden connected differs from the rated one, a recalculation of ALF is required. This implies that the internal EMF, corresponding to the saturation voltage of the CT, has the same value in both cases. Assuming that the burden connected at the secondary is purely resistive –in case of numerical protection relays, the reactive component of the burden is neglected-, the nominal power supplied at the secondary side is given by the equation below:

$$P_n = U_2 \cdot I_2 = I_2^2 \cdot R_{Bn} \quad (3-4)$$

The internal EMF, E_2 , under nominal operating conditions of the CT is:

$$E_2 = I_2 (R_{CT} + R_{Bn}) \quad (3-5)$$

When the rated accuracy limit current, $I_{2,al}$, is flowing through the secondary winding, the internal EMF, E_{al} , corresponds to the saturation voltage of the CT. Equation (3-6) describes the latter:

$$E_{al} = ALF \cdot I_2 (R_{CT} + R_{Bn}) \quad (3-6)$$

As it was mentioned above, when a different burden is connected at the secondary, ALF has to be re-calculated, so that the internal saturation EMF does not change its value:

$$E_{al} = ALF' \cdot I_2 (R_{CT} + R_{B,real}) \quad (3-7)$$

Using equations (3-6) and (3-7), the re-calculated value of ALF' is derived:

$$\begin{aligned} ALF \cdot I_2 (R_{CT} + R_{Bn}) &= ALF' \cdot I_2 (R_{CT} + R_{B,real}) \\ \Rightarrow ALF' &= ALF \frac{R_{CT} + R_{Bn}}{R_{CT} + R_{B,real}} \quad (3-8) \end{aligned}$$

The secondary winding resistance of the CTs installed in the mixed transmission system is equal to 5.3Ω , while the rated burden is 10Ω , as it is calculated with the help of (3-4). Nonetheless, the real burden connected at the secondary side of the CTs is that of the protection relays, which is lower than the nominal one. For instance, the resistance of the SIEMENS differential relay 7SD52, R_R , is approximately 0.5Ω and the resistance of the wiring connections, R_L , is assumed to be 2.5Ω . Thus, the total real burden of the secondary is $R_b = R_R + R_L = 3\Omega$. By making use of (3-8), the re-calculated value of ALF' is defined:

$$ALF' = ALF \frac{R_{CT} + R_{Bn}}{R_{CT} + R_{B,real}} = 60 \frac{5.3+10}{5.3+3} = 110.6$$

As a result, the protection CTs will erroneously transform the primary currents to the secondary side, when the latter will exceed the value $110.6 \cdot I_{1n}$ and no DC offset component is present. In other words, the accuracy limit margin increases conversely with the resistive burden connected at the secondary side.

3.3 CT Saturation

The ferromagnetic core of a CT is not linear and it is characterized by its magnetization curve, which consists of the linear and the saturated part respectively. When the CT is operating in its linear range, the primary current is transformed to the secondary without significant errors, since the excitation current has low values. However, this is not the case when the CT is driven into saturation, because the magnetizing branch draws higher currents and the magnetic induction goes beyond the knee point, resulting into a secondary current, which deviates from the ideal case. Based on the latter, large errors arise that exceed the permissible limits and the correct operation of the protective relays may be affected. Thus, the transient response of a CT in its saturated range is necessary to be known for ensuring the proper operation of the protection configurations.

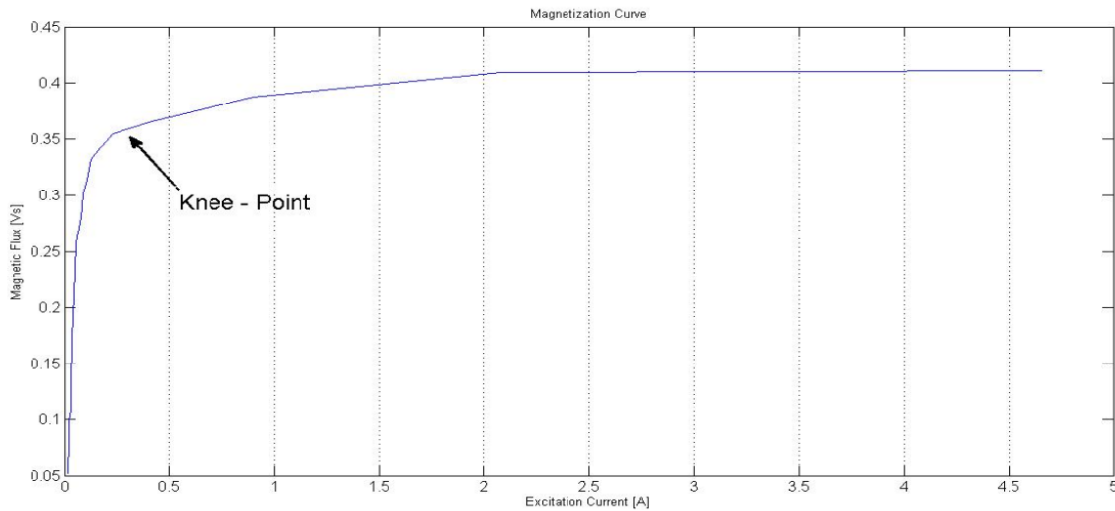


Figure 3-5. Typical magnetization curve of the applied CT in the mixed transmission configuration

A CT may be driven into saturation due to two different cases: a pure AC primary fault current exceeds the accuracy limit current, which is defined in (3-3), or the fault current consists of AC and DC offset components. Both cases are described briefly in the next two paragraphs.

3.3.1 CT Saturation due to pure AC fault current

As it was mentioned in paragraph 3.2.1, when the CT is loaded with a certain secondary burden, the re-calculated ALF' determines the point at which the magnetic core will start saturating, assuming a pure AC primary current. The accuracy limit current determines the knee point of the magnetization curve, as it is shown in Figure 3.6. For higher currents than I_{al} the magnetic core is saturated and the excitation current, I_e , increases. Thus, the secondary current is decreasing, since the ideal transformed current is defined as below:

$$\frac{\vec{I}_1}{N} = \vec{I}_2 + \vec{I}_e \quad (3-9)$$

By subtracting the excitation current from the ideal secondary, the real secondary current is determined, as it is shown in Figure 3-7.

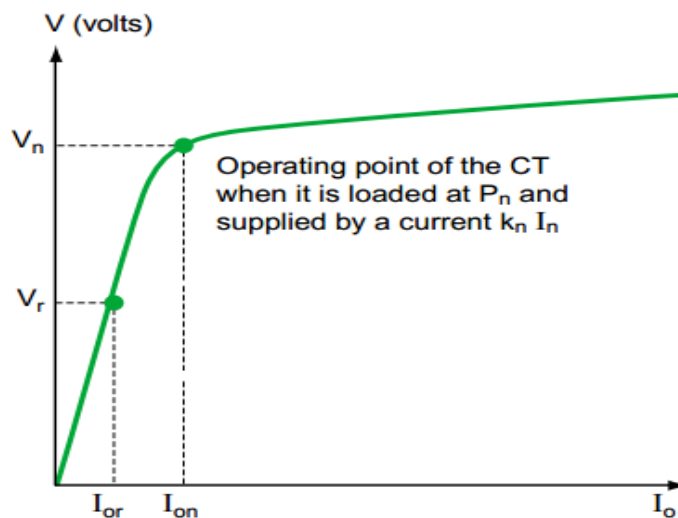


Figure 3-6. Operating point of a CT when the accuracy limit current flows in the primary side

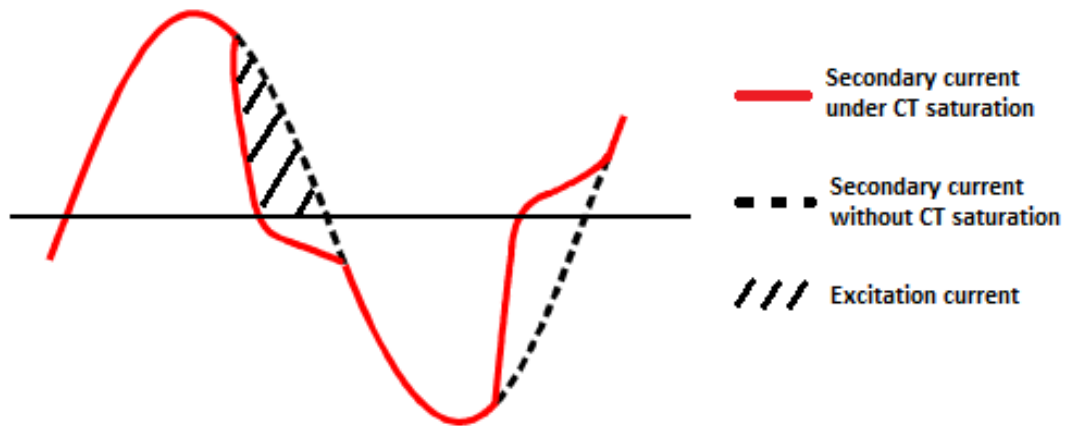


Figure 3-7. Graphic representation of I_2 , $I_{2,sat}$, I_e

3.3.2 CT Saturation due to DC offset fault current component

The most important factor, which may affect the transient response of a protection CT, is the unipolar exponentially decaying DC component of the primary fault current. The DC offset is responsible for the steep increase of the core's induction and together with the AC component of the flux, may lead to saturation [14]. This is shown in the figure below, where the total flux is equal to the sum of the AC and DC component respectively.

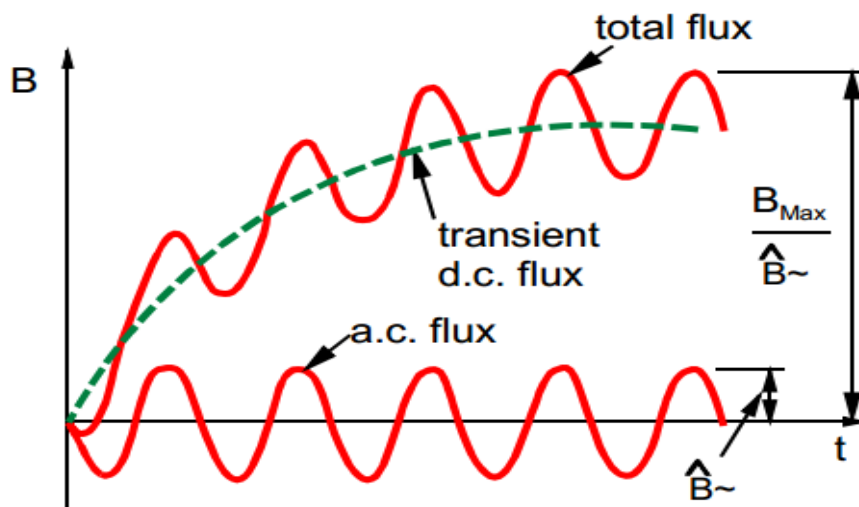


Figure 3-8. Total flux in the CT magnetic core under offset fault current conditions [Source: SIEMENS, "Basics of Current and Voltage Transformers"]

When an offset fault current flows in the primary side of a protection CT, the core flux will steeply increase, reaching high values. If the saturation level is reached, the secondary current, which is transformed without significant errors till the knee point of the magnetization curve is reached, will start decreasing to lower values. During the negative (or positive, depending on the DC component's polarity) cycle of the primary current, the latter will be correctly translated to the secondary side, without any saturation occurring. Thus, a sequence of saturated and non-saturated intervals will result till the DC component significantly decays. Figure 3.9 shows the secondary current under saturation and no saturation conditions, while Figure 3-10 gives a graphic representation of the situation analyzed above.

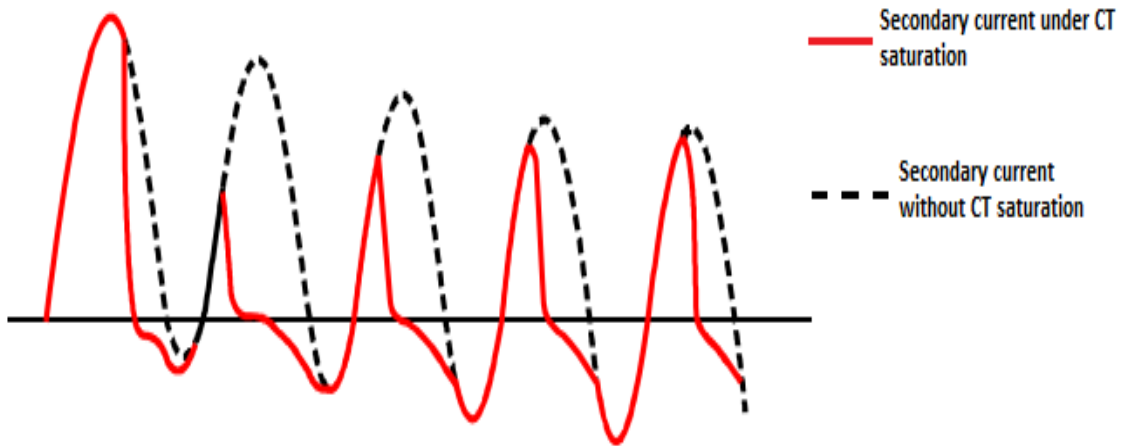


Figure 3-9. Graphic representation of I_2 and $I_{2,sat}$

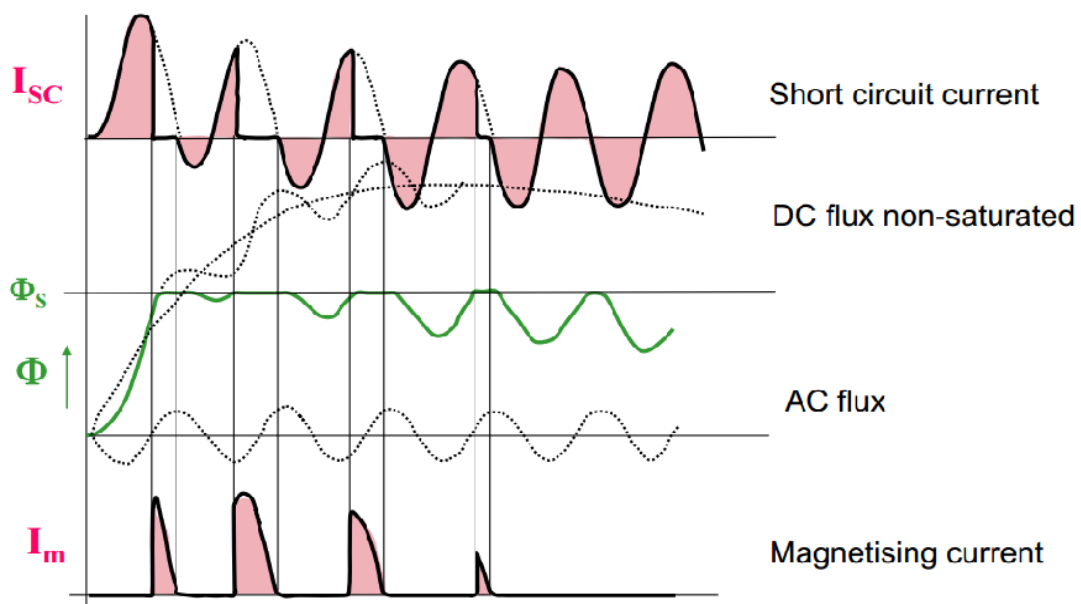


Figure 3-10. Secondary current, flux and magnetization current under CT saturation [Source: SIEMENS, “Basics of Current and Voltage Transformers”]

3.3.3 Classes of Protection CTs

Apart from their basic technical specifications, the current transformers that are used in the different protection schemes, are also characterized by their response under transient conditions. For that reason, four classes are defined, according to the transient performance (TP) of the CTs. Moreover, the response of a CT during a DC offset fault current depends on the construction of its magnetic core, as it is shown in the table below:

Current Transformers TP classes	
TPS	Closed iron core with low leakage reactance
TPX	Closed iron core without remanence limits
TPY	Anti-remanence air gaps are present ($B_r < 10\%$)
TPZ	Linear core, remanent flux is negligible

Table 3-2. Transient performance classes of the protection CTs

- **TPS class:** The response of the CT depends on the magnetization curve and the secondary winding resistance. Thus, there are no limits regarding the residual flux, as it is also defined in the IEC standards [15].
- **TPX class:** Although the CT transforms the AC and DC offset components of the transient current with high accuracy, the residual flux is also high and may reach values of more than 80%. The latter is trapped in the magnetic core and it can be removed by forced de-magnetization. However, errors may arise in the case of an unsuccessful auto-reclosure operation, because of the extra significant increase of the flux. This is shown in Figure 3-11, in comparison with the flux built-up in a TPY class CT.
- **TPY class:** The magnetic core of the CT has small air gaps –in the range of some millimeters– and by this way the residual flux is considerably limited, i.e. up to 10% of the saturation flux. CTs of this class are mainly used for line protection with auto-reclosure, since the core is partially de-magnetized during the dead time of the AR operation [16].
- **TPZ class:** In this case, the air gaps in the magnetic core are centimeter sized. Consequently, the residual flux is limited in such an extent that it may be neglected. In addition, DC offset component of the fault current is heavily dampened, resulting in a small flux increase during an AR operation.

The two figures below show the differences between the TPX, TPY and TPZ CT classes. More specifically, in Figure 3-12 the typical magnetization curves in terms of flux, B , and magnetic field strength, H , are shown. It can be seen that the residual flux, B_r , has high value in case of a TPX CT, while for a TPY and a TPZ CT the values are very low and negligible respectively. Figure 3-12 shows the flux building-up during an AR operation for a TPX and TPY CT. Contrary to the TPX CT, it is clear that the anti-remnance air gaps in the TPY magnetic core limit the B_r to much lower values.

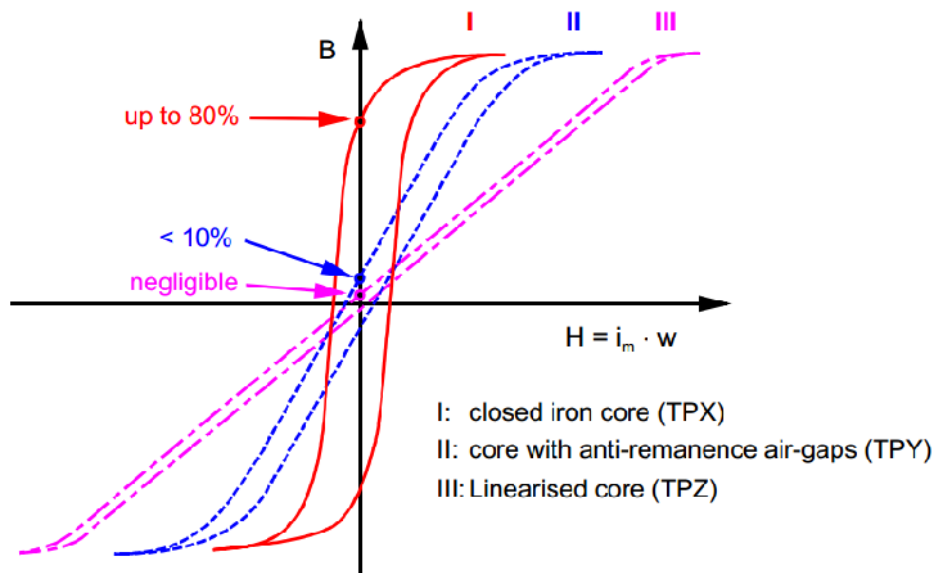


Figure 3-11. Magnetization curves for the different CT classes [Source: SIEMENS, “Basics of Current and Voltage Transformers”]

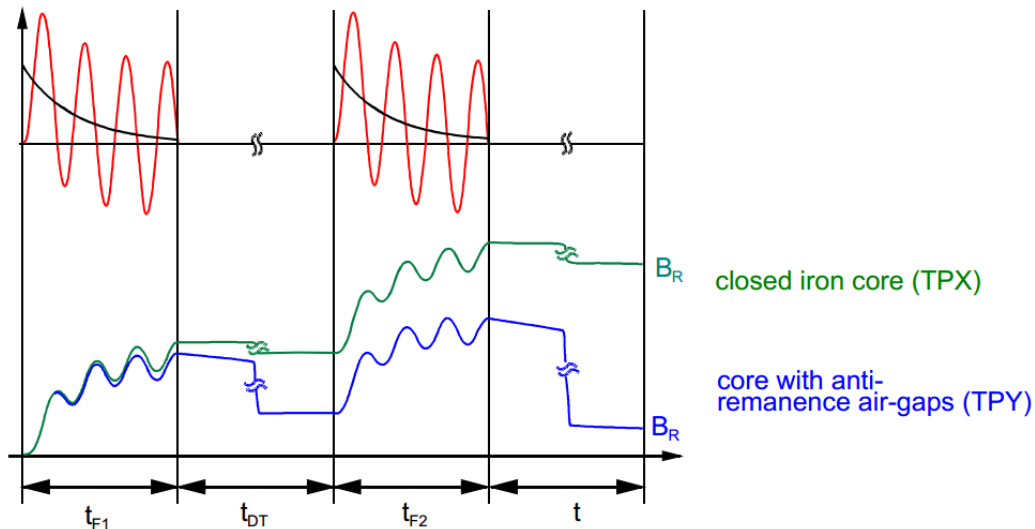


Figure 3-12. Transient magnetization of the TPX and TPY CTs during an AR operation [Source: SIEMENS, "Basics of Current and Voltage Transformers"]

3.4 Protection CT model in ATP – EMTP

3.4.1 CT Equivalent per Phase Circuit in ATP - EMTP

For an accurate model of a protection CT through ATP – EMTP, apart from the basic technical specifications of the latter, the magnetization curve has to be available too. Consequently, the transient response of the CT can be thoroughly studied, since the CT's behavior under saturation conditions can be simulated. The equivalent per phase circuit of a CT, as modeled in ATP – EMTP [17], is based on the equivalent per phase circuit of Figure 3-2 and it is shown in the figure below:

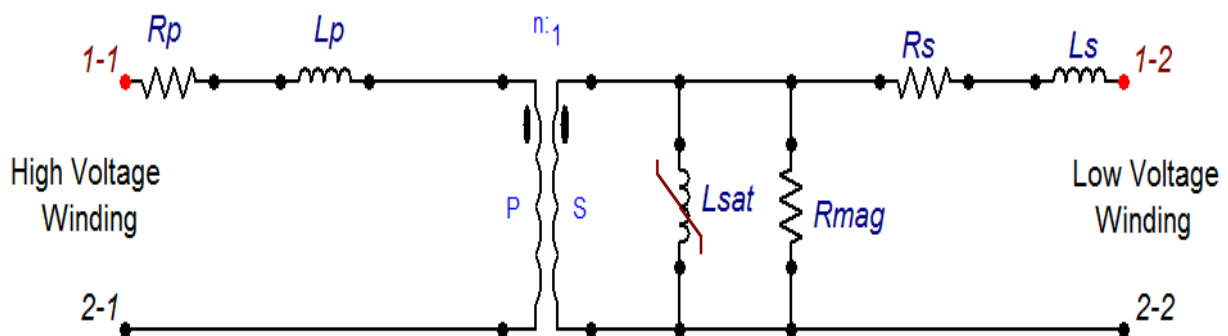


Figure 3-13. Equivalent per phase circuit of a protection CT as modeled in ATP – EMTP

- For the representation of the ideal transformer, the single phase ideal transformer of Type-18 is used, which represents the relation between the turns number of the two windings
- To take into account the saturation effect of the magnetic core, a true non-linear inductor of Type-98 is used, which generates the magnetization curve, by having as input data pairs of excitation current and magnetic flux values [18]. More precisely, the non-linearity is defined as a number of linear segments, while the flux is recorded at each time step. By this way, at the end of every time step the next linear segment is chosen and the non-linear inductance is calculated.

- Although Figure 3-13 shows the complete per phase equivalent of the CT circuit, the primary winding can be neglected in the ATP – EMTP model, without causing any significant deviations in the accuracy of the final results.
- The ideal transformer, together with the secondary winding, can be replaced by a single phase saturable transformer. The latter includes in its input data the values of the primary and secondary branches, the magnetizing resistance and the turns ratio of the CT. The simplified per phase equivalent of the CT, as modeled in ATP – EMTP, is shown below:

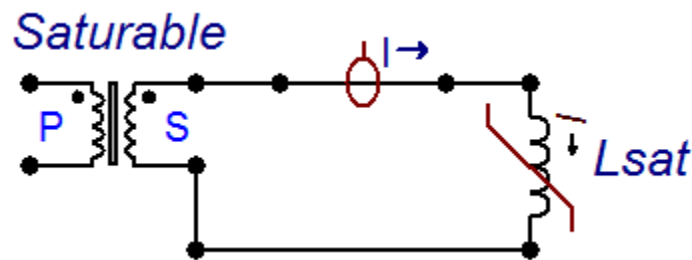


Figure 3-14. Simplified equivalent per phase CT circuit as modeled in ATP - EMTP

3.4.2 Magnetization Curve and SATURA routine in ATP – EMTP

As it was mentioned above, pairs of excitation current and magnetic flux values are needed for generating the magnetization curve in the non-linear inductor of Type-98. However, the CT data provided by the manufacturers represent the saturation curve in terms of excitation current and the voltage at the secondary winding. For that reason, ATP – EMTP supports an additional routine called “SATURA”, which can convert the $i_e - V_2$ pairs of RMS values into $i_e - \Phi$ peak values, while the hysteresis loop is not taken into account. Figure 3-14 shows the magnetization curve given in the specifications data sheet of the CTs used in the mixed transmission system studied. The knee and curve points are also mentioned on the graph, based on the calculations below.

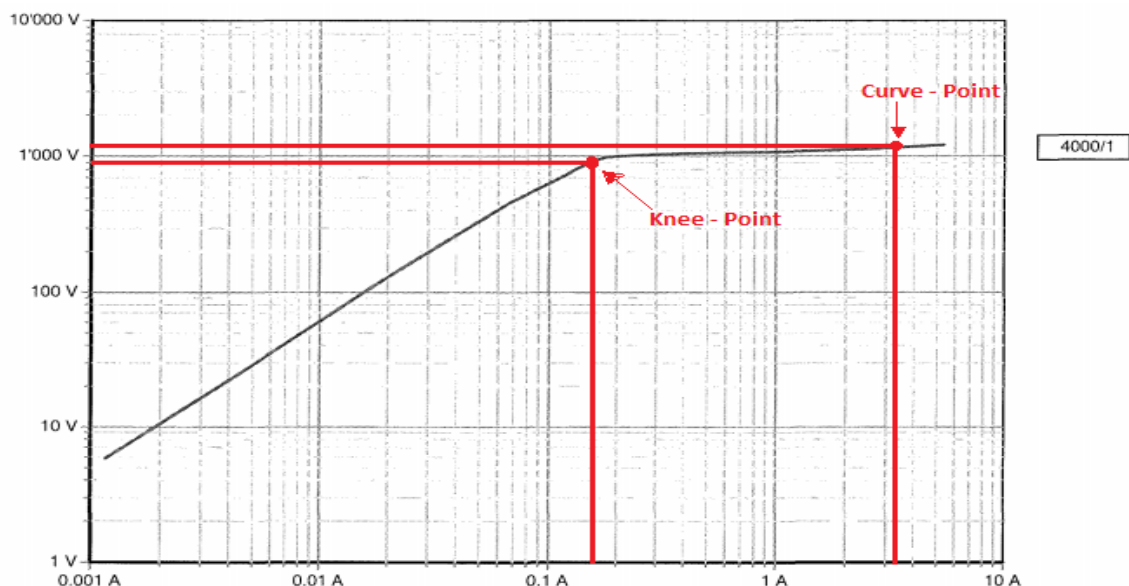


Figure 3-15. Magnetization curve of the 4000/1 protection CTs used in the mixed transmission system

According to [19], the knee point of the saturation curve can be calculated as:

$$E_k = ALF \cdot (R_{CT} + R_B) \cdot I_{2n} = 913.8V \quad (3-10)$$

where E_k : the voltage at the secondary winding of the CT [V]

ALF: the accuracy limit factor

I_{2n} : the nominal secondary current [A]

R_B : the rated burden connected at the secondary [Ω]

R_{CT} : the nominal resistance of the secondary winding [Ω]

Also, the curve point corresponds to the excitation current, which results to the composite rated error of the protection CT:

$$I_e \leq \frac{CE \cdot ALF \cdot I_{2n}}{100\%} = 3A \quad (3-11)$$

Based on the value of (3-11), the curve point is approximately 1050V.

From the magnetization curve of Figure 3-15, 20 pairs of RMS values of i_e and V_2 were chosen along the linear and saturated lines and they were used as input values in the "SATURA" routine, which in turn generated 20 pairs of peak values of i_e and Φ . The two tables below include the $i_e - V_2$ and $i_e - \Phi$ pairs:

RMS Values of i_e and V_2	
$i_{e,RMS}$ [mA]	$V_{2,RMS}$ [V]
2.10634	11.00694171
2.95521	16.15598098
5.08021	26.10157216
7.62698	46.41588834
19.684194	133.3521432
29.552092	177.827941
50.80218	348.0700588
81.614007	510.8969775
150.131072	749.8942093
171.90722	908.5175757
196.841944	1000
295.520923	1019.373486
387.4675	1049.139729
581.709132	1079.775162
762.698585	1100.694171
1145.04757	1122.018454
1403.003723	1143.755863
1968.419447	1165.914401
2955.209235	1188.502227
3974.67512	1211.527659

Table 3-3. Pairs of $i_e - V_2$ RMS values



Peak Values of i_e and Φ	
$i_{e,peak}$ [mA]	Φ_{peak} [Vs]
2.97881459	0.0495486461
4.0704743	0.0727274664
7.39904568	0.117498356
9.96943612	0.208944908
27.625578	0.600295552
45.0434867	0.800506984
67.6858511	1.56686577
121.732527	2.2998442
232.210553	3.37570996
236.131071	4.08976598
300.087608	4.50158158
843.059016	4.58879291
846.437526	4.72278808
1514.07113	4.86069598
1951.29738	4.95486461
3266.92372	5.05085761
3332.2204	5.14871033
5438.6377	5.24845879
8359.11017	5.35013973
9916.59508	5.45379059

Table 3-4. Pairs of $i_e - \Phi$ peak values

With the values of table 3.3, together with the help of MATLAB, the CT's magnetization curve –in terms of excitation current and secondary voltage- is generated, as it is shown in the figure below:

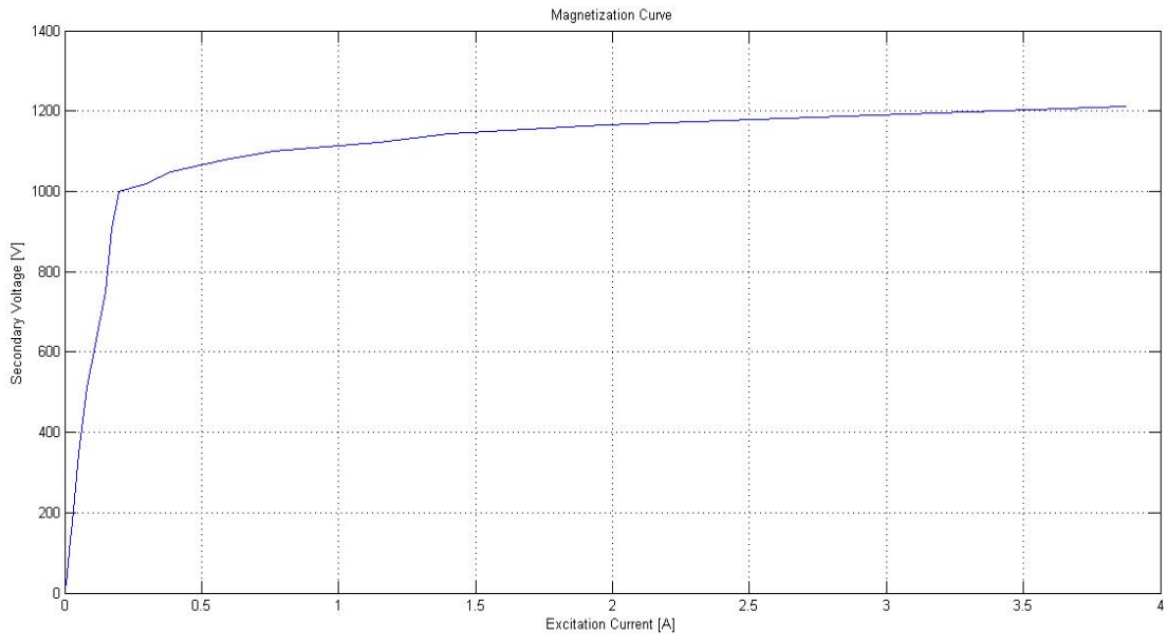


Figure 3-16. Magnetization curve ($i_e - V_2$) of the protection CTs

Using the values of table 3-4, the saturation curve of the CTs in terms of excitation current and magnetic flux is generated through MATLAB. However, it has to be noticed that the curve is accordingly fitted and smoothed, while the saturation line is extended, compared to the curve provided by the manufacturer. By this way, the behavior of the CT can be simulated under deep saturation conditions. The latter is shown in Figure 3.17, where the two curves are compared.

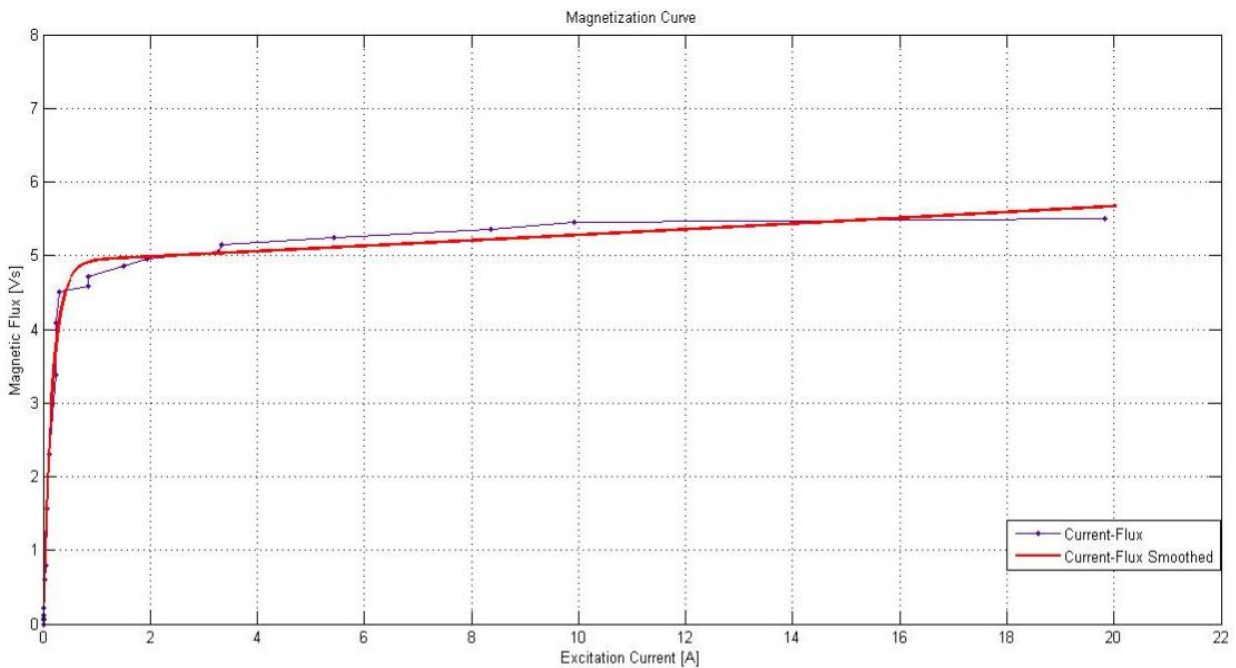


Figure 3-17. Magnetization curve ($i_e - \Phi$) of the protection CTs

3.4.3 Transient Response of the Protection CT model in ATP – EMTF

The transient response and the accuracy limit of the protection CT are studied through a test circuit model in ATP – EMTF. More specifically, a three-phase voltage source is connected in the primary

winding of the CT, while a resistive load determines the primary current generated by the source. By modifying the value of the load resistance, the value of the primary current is varied too and by this way the response of the CT and the saturation limit are studied.

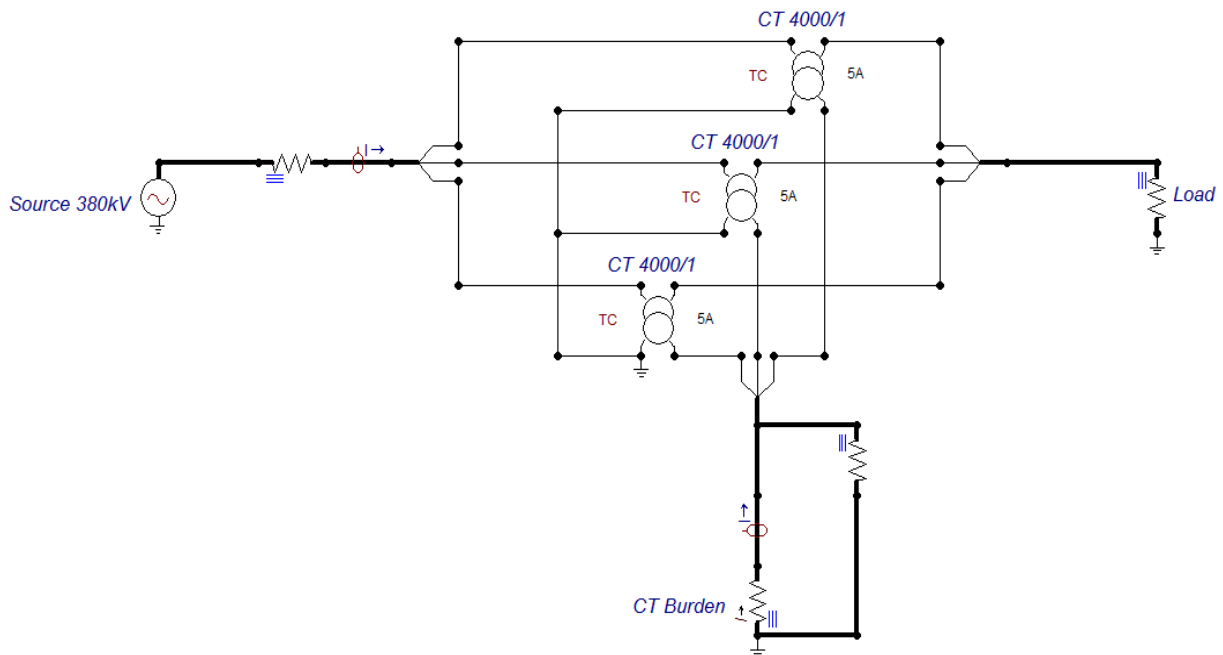


Figure 3-18. Test circuit of the protection CT in ATP – EMTP

- Rated burden connected in the secondary winding of the protection CT

With the rated burden connected in the secondary winding of the CT ($R_B=10\ \Omega$), the primary current varies from a value equal to the nominal primary current of the protection CT ($I_{1N}=4000\ \text{A}$) to a value equal to $84.3 \cdot I_{1N}$. The table below shows the results obtained at each simulation step, regarding the peak values of the primary and excitation current respectively.

Sensitivity Analysis results of the Protection CT with nominal burden connected in the secondary				
I_1 [kA]	$I_{1N,multiples}$	$I_{1,peak}$ [kA]	$I_{e,peak}$ [A]	R_{Load} [Ω]
4	$1 \cdot I_{1N}$	5.65	0.0059975	54.8
40	$10 \cdot I_{1N}$	56.5	0.02895	5.48
80	$20 \cdot I_{1N}$	113.14	0.05946	2.73
120	$30 \cdot I_{1N}$	169.7	0.09604	1.8185
160	$40 \cdot I_{1N}$	226.27	0.1465	1.361
200	$50 \cdot I_{1N}$	282.84	0.2067	1.0875
240	$60 \cdot I_{1N}$	339.41	0.311	0.9038
260	$65 \cdot I_{1N}$	367.69	0.4026	0.835
286.75	$71.69 \cdot I_{1N}$	405.53	1.052	0.755
337.2	$84.3 \cdot I_{1N}$	477.26	20.16	0.64

Table 3-5. Saturation analysis results of the protection CT model in ATP – EMTP ($R_B=10\ \Omega$)

The protection CT is driven into significant saturation, when a pure AC primary current of 286.75 kA RMS value flows through the primary winding. The excitation current is then equal to 1.052 A, which corresponds to the saturated part of the magnetization curve, as it is shown in Figure 3-17 above. When the excitation current is lower than the value mentioned above, the primary current is transformed to the secondary with insignificant errors, as it is shown in Figure 3-19, where the

primary, secondary and excitation currents are represented for the case that nominal primary current flows through the CT.

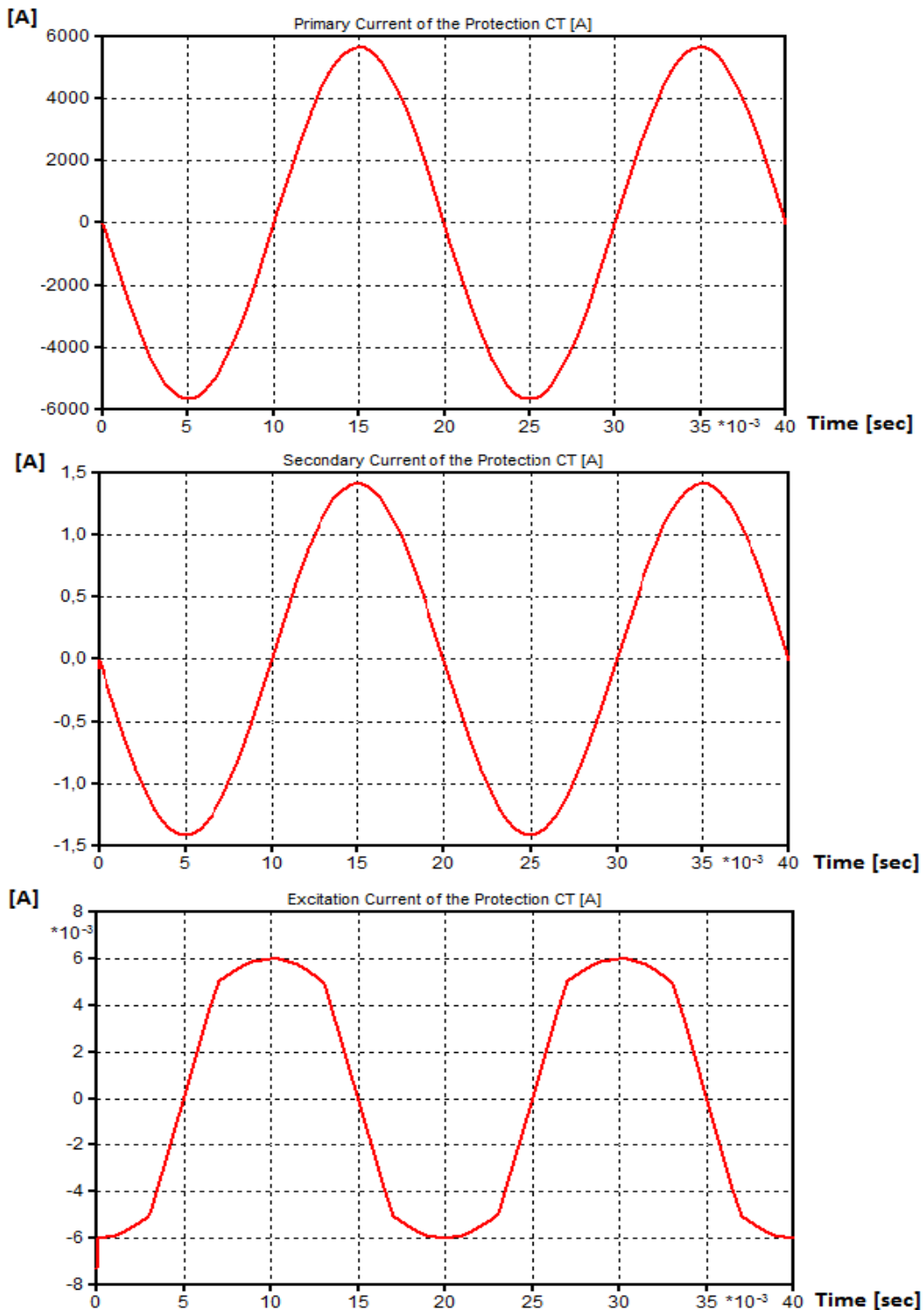


Figure 3-19. Primary, secondary and excitation currents of the protection CT with nominal current flowing in the primary winding

On the other hand, when the CT is driven into saturation, the primary current is transformed to the secondary side with errors and the secondary current is distorted. The higher the excitation current, the more significant the distortion is in the current flowing in the secondary winding. The figures

below show the primary, secondary and excitation currents when primary currents equal to 71.69 and 84.3 times the nominal one flow in the primary side of the CT.

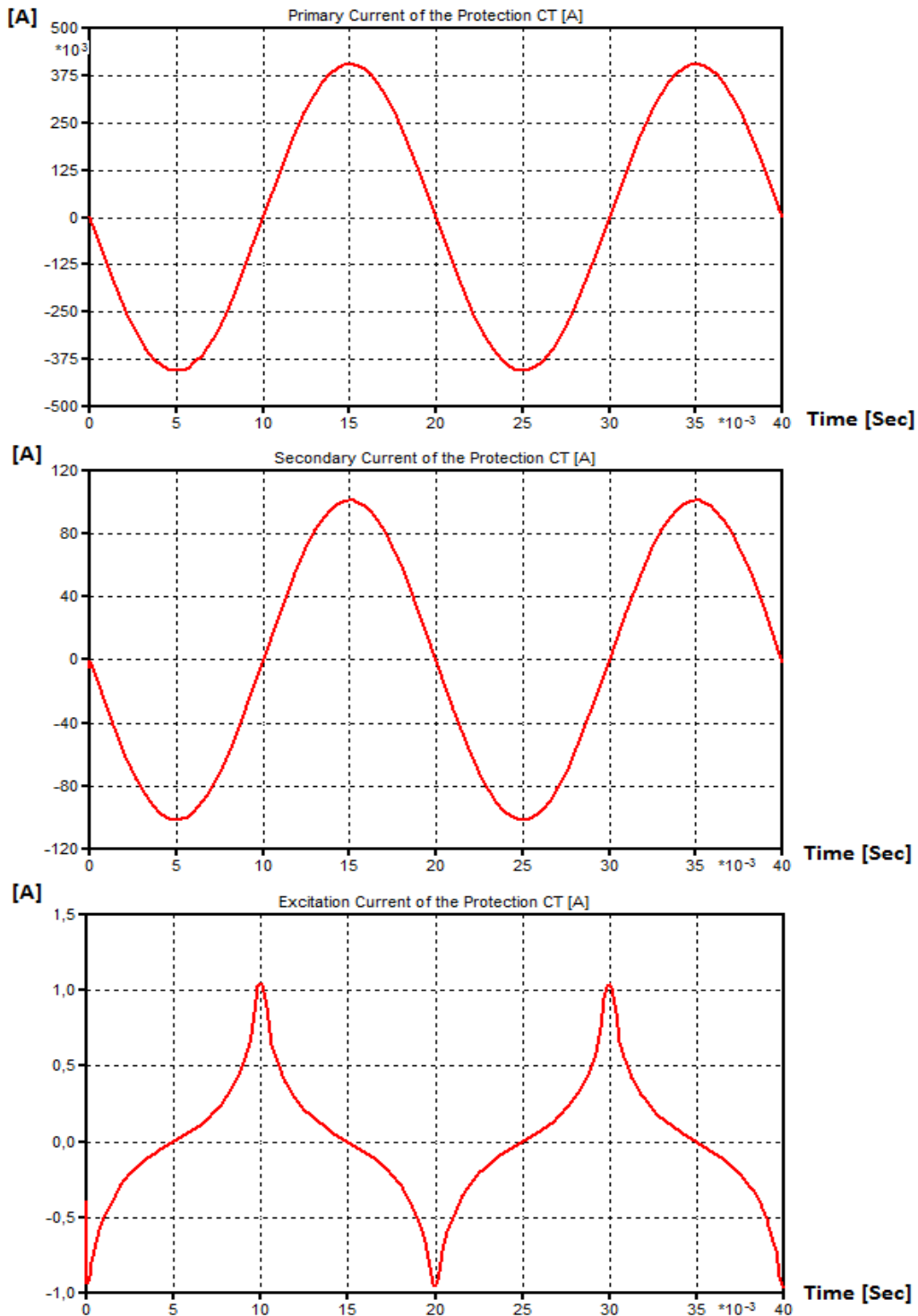


Figure 3-20. Primary, secondary and excitation currents of the protection CT with current 71.69 times the nominal one flowing in the primary winding

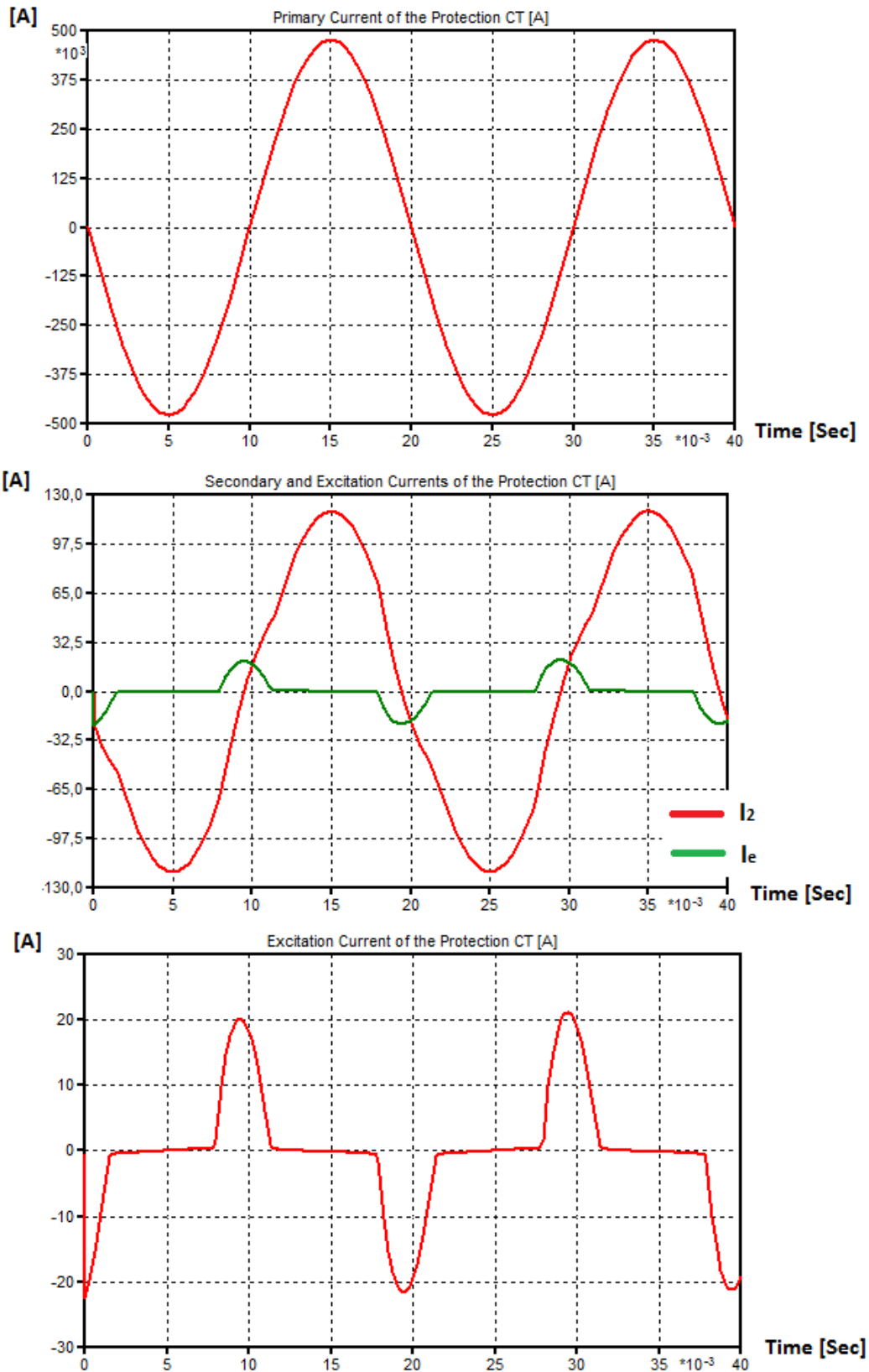


Figure 3-21. Primary, secondary and excitation currents of the protection CT with current 84.3 times the nominal one flowing in the primary winding

Figure 3-22 shows an extreme situation of CT saturation, where the excitation current is comparable with the secondary current. In this case, the high distortion of the secondary current and the significant errors are obvious.

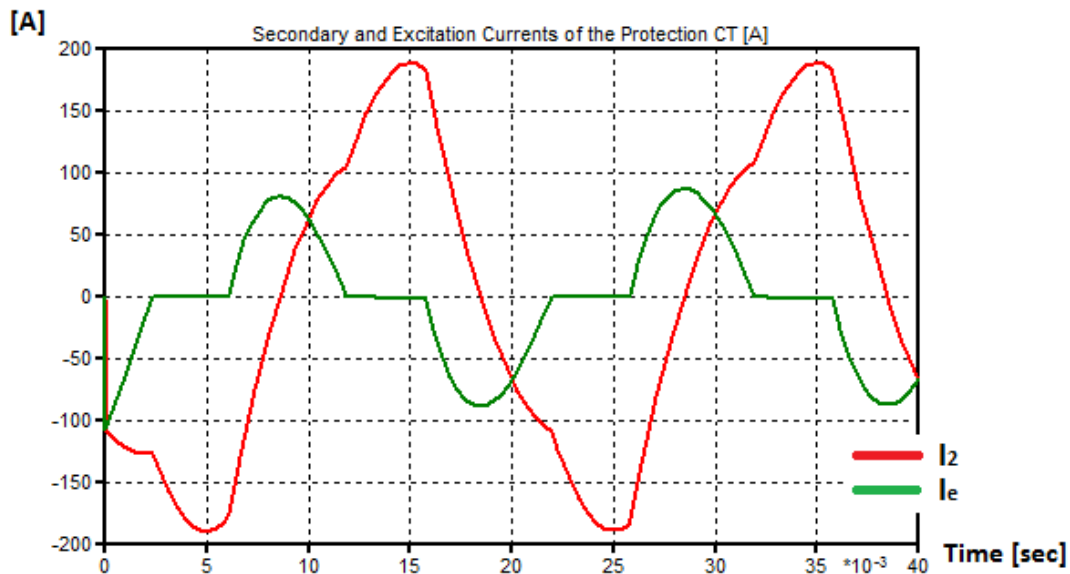


Figure 3-22. Secondary and excitation currents under extreme saturation conditions of the protection CT

- Real burden connected in the secondary winding of the protection CT

As it was mentioned in paragraph 3.2.1, the value of the resistive burden connected in the secondary winding of the CT affects the accuracy limit of the latter. Thus, in the case of connecting a real burden in the secondary side (i.e. wiring connections and protective relay), the transient response of the CT is enhanced, since the value of ALF increases accordingly. This is shown in the table below, which summarizes the results obtained from the sensitivity analysis of the CT for $R_B=3\ \Omega$.

Sensitivity Analysis results of the Protection CT with $R_B=3\ \Omega$ connected in the secondary				
I_1 [kA]	$I_{1N,multiples}$	$I_{1,peak}$ [kA]	$I_{e,peak}$ [A]	R_{Load} [Ω]
4	$1 \cdot I_{1N}$	5.65	0.0046385	54.9
240	60	339.41	0.1053	0.904
440	110	622.25	0.2999	0.4885
531.08	132.77	751.06	1.0373	0.403

Table 3-6. Saturation analysis results of the protection CT model in ATP – EMTP ($R_B=3\ \Omega$)

In this case, the CT is driven into significant saturation when the current flowing in the primary winding reaches an RMS value of 531.08 kA, which corresponds to a value 132.77 times the rated current. Thus, the transient response of the CT is enhanced, when compared with the previous case. The latter confirms the fact that a lower burden than the nominal one, which is connected to the secondary winding of the protection CT, increases the accuracy limit of the device.

Chapter 4

Line Differential Protection (DP)

4.1 Introduction

Protection of power systems and of their equipment is essential and crucial for the proper operation of the electrical networks and for the uninterrupted transmission and distribution of the generated power. Additionally, the high costs of the installed equipment increase the need of reliable protection systems, which can provide suitable and fast clearance of the possible faults in a system. Current differential relay is one of the very first protection systems, which were implemented, because of its simplicity, high reliability and fast tripping operation. This is the reason why the differential protection is widely used in various power systems' equipment, i.e. generators, power transformers, busbars, overhead lines and underground cables [20].

The operating principle of DP is based on comparing the currents, which flow into the sending end and flow out of the remote end of the protected area [21]. By this way, it is determined whether a fault takes place within the protected zone or not, if the differential current has a non-zero value. DP can be implemented in parts of a power system, where the measured currents do not have to be transmitted (generators, power transformers, busbars). However, DP can also be implemented in the case of OHL and underground cables, where the measured quantities are transmitted to the opposite far end, via communication channels. Thus, the independent differential protection of a cable system is possible in a mixed circuit, consisted of overhead line and underground cable parts [22].

In this chapter, the basic operating principles of the differential protection are presented, while the SIEMENS differential relay 7SD52, which is installed in the mixed configuration between the Maasvlakte and Westerlee substations, is studied too. Last but not least, the differential relay model, which was investigated in ATP – EMTP, is presented along with the results obtained from a test circuit.

4.2 Basic Principles of Differential Protection

The main operation of the DP corresponds to the clearing of a fault within the protected area, which is defined only by the location of the installed protection CTs. Thus, the DP is highly selective and no time grading is needed with other protection schemes, unless any time delay is inserted to the tripping signals at special cases (i.e. isolated or resonant/earthed networks). As it was mentioned above, the operating principle of the DP is based on the comparison of the currents, which flow in and out of the protected zone. More specifically, the instantaneous values of the CTs' secondary currents are directly compared with regard to their magnitude and phase. In the case of an external fault, the current which flows into the protected object is equal to the one that flows out of the object. Consequently, the geometric sum of the current vectors, which corresponds to the differential current, is equal to zero. On the other hand, the differential current gets a non-zero value in the case of an internal fault, which results to the generation of a tripping signal by the differential relay.

Figures 4-1 and 4-2 show the basic operation of the differential protection, under internal and external fault conditions. During an external fault, the secondary currents of the CTs flow into the opposite direction and since they are equal in terms of magnitude and phase, the differential current

ΔI will be zero. To the contrary, under internal fault conditions, the secondary currents will add up in the differential branch, resulting into a non-zero differential current.

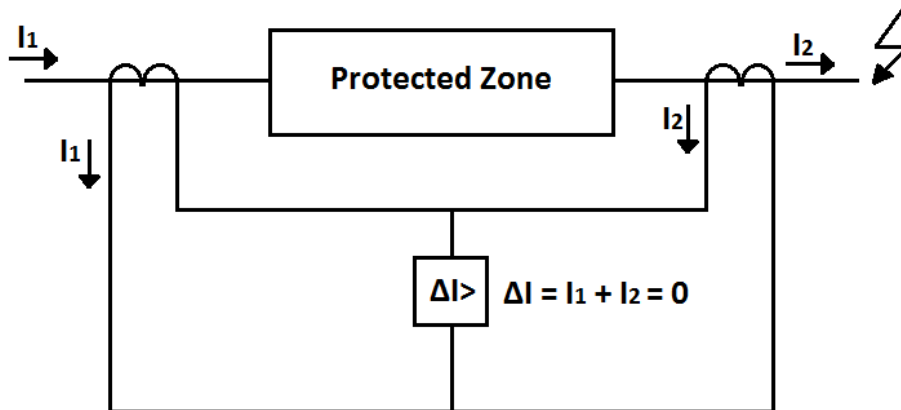


Figure 4-1. Differential protection under an external fault

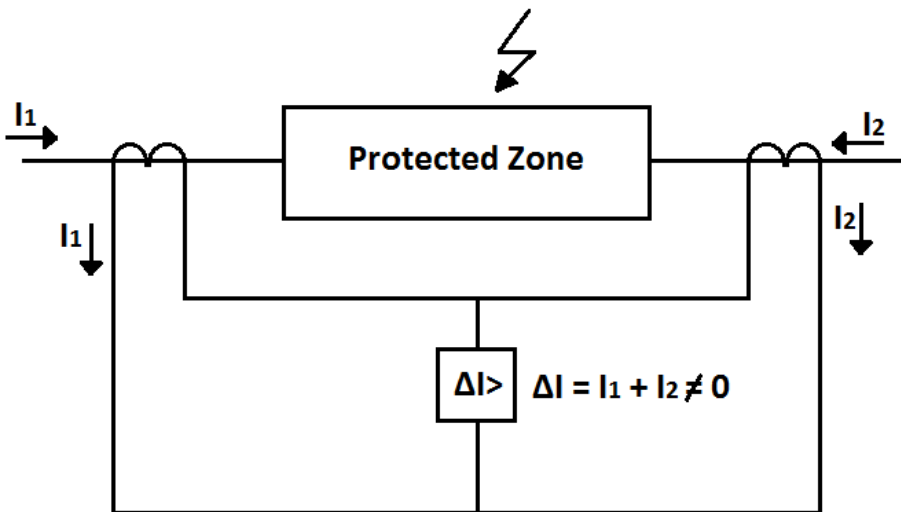


Figure 4-2. Differential protection under an internal fault

The differential current, which is defined as in the equation (4-1), is compared to the restraint current and not to a fixed pick – up threshold. This is because various errors may affect the proper operation of the differential protection, as it is explained below.

$$I_{Diff} = \left| \overline{I}_1 + \overline{I}_2 \right| \quad (4-1)$$

$$I_{Res} = \left| \overline{I}_1 \right| + \left| \overline{I}_2 \right| \quad (4-2)$$

where \overline{I}_1 : the secondary current at the sending end of the protected zone

\overline{I}_2 : the secondary current at the remote end of the protected zone

Errors during the calculation of the differential current could be introduced due to CT transformation errors, line charging currents, time delays in the communication channels or transformer tap changer errors [23]. For instance, the CTs may be driven into saturation under large fault currents, leading to

an incorrect calculation of I_{Diff} . This is undesirable under external fault conditions, since a false tripping signal could be generated by the differential relay. Thus, the restraint current depends on the through current and it increases when the latter increases too. Consequently, the sensitivity of the relay is highly enhanced.

Based on the above, a standard stabilized pick – up characteristic is defined for the differential relay, as it is shown in the figure below. The relay will generate a tripping signal, if only the differential current lies in the “Operate” area, which is defined by the two lines with slopes k_1 and k_2 respectively [24]. In other words, the pick – up criterion is:

$$I_{Diff} \geq k_1 \cdot |I_{Res}| + I_0 \quad (4-3)$$

Or

$$I_{Diff} \geq k_2 \cdot |I_{Res}| - (k_2 - k_1) \cdot I_{S2} + I_0 \quad (4-4)$$

where I_0 : the pick – up setting of the differential relay
 k_1 : the slope of the first part of the characteristic
 k_2 : the slope of the second part of the characteristic

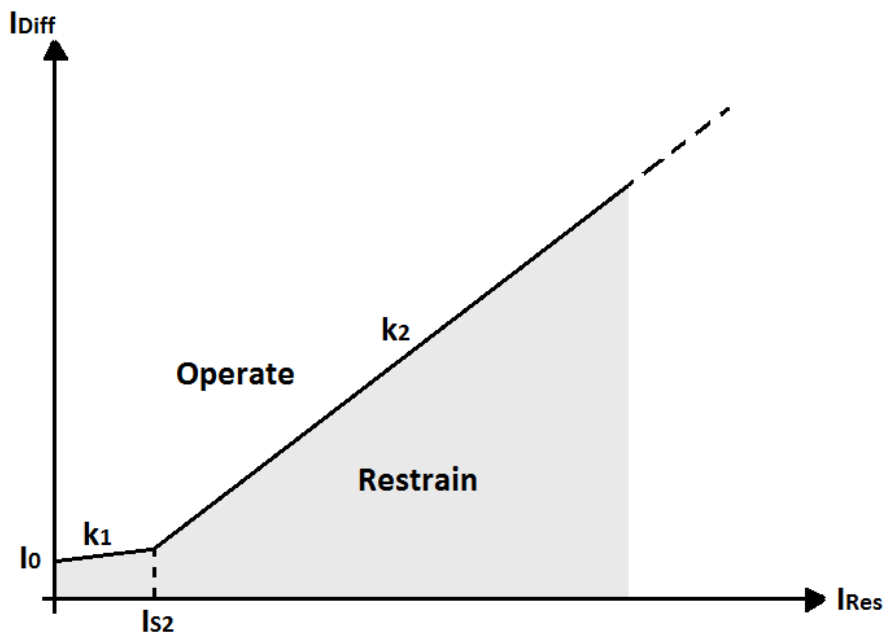


Figure 4-3. Stabilized pick – up characteristic of the differential relay

Modern numerical relays analyze the instantaneous values of the secondary currents and the dynamic response is defined based on the pick – up characteristic. The process and analysis of the measured quantities is done numerically, with filters and intelligent algorithms providing high accuracy, flexible setting characteristics and short operating times.

4.3 Numerical Measuring Technique – Discrete Fourier Transform (DFT)

A differential relay consists of various block models, forming the signal conditioning, data acquisition and analysis, before reaching the logic block, where the tripping and blocking commands are generated. These blocks are responsible for the filtering of the analog signal, the sampling of the values, the conversion of the instantaneous values from analog to digital and the buffering of the digital samples. The most important block is responsible for estimating the current phasors, which

are calculated, based on the sampled values [25]. Figure 4-4 shows a schematic representation of the blocks and their sequence, while the output of the relay logic is directly linked with the circuit breaker (CB).

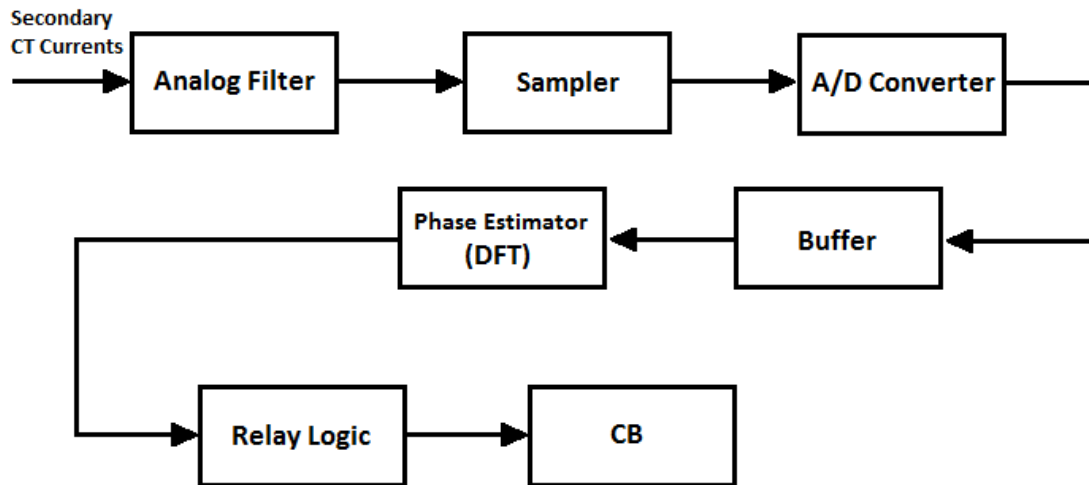


Figure 4-4. Block diagram of a numerical differential relay

- **Analog Filter:** It removes the high frequency components, by using sharp cut – off bandwidths. However, passive RC filters are also used, providing simplicity and reliability when damping the high frequencies.
- **Sampler:** It is responsible for choosing and storing samples of the instantaneous measured values with a specific sampling rate. The latter is defined as the time between two consecutive samples and for differential protection, a sampling rate of 1 kHz, which corresponds to 1 ms, is sufficient according to [26].
- **A/D Converter:** It is responsible for converting the analog signal into digital, by assigning a specific binary number to each of the samples. The digitalized samples maintain the sequence they primarily had, while the number of bits used in the binary system differs according to the technique that is implemented.
- **Buffer:** This block stores the converted samples, before they are processed to the phasor estimator block. The buffer's size is of n+1 samples, with n being the number of the samples during a cycle.
- **Phase Estimator:** In this block the phasors of the measured signals are computed in terms of magnitude and phase, so that they can be used in the relay algorithm following. Numerical differential relays commonly use two techniques, namely: the Discrete Fourier Transform (DFT) and the Least Squared Algorithm. The SIEMENS differential relay 7SD52 implements the DFT method, which is examined in the next paragraph.

4.3.1 Discrete Fourier Transform (DFT)

The DFT expresses a periodic time waveform, $f(t)$, in the frequency domain $F(j\omega)$, where all the frequency components of the original input signal are present. Consequently, the undesired harmonics can be excluded and the fundamental frequency component can be extracted. DFT makes use of two orthogonal functions in order to derive the real and imaginary parts of the estimated

phasors [27]. Two functions, $f(x)$ and $g(x)$ are orthogonal within an interval $[a, b]$, when the following expression is true:

$$\langle f(x) \perp g(x) \rangle = \int_a^b f(x) \cdot g(x) dx = 0 \quad (4-5)$$

Equation (4-5) is confirmed in the case of the sine and cosine functions, which are used in DFT of the numerical relays, as it is shown below:

$$\langle \sin(x) \perp \cos(x) \rangle = \int_{-\pi}^{\pi} \sin(x) \cdot \cos(x) dx = 0 \quad (4-6)$$

The basic principle of the DFT is based on the convolution theory, where the samples of the input signal are multiplied and summated with the sine and cosine functions respectively for each sampling rate. Thus, the sampling rates of the two orthogonal functions have to be the same with the sampling rate of the original signal. By this way, each sample of the periodic waveform is multiplied with the corresponding sample of the sine and cosine functions and they are summated in the end of each cycle. The real and imaginary parts of the estimated phasors are calculated according to the equations (4-7) and (4-8):

$$I_{r(k)} = \frac{2}{N} \cdot \left[\sum_{n=1}^{N-1} i_{k-N+n} \cdot \sin\left(2\pi \cdot \frac{n}{N}\right) \right] \quad (4-7)$$

$$I_{im(k)} = \frac{2}{N} \cdot \left[\frac{i_{k-N} + i_k}{2} + \sum_{n=1}^{N-1} i_{k-N+n} \cdot \cos\left(2\pi \cdot \frac{n}{N}\right) \right] \quad (4-8)$$

where k : the sample at the sampling time $k \cdot \Delta t$
 N : the total number of the samples

The magnitude and phase of the phasors are calculated based on the equations (4-9) and (4-10):

$$I_{(k)} = \sqrt{I_{r(k)}^2 + I_{im(k)}^2} \quad (4-9)$$

$$\Phi_{(k)} = \arctan\left(\frac{I_{r(k)}}{I_{im(k)}}\right) \quad (4-10)$$

Furthermore, it has to be noticed that the estimated phasors will be available for the relay algorithm only in the end of each data window of the DFT. Although the phasors are re-computed at fixed time intervals, the data window cannot be excessively shortened due to noise interference. Figure 4-5 shows the basic principle of the DFT, where the sampled values are correlated with the sine and cosine functions to calculate the real and imaginary parts of the estimated phasors.

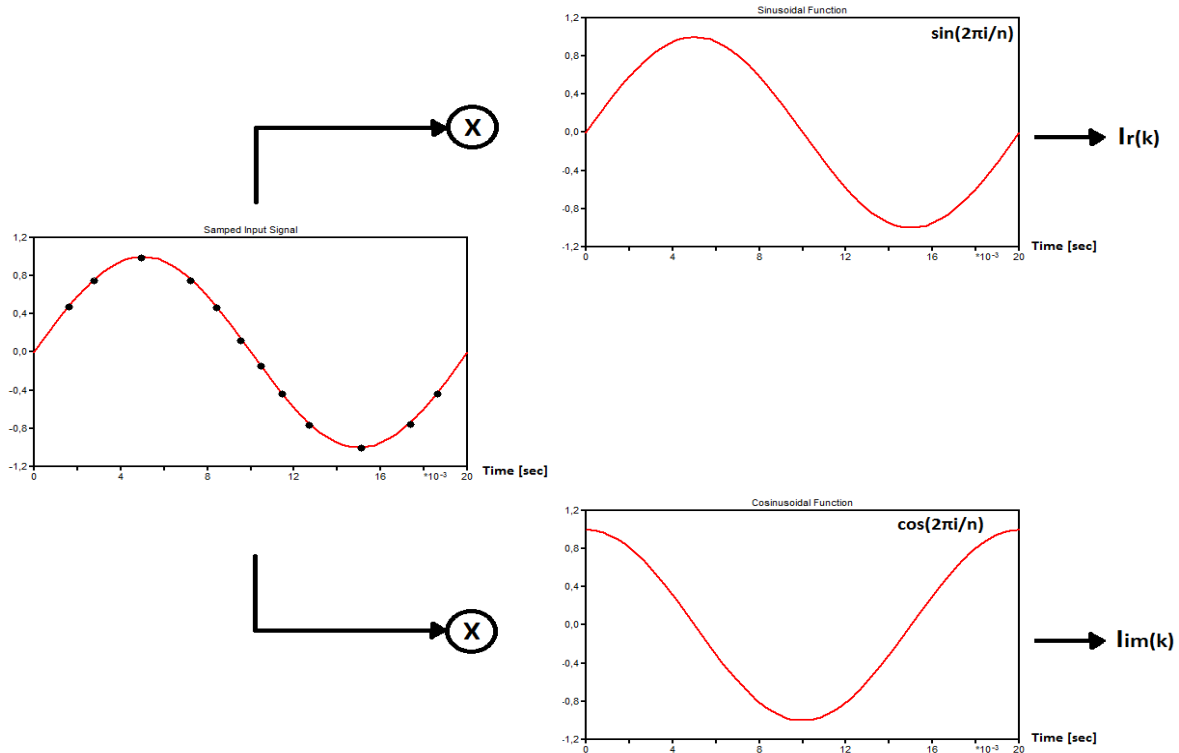


Figure 4-5. Basic principle of the Discrete Fourier Transform

4.4 SIEMENS Numerical Line Differential Relay 7SD52

In the mixed transmission configuration studied, between the Maasvlakte and Westerlee substations, TenneT TSO has installed SIEMENS relays of the 7SD52 series, for the line differential protection and the differential protection of the HV underground cables. For each protected zone, two relays are used and installed in the remote and sending end of the object. The relays receive the measured secondary currents from the corresponding CTs, while exchanging at the same time the acquired signals via communication links. This is schematically shown in Figure 4-6, where the protected zone refers to an underground HV cable (two-end relay configuration).

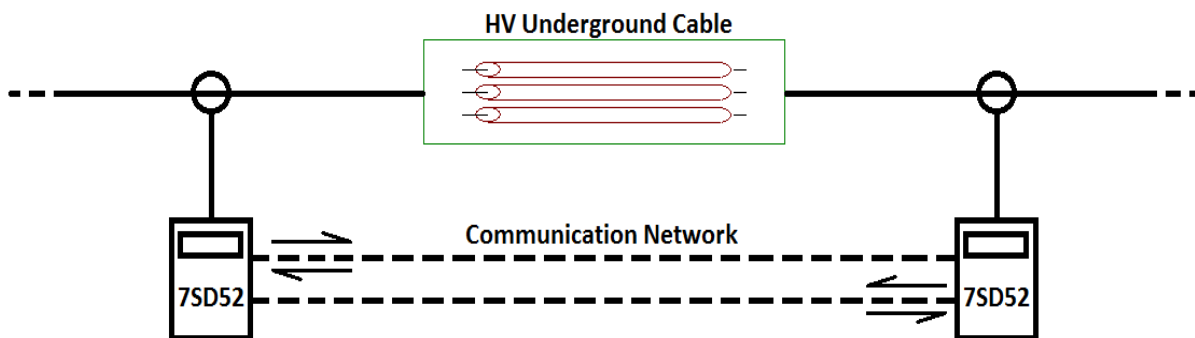


Figure 4-6. SIEMENS 7SD52 differential protection scheme

Contrary to the standard numerical differential relays, SIEMENS relay employs a different stabilized pick – up characteristic. More specifically, the restraint current is calculated by taking into account all the possible errors introduced by the CTs and the communication links between the relays and the characteristic adapts accordingly:

- Constant value of the pick – up current, $I_{Diff>}$: This value is determined by the charging current of the protected line/cable, since the latter could lead to a false tripping signal generated by the relay. However, this setting should not be less than the 15 – 20% of the system’s nominal current.
- Communication network errors, Σe_{sync} : Because of the communication links between the two relays, delays are introduced to the calculated phasors, which are exchanged through the data channels. These delays are translated into angle errors, leading to miscalculation of the differential current.
- CTs errors, Σe_{CT} : The errors of the current transformers depend on the operating conditions (normal load or short circuit). Under normal operating conditions the errors are low, contrary to the errors under fault conditions, when they reach the composite values.
- Harmonic distortion, f_{sn} : As it was mentioned above, the phasor estimator is able to calculate all the harmonic components of the input signal. Thus, when desired (i.e. differential protection of power transformers), an additional factor is taken into account, which corresponds to the distortion of the currents due to the harmonic content.

The above factors are included in the expression, which defines the restraint current, as it is shown in the equation below:

$$I_{Res} = I_{Diff>} + \sum e_{sync} + \sum |I_n| \cdot f_{sn} \cdot e_{CT} \quad (4-11)$$

The above results in the following pick – up characteristic, which consists of a straight line, corresponding to the pick – up constant threshold, and the 45° line:

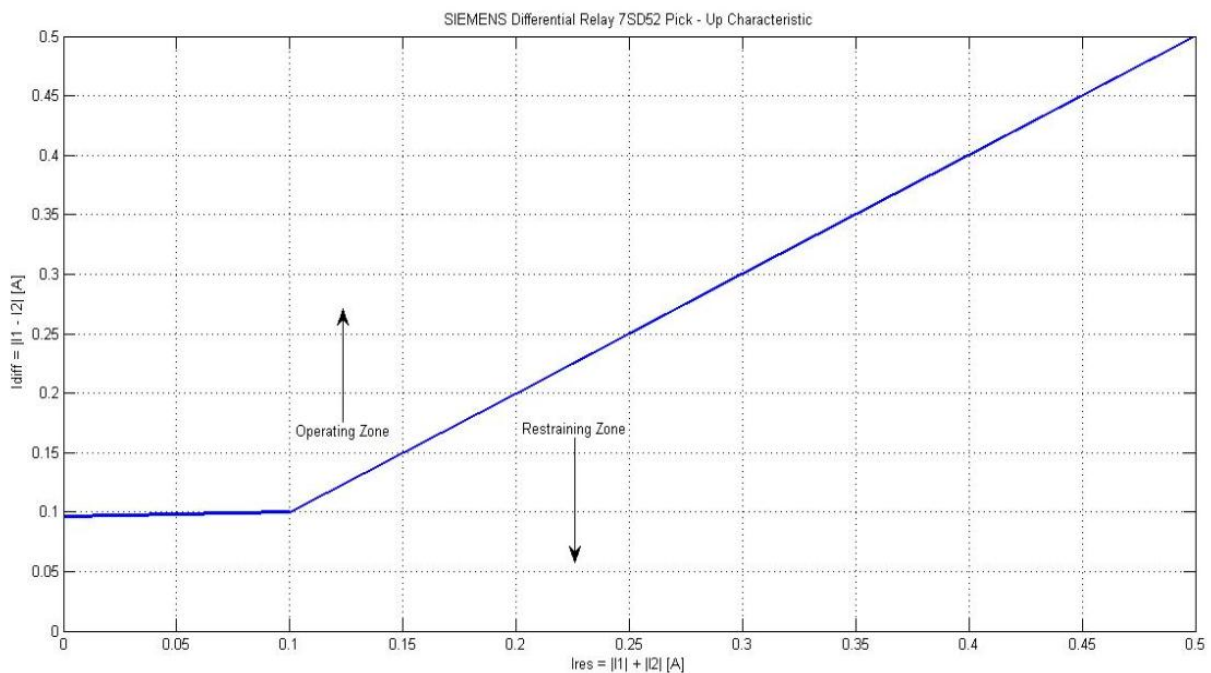


Figure 4-7. Adaptive pick – up characteristic of the SIEMENS differential relay 7SD52

4.4.1 SIEMENS Differential Relay Model in ATP – EMTP

Using the “Models” programming language [28], the algorithm of the differential protection was developed based on the logic diagram of the SIEMENS differential relay 7SD52 [29], which is shown in Figure 4-8. In this diagram, the following terms are defined:

- Diff>>L_i: Highest pick – up threshold for instantaneous tripping, defined for each phase
- Diff>L_i: Differential current calculated for each phase separately
- I>Release: Restrain current, as defined in equation (4-11)
- T-Delay I-Diff>: Time delay after a fault is detected
- T3I0 1Phase: Time delay or blocking signal after a single phase fault is detected in an isolated or resonant – earthed network
- Diff. Gen. TRIP: General tripping signal, value 1 corresponds to internal fault, value 0 corresponds to normal operation of the protected zone
- Diff TRIP 1p L_i: Tripping signal for phase and earth faults, with phase i being involved
- Diff TRIP L123: Tripping signal for three - phase faults
- Diff TRIP 1pole: Tripping signal for single phase faults (one pole of the CB opens)
- Diff TRIP 3pole: Tripping signal for two – phase or three – phase faults (all the three poles of the CB open)

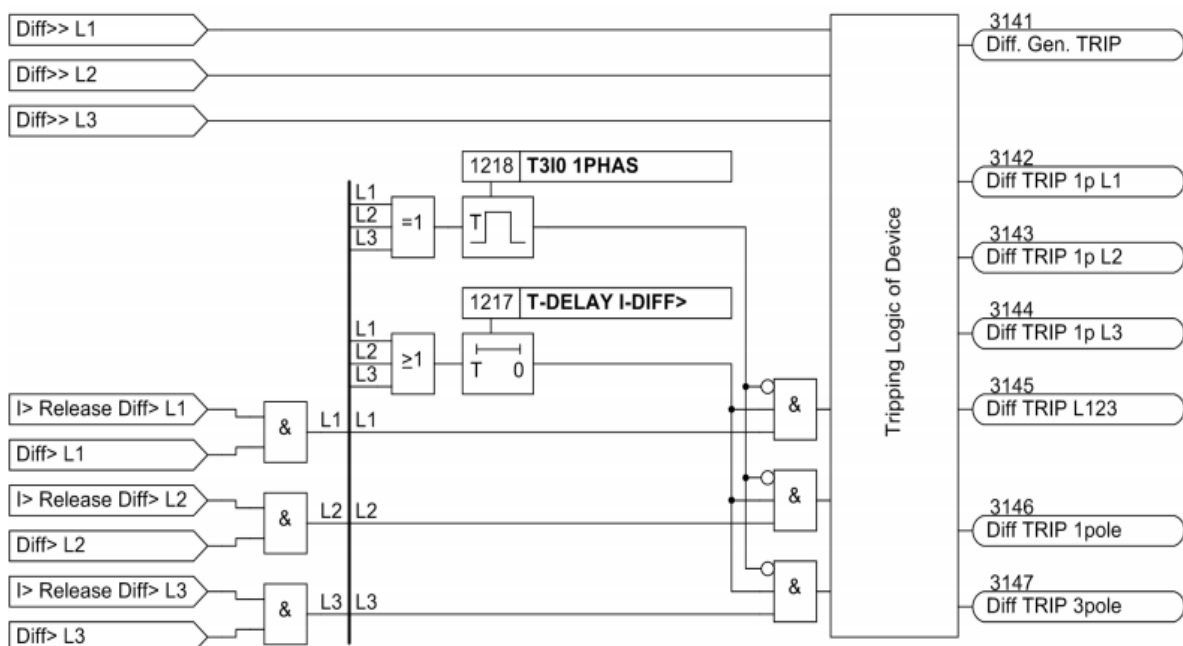


Figure 4-8. Tripping logic of the SIEMENS differential relay 7SD52

Firstly, a comparison takes place between the calculated differential and restraint currents for each phase independently. In case of an internal fault, where $I_{Diff} > I_{res}$, the comparison results in a “True” signal (=1) in the output of the “AND” block, otherwise a “False” signal (=0) is generated. These signals are delayed (T-Delay I-Diff>), if desired by the user, while a delay is introduced, if only a single phase fault takes place within the protected area. The latter is desired in an isolated or resonant – earthed network, and if the time delay is set equal to ∞ , then the delay is translated into a generated blocking signal. At the same time, the differential current is compared to the highest pick – up setting for clearing the internal fault instantaneously.

It has to be noticed, that these currents refer to the phasor components, as calculated by the DFT. More precisely, the phase currents flowing in the secondary side of the protection CTs belong to the

time domain, when measured by ATP – EMTP. Nonetheless, the developed DFT algorithm of the relay model extracts the phasors of the currents in terms of magnitude and phase, which lie on the frequency domain. Thus, the differential and restraint currents for each phase are based on the phasors, as computed by the DFT.

However, a few assumptions were taken into account for building up the relay algorithm in ATP – EMTP. More precisely, the restraint current is calculated at each time step according to the equation (4-11), with no signal delays occurring in the communication channels ($\sum e_{sync} = 0$). Moreover, for the line/cable differential protection, only the fundamental frequency component is extracted from the DFT. Thus, the harmonic distortion factor, f_{sn} , is set equal to unity, while the composite error of the CTs, $\epsilon_c = 5\%$, is set in the equation. Also, the developed algorithm does not take into account any extra multiplication factor for the increase of the restraint current under CTs saturation conditions, since the logic behind this operation is classified by the manufacturer.

According to the data provided by TenneT TSO, no delays are introduced in the generated tripping signals under any fault conditions. The flowchart below shows the logic that was implemented in the model's algorithm:

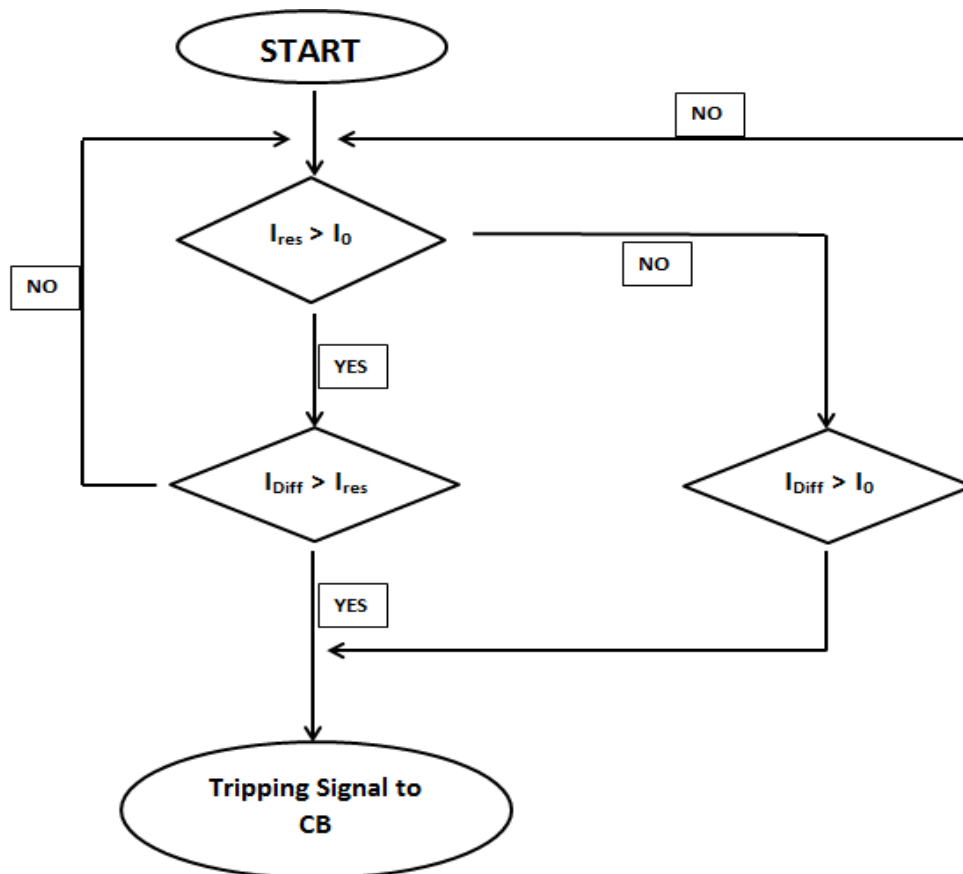


Figure 4-9. Logic flowchart of the differential relay's model implemented in ATP – EMTP

At the end of each DFT data window, the computed differential current is compared either to the restraint current or to the constant pick – up setting of the relay. The latter depends on the comparison between the restraint current and the lower threshold, I_0 , so that the correct part of the relay's pick – up characteristic is chosen. When the pick – up criteria are satisfied, a tripping signal of value equal to unity is generated and sent to the corresponding circuit breakers to clear the fault. In any other case (normal operating conditions, external faults), no tripping signals are generated, thus,

the set value is equal to zero. It has to be noticed that the procedure described above, is implemented for each phase separately.

The differential relay model was studied in a simple test circuit, as shown in Figure 4-10. The protected zone is defined by the two current probes, connected at the sending and at the remote end of the resistive area. The internal and external ground faults are simulated by connecting the main circuit to the ground through a very low fault resistance of $10^{-5} \Omega$. Time controlled phase switches are used, for simulating the ground faults at the desired instant.

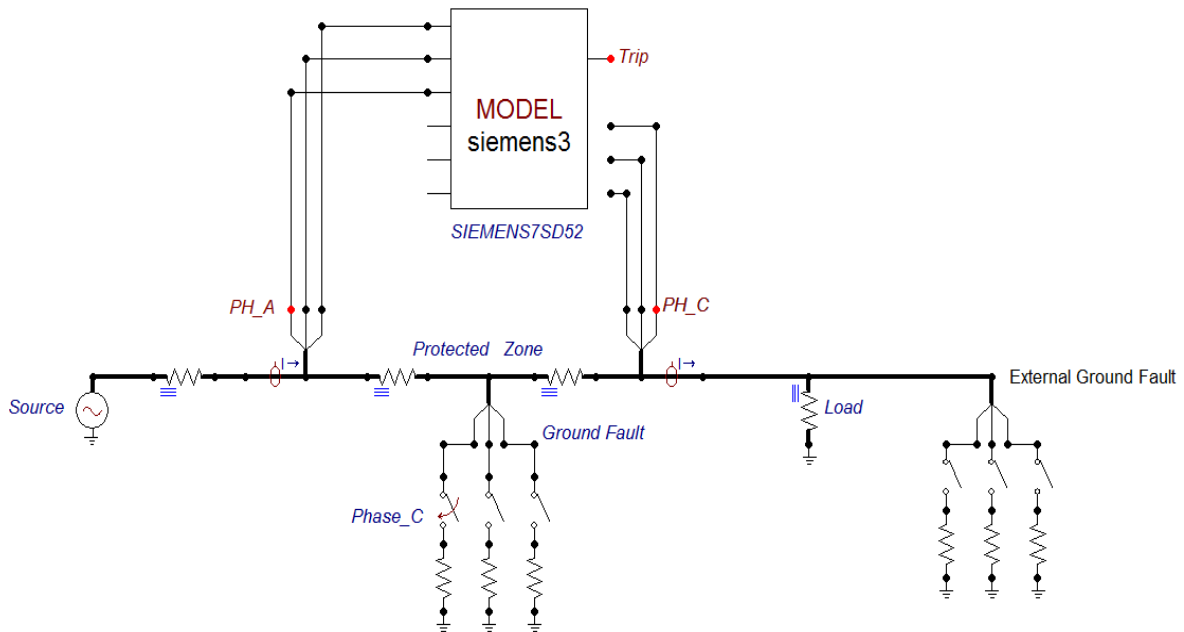


Figure 4-10. Test circuit of the differential relay model in ATP - EMTP

- Response of the Differential Relay model under normal operating conditions

Under normal operating conditions, the relay should not generate a tripping signal, since the trajectory of the differential current do not enter the tripping area of the pick – up characteristic. Thus, the “TRIP” signal generated at the output of the model should have a value equal to zero, as it is shown in the figure below.

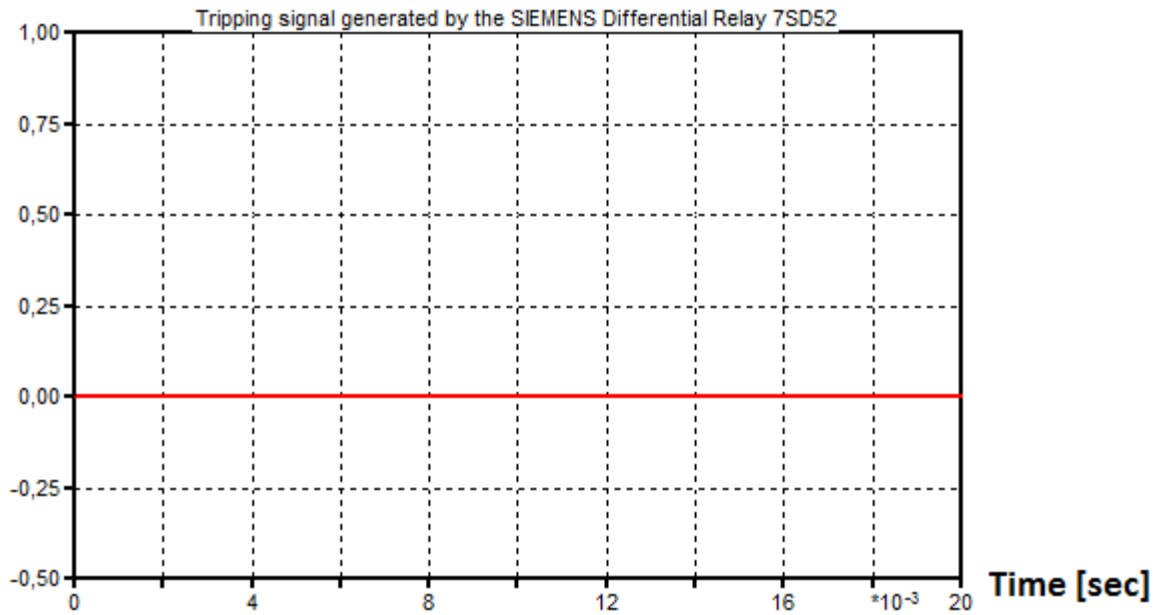


Figure 4-11. Tripping signal of the differential relay under normal operating conditions

- Response of the Differential Relay model under ground fault conditions outside the protected zone

As in the previous case, the differential relay must not trip under external fault conditions. Thus, the generated tripping signal is equal to zero, before and after the occurrence of the external fault.

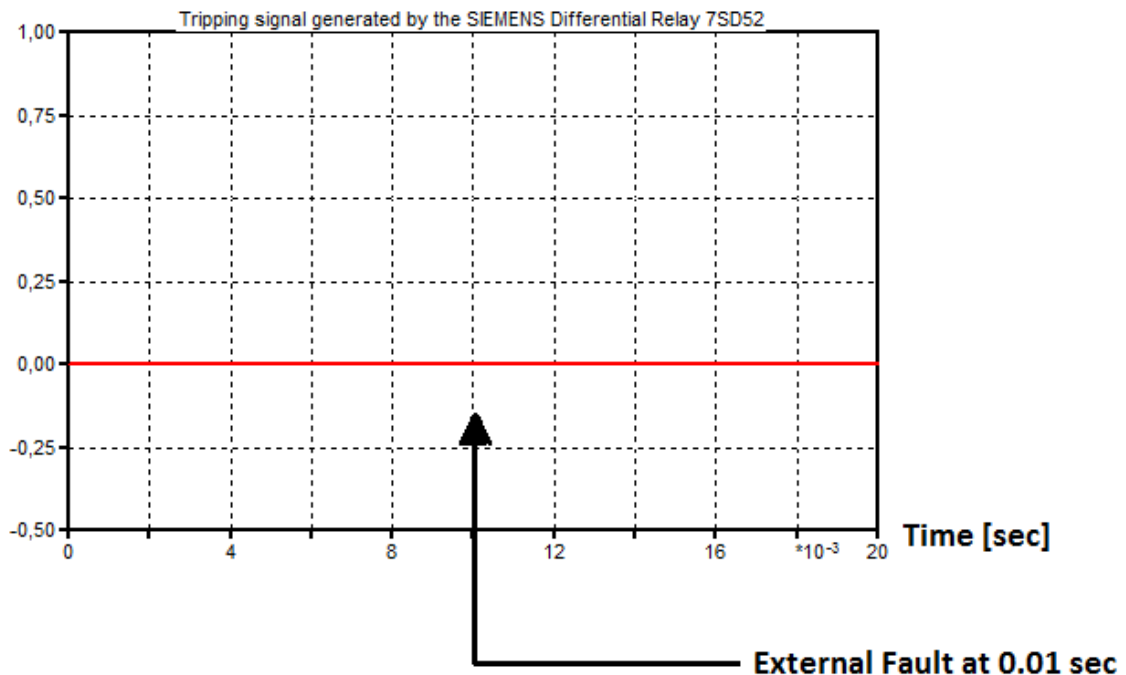


Figure 4-12. Tripping signal of the differential relay under external fault conditions

- Response of the Differential Relay under fault conditions within the protected zone

When an internal fault (ground or phase) takes place, the differential relay should respond within a short time of 30-50 ms, by taking into account the transmitting time of the communication channels. Faster tripping times (< 15 ms) can be reached, when fast current comparison techniques are adopted by the protective relay. A ground fault at phase C is simulated at the time point $t = 0.01$ sec

and a tripping signal for phase C is generated 5 ms after the occurrence of the fault. For the phases A and B no tripping signal are generated, since they are not involved in the fault.

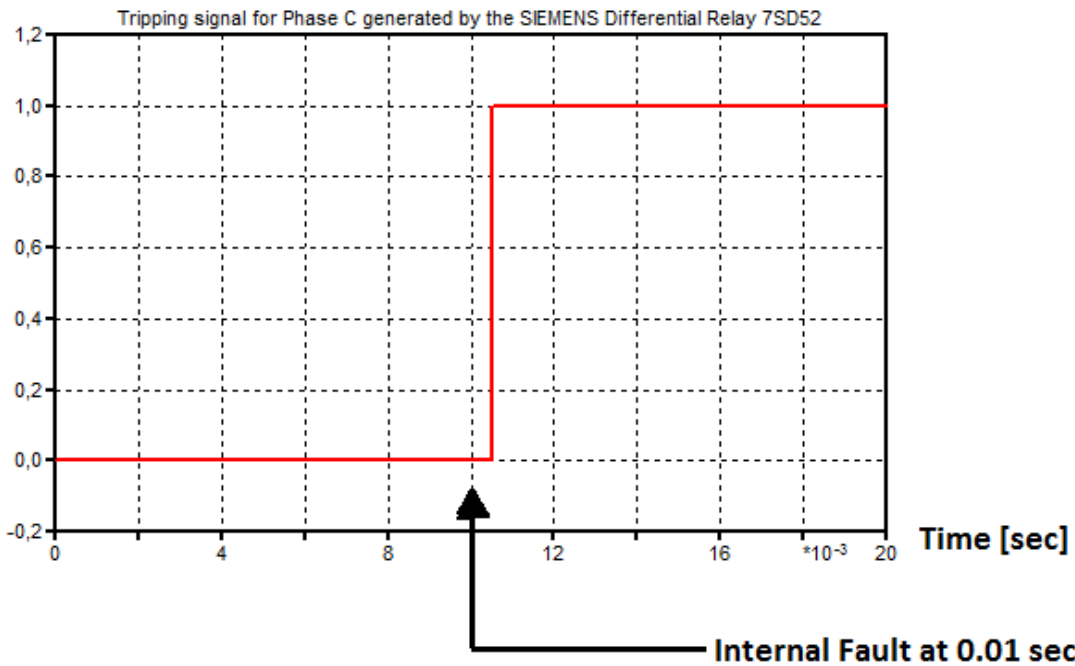


Figure 4-13. Tripping signal generated for the faulty phase under internal fault conditions

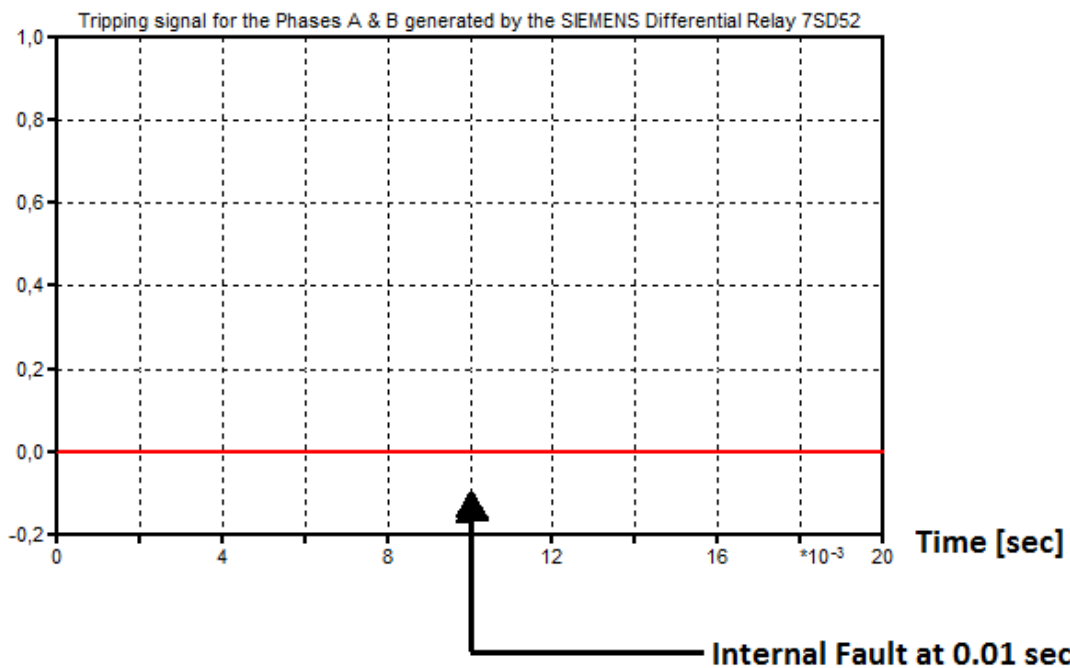


Figure 4-14. Tripping signals generated for the healthy phases under internal fault conditions

Differential Protection of the Randstad 380 kV South Ring HV Cable – Results and Conclusions

5.1 Introduction

The south ring of the Randstad 380 kV project constitutes a small part of the Dutch transmission system, thus, appropriate protection systems are required for its normal, consistent and uninterrupted operation. TenneT TSO implements specific schemes to provide the adequate protection needed in the mixed configuration between the Maasvlakte and Westerlee substations. The main protection scheme consists of an appropriate and selective combination between differential and distance protection relays, while differential protection is independently implemented at the High Voltage underground cable.

In this chapter, the general protection scheme that is applied between the MVL – WTL substations is presented, while the calculated settings of the SIEMENS differential relays 7SD52 are discussed too. Moreover, the configuration's complete model in ATP – EMTF is studied together with the simulation results, regarding the operation of the differential relay model.

5.2 Protection Scheme of the Maasvlakte – Calandkanaal – Hoek van Holland – Westerlee 380 kV mixed connection

5.2.1 Description of the General Protection Scheme

As it was mentioned above, TenneT TSO implements both differential and distance protection schemes in the studied configuration. The general scheme is shown in Figure 5-1, where the four – point current DP system and the distance relays are presented too, as it is mentioned in [30]. More specifically, two differential relays are installed in each substation (Δ_1 and Δ_2 in MVL and Δ_3 and Δ_4 in WTL), while differential relays Δ_7 - Δ_8 and Δ_9 - Δ_{10} protect the HV cable and the series reactor respectively. The directional distance relays Z_5 and Z_6 cover three setting zones and they are communicating with the differential relays installed in the two substations.

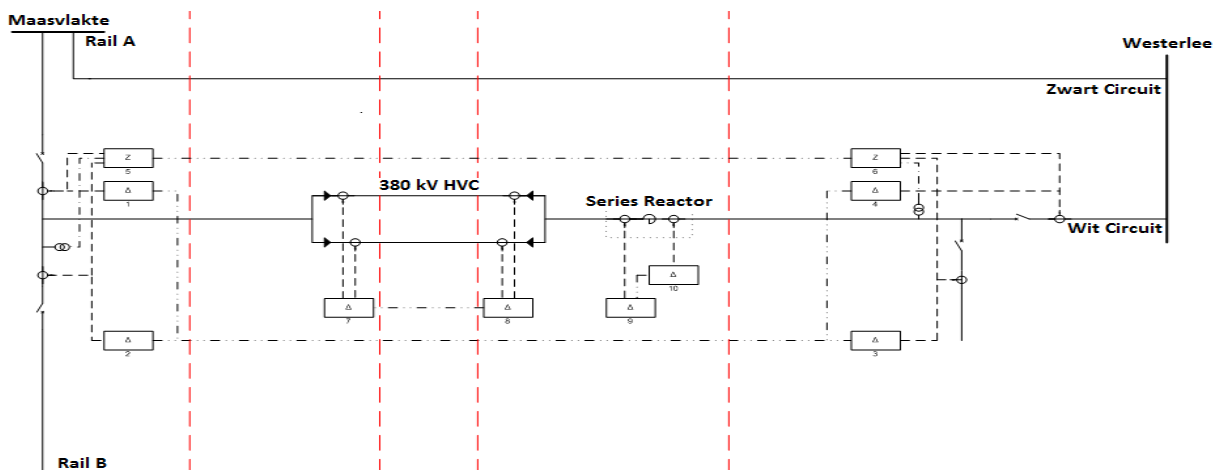


Figure 5-1. Basic protection scheme of the MVL – WTL mixed transmission connection

- *HV underground cable*: Two differential relays constitute the main protection of the 380 kV cable part and they will operate only in the case of an internal fault. When a fault within the cable occurs, the operation of the distance relays and the auto – reclosure function of the circuit breakers are blocked. The latter is based on the fact that cable faults are permanent, contrary to the faults on overhead lines, which in most cases are temporary [31].

- *Series reactor*: Differential protection is used for this equipment too, consisting of two protective relays. However, a back – up protection system is installed together with the DP, where a Buchholz relay monitors the oil – filled reactor. As in the case of the HV cable, under internal fault conditions the differential protection will generate and send tripping signals at the circuit breakers, while blocking signals will be sent to the distance relays.

- *Distance protection relays*: Three main zones are defined in the mixed connection, which are distinguished with appropriate time grading. Also, an extended zone is defined with instantaneous tripping setting for back – up reasons.

5.2.2 Settings of the SIEMENS Differential Relays 7SD52

As it was mentioned in paragraph 4.4 of Chapter 4, the pick – up threshold and the CTs errors should be defined in the differential relay algorithm, so that the latter can generate the correct adaptive pick – up characteristic. For that reason, series of calculations are needed according to [32]:

- *Pick – up threshold, I_0* : For this setting, either the charging current of the whole transmission line or the nominal current of the transmission connection have to be taken into account. More precisely, the charging current, I_c , may cause false operation of the differential protection under normal operating conditions of the protected zone, thus, a specific pick – up value is needed to overcome a possible maloperation of the DP. This value is set to three times the value of I_c . The charging current depends on the nominal frequency, the operating voltage, the total length and capacitance of the line and it is given by (5-1):

$$I_c = 3.63 \cdot 10^{-6} \cdot U_{nom} \cdot f_{nom} \cdot C \cdot l \quad (5-1)$$

where U_{nom} : the nominal voltage of the system [kV]
 f_{nom} : the nominal frequency of the system [Hz]
 C : the capacitance of the line [nF/km]
 l : the total line length [km]

In the case of the mixed transmission connection, the charging current is equal to:

$$I_c = 3.63 \cdot 10^{-6} \cdot 380 \cdot 50 \cdot 36.78 \cdot 21.52 = 54.59 \text{ A}$$

However, the calculated charging current has to be higher than the 15-20% of the nominal current flowing in the system, otherwise it is ignored and a higher pick – up current is used as the setting value. The nominal current of the system is 1925 A \gg ($3 \times 54.59 = 163.77$ A), thus, it will define the pick – up setting of the differential relays. According to the technical report of TenneT TSO, the 20% portion of I_{nom} is selected as the pick – up threshold, which has to be translated into the secondary side of the CTs:

$$I_0 = \frac{0.2 \cdot 1925}{4000} = 0.09625 \text{ A}$$

At the same time, the CT errors are introduced for defining the pick – up characteristic of the differential relays. As it was mentioned in paragraph 4.4.1 of Chapter 4, the constant composite error, 5%, of the current transformers is taken into account and used in the equation (4-11). It has to be noticed, that no delay times are introduced in the generated signals and the tripping operation occurs instantaneously.

The double – circuited mixed configuration between the Maasvlakte and Westerlee substations, consisting of the generating sources, the overhead transmission lines, the HV underground cable, the series reactors, the protection CTs and the protective relays, was modeled through ATP – EMTP and it is shown in the figure below. An overhead transmission line, “MVL – WTL 1” is responsible for the connection part between the Maasvlakte substation and the sending end of the HV cable, while the second OHL, “MVL – WTL 2”, transmits power between the series reactor and the Westerlee substation. The HV cable is divided into two parts connected in series, so that an internal ground or phase fault can be simulated. The differential protection implemented for the cable and its protected zone are defined by the current transformers installed at the sending and remote ends of the cable. However, it has to be noticed that for simplicity and redundancy reasons, DP was studied only in the “White” circuit of the configuration, since the same scheme is used in the “Black” one. The faults are simulated by connecting the main circuit to the ground through resistances of very low value, whereas time controlled switches define the instant of the fault occurrence. Likewise, the fault outside the protected zone is selected to be a ground fault on the overhead transmission line “MVL – WTL 2”, which is divided into two parts, as in the case of the cable. The two – end scheme of the protective relays is represented by the “SIEMENS – 3Phase” model, which receives as inputs the secondary phase currents of the two CTs, in order to execute the current differential algorithm.

Various internal and external faults are simulated and the response of the DP scheme is studied. More specifically, single phase to ground fault, two – phase fault and three – phase to ground fault within the cable are simulated, while an external three – phase fault is simulated too. The results are presented and discussed in the following paragraphs.

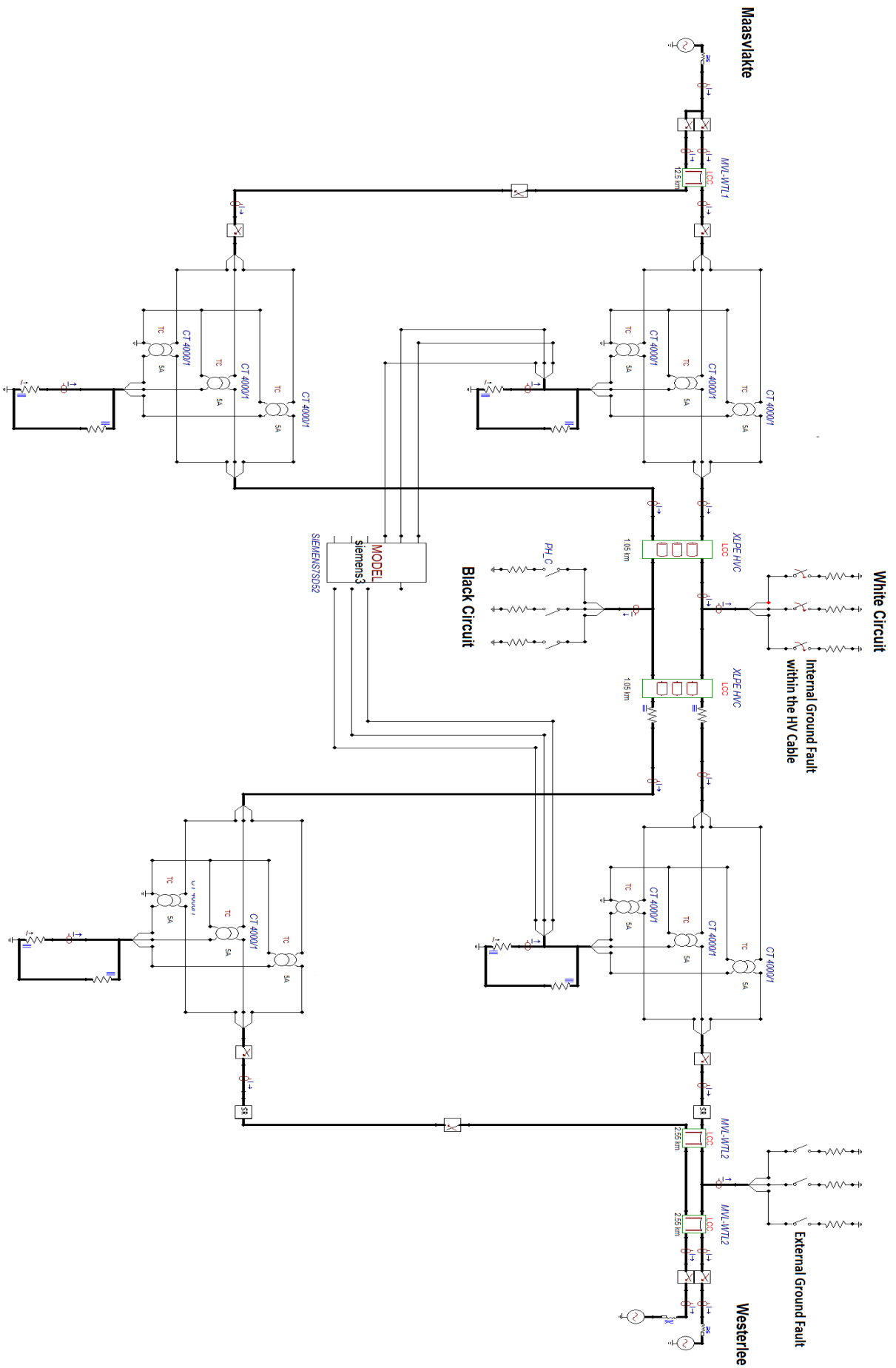


Figure 5-2. Schematic diagram of the mixed transmission configuration in ATP - EMTP

5.3 Fault Simulation Results

5.3.1 Single Phase to Ground Fault within the Protected Zone

At first, an internal single phase to ground fault is simulated in phase A of the HV underground cable. Phase A is connected to the ground through a resistance of $1 \mu\Omega$ and the fault occurs 50 ms after the simulation starts. Figure 5.3 shows the phase currents flowing at the primary side of the two CTs installed at the sending and remote end of the cable respectively, while Figure 5.4 shows the fault current to the ground. It can be noticed that when the fault occurs, an unsymmetrical current with DC offset appears in the faulty phase, while the currents of the healthy phases are not affected. Furthermore, the peak value of the initial fault current to ground is approximately 64 kA, a value close to the one calculated at the report of KEMA Consulting, as mentioned in paragraph 2.5 of Chapter 2.

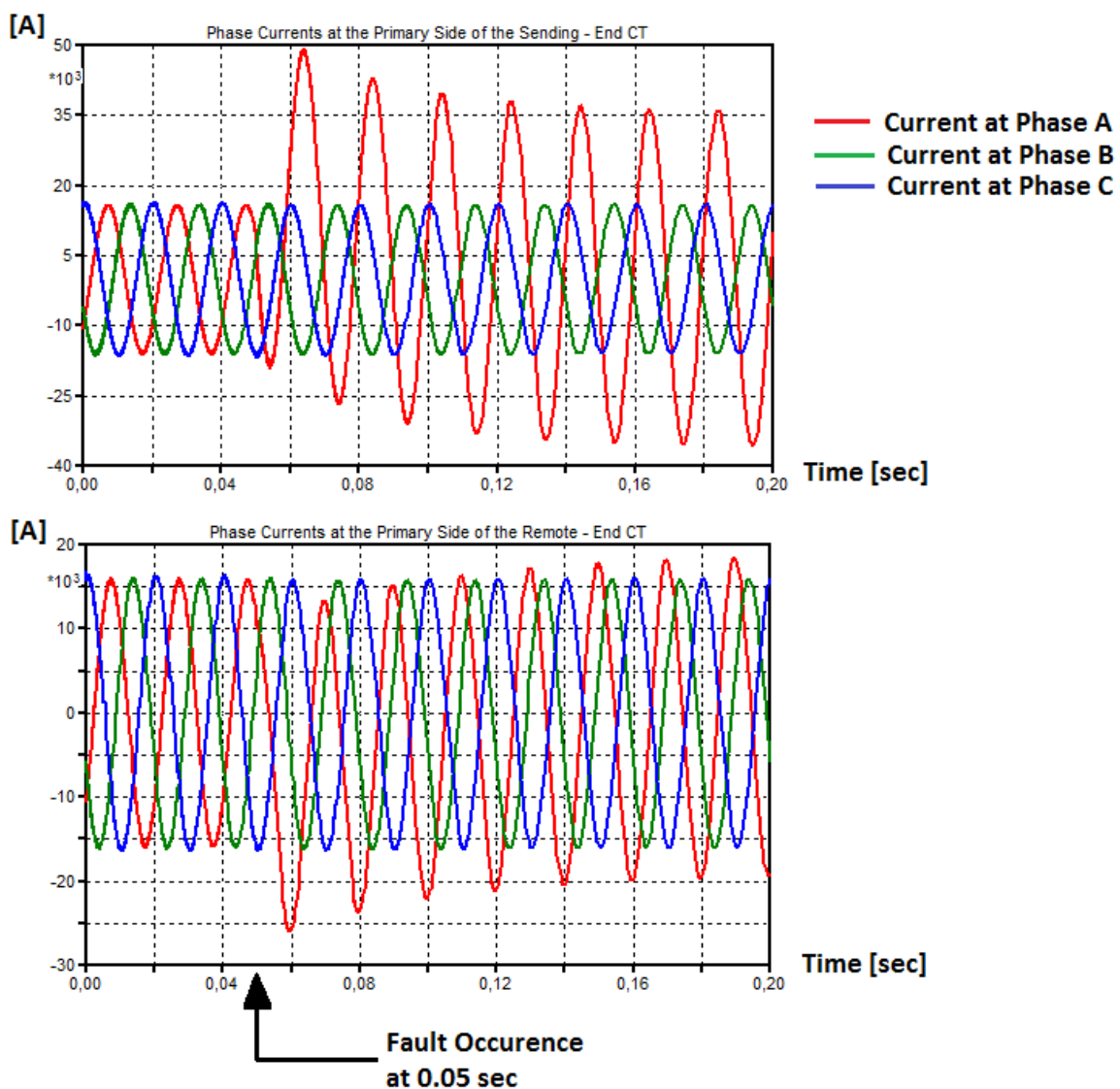


Figure 5-3. Phase currents flowing at the primary side of the protection CTs

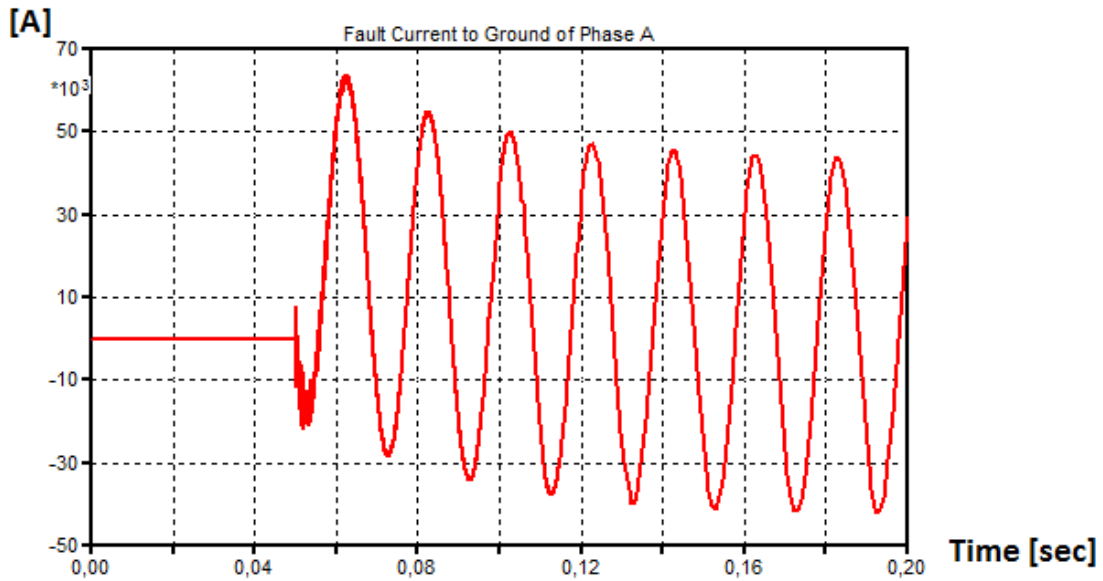


Figure 5-4. Current to ground of the cable’s faulty phase A

The secondary currents of the protection CTs are of importance for the SIEMENS 7SD52 differential relays, since the comparison of the estimated phasors computed by the relay’s algorithm, is based on the instantaneous values of these currents. In the figures below, the CTs secondary phase currents are shown, as well as a comparative figure between the secondary faulty currents is listed too.

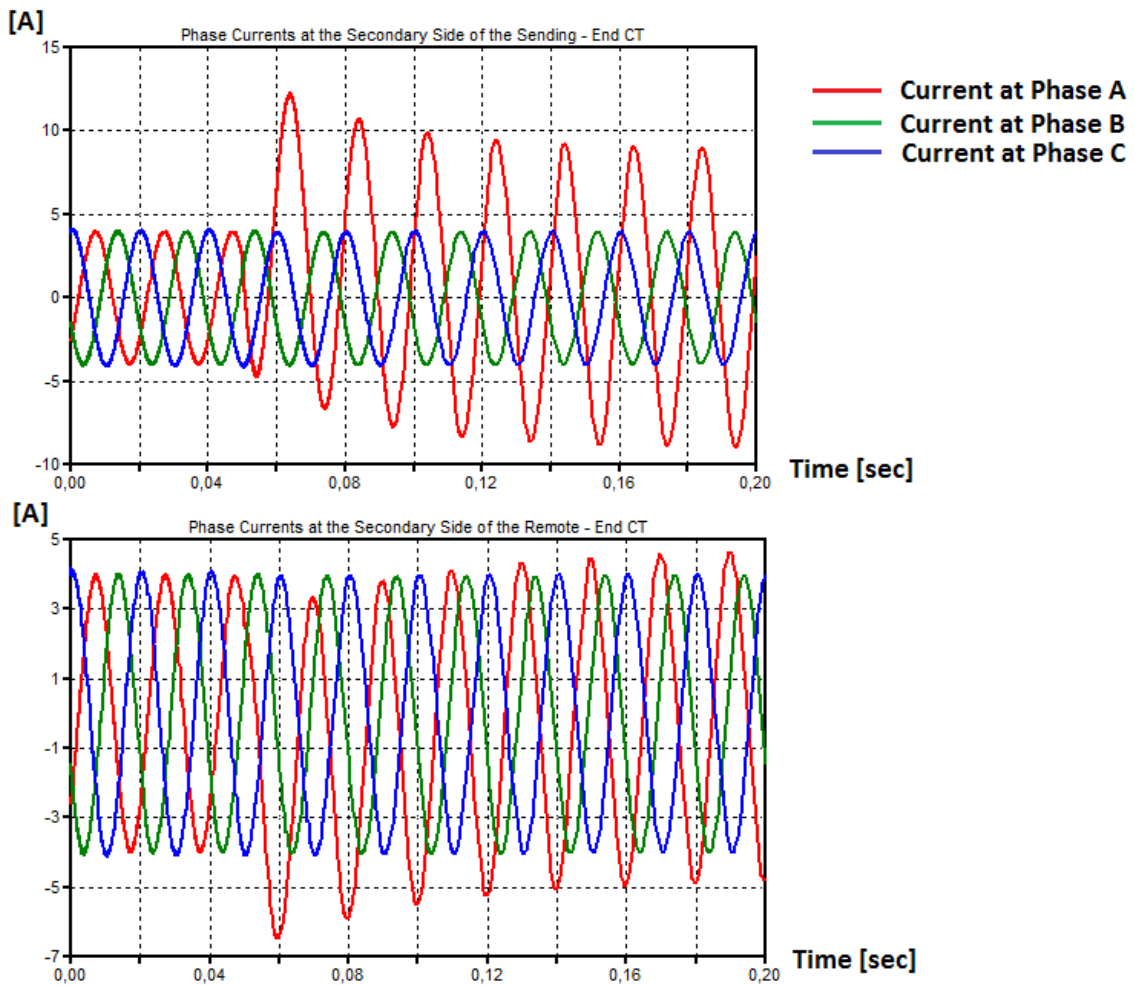


Figure 5-5. Phase currents flowing at the secondary side of the protection CTs

From the comparative Figure 5-6, the difference between the secondary fault currents of Phase A at the sending and remote end of the HV cable can be noticed. Additionally, since the healthy phases remain unaffected by the fault conditions, the secondary currents of Phase B at both ends of the cable will be equal – this is also the case for the secondary currents of Phase C-. Besides, the CTs primary currents are correctly transformed to the secondary side with the nominal ratio of 4000/1. For instance, the primary current of Phase A at the sending end has a peak value of approximately 49 kA, while the secondary current has a peak value of 12.25 A ($12.25 \times 4000 = 49$ kA).

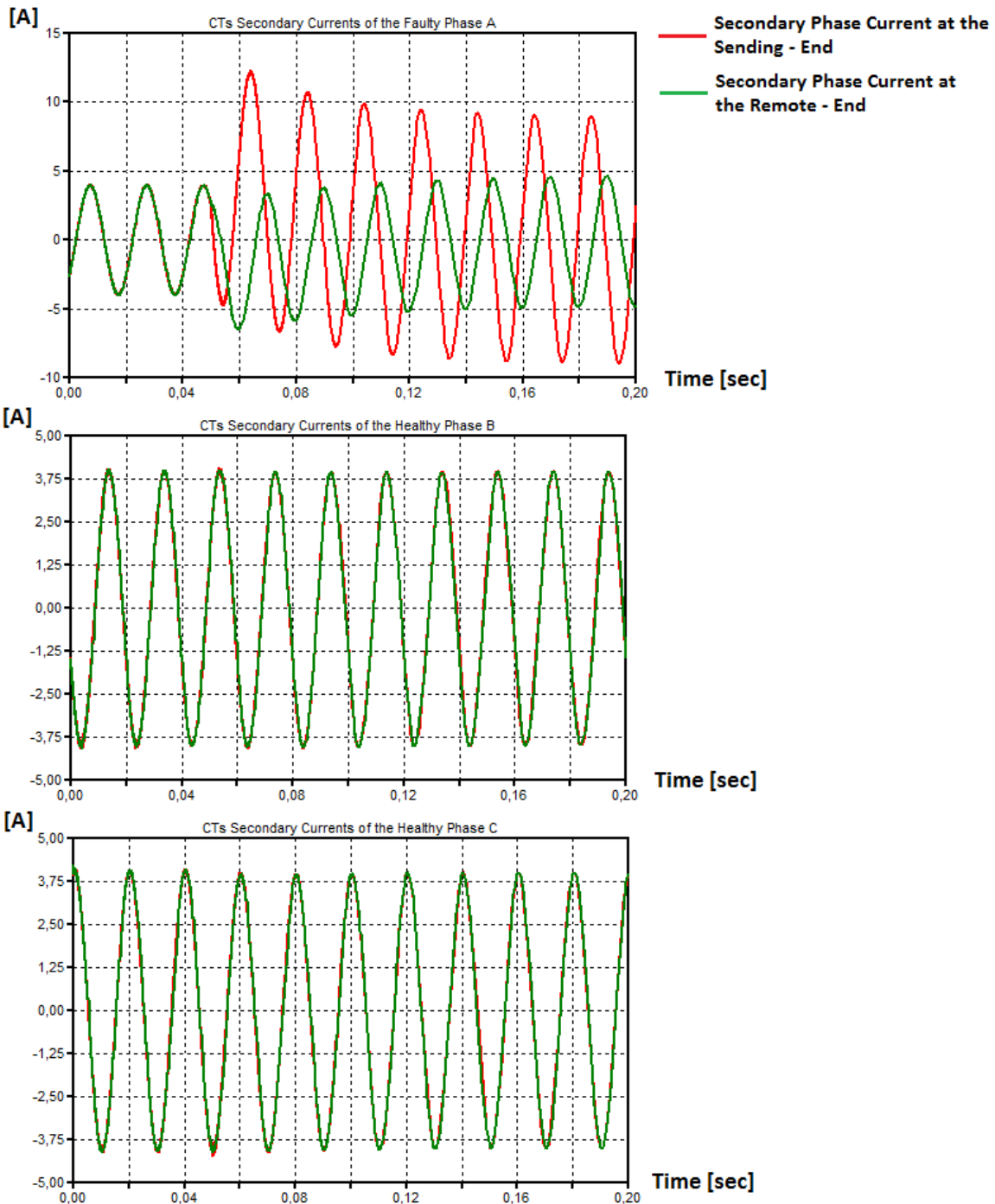


Figure 5-6. Comparison between the CTs secondary phase currents at the sending and remote end of the HV cable respectively

The following figures show the differential and restraint currents for each phase, as they are computed through the algorithm of the differential protection relay. When the internal single phase to ground fault occurs, the differential current of the faulty Phase A starts building up to exceed the restraint current. On the other hand, this is not the case for the healthy phases B and C, where the differential current has a lower value than the value of the restraint current at each computation time step.

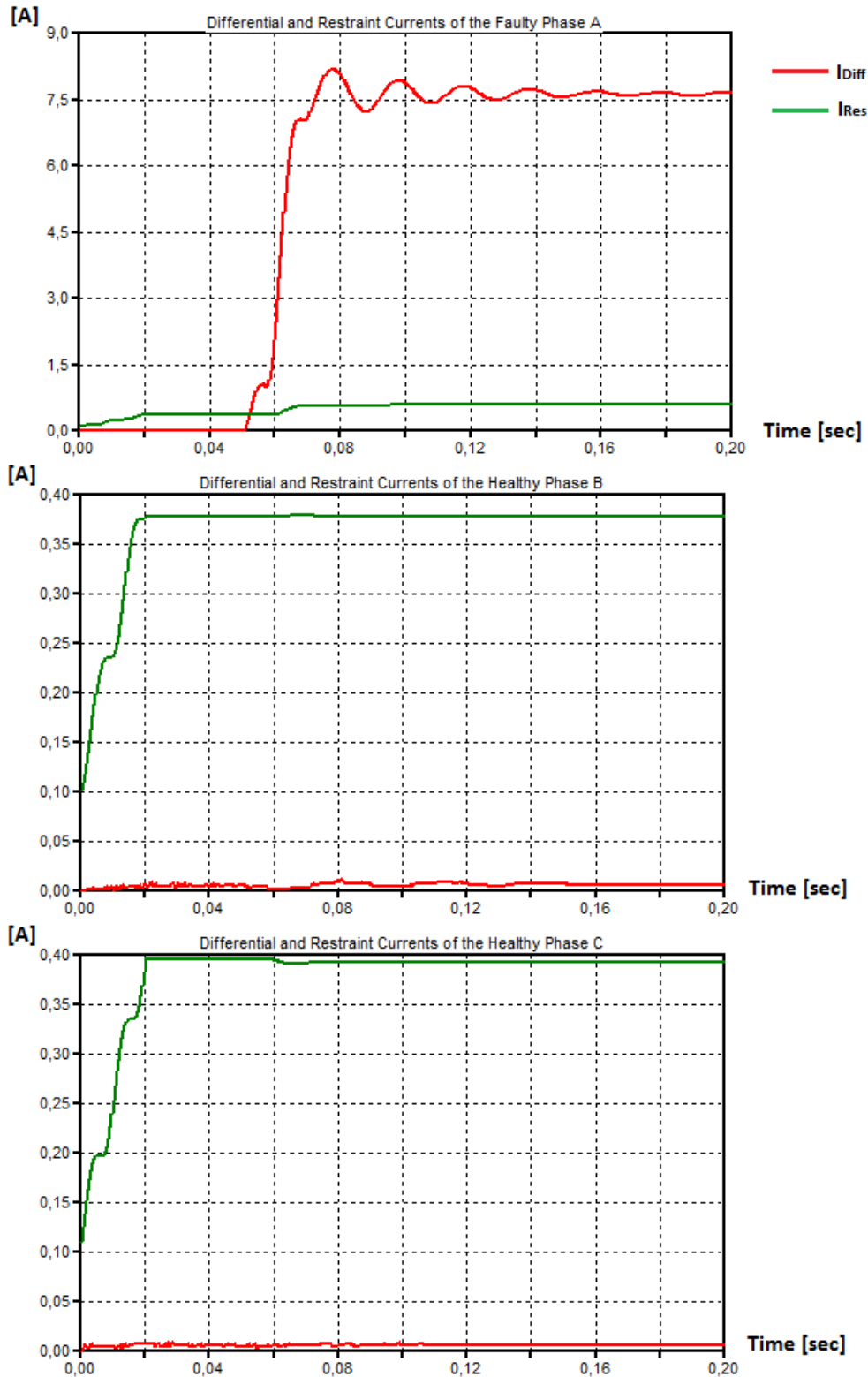


Figure 5-7. I_{Diff} and I_{Res} as calculated for each phase

Since only the differential current of Phase A exceeds the computed restraint current, the trajectory of these two currents is of importance. The latter will confirm whether the differential relay operates correctly or not. More specifically, Figure 5-8 shows the trajectory formed by the calculated values of I_{Diff} and I_{Res} at each time step of the relay algorithm, compared to the pick – up characteristic of the SIEMENS 7SD52 relay. The trajectory enters the tripping zone of the characteristic, causing the protective relay to generate a tripping signal for Phase A, as it is shown below.

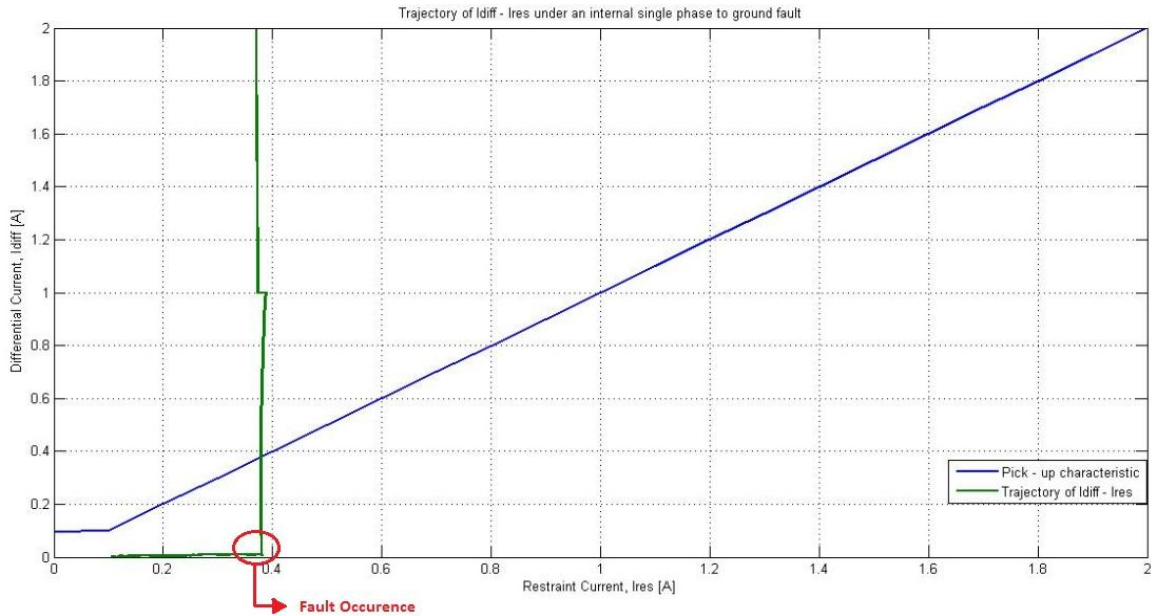


Figure 5-8. $I_{Diff} - I_{Res}$ trajectory and adaptive pick – up characteristic of the differential relay

In the case that the single phase fault is cleared after a certain period of time, a different trajectory will be generated, as it is shown in Figure 5-9. More precisely, the single phase to ground fault occurs at $t = 0.05$ sec and it is cleared after 50 ms. Thus, the trajectory will first enter the tripping zone of the characteristic, but the differential current will start decreasing as soon as the fault is detected and cleared. As a result, the trajectory will return at the restraint zone, which is defined as the part underneath the pick – up characteristic. (The red arrows show the build – up path that is followed by the trajectory)

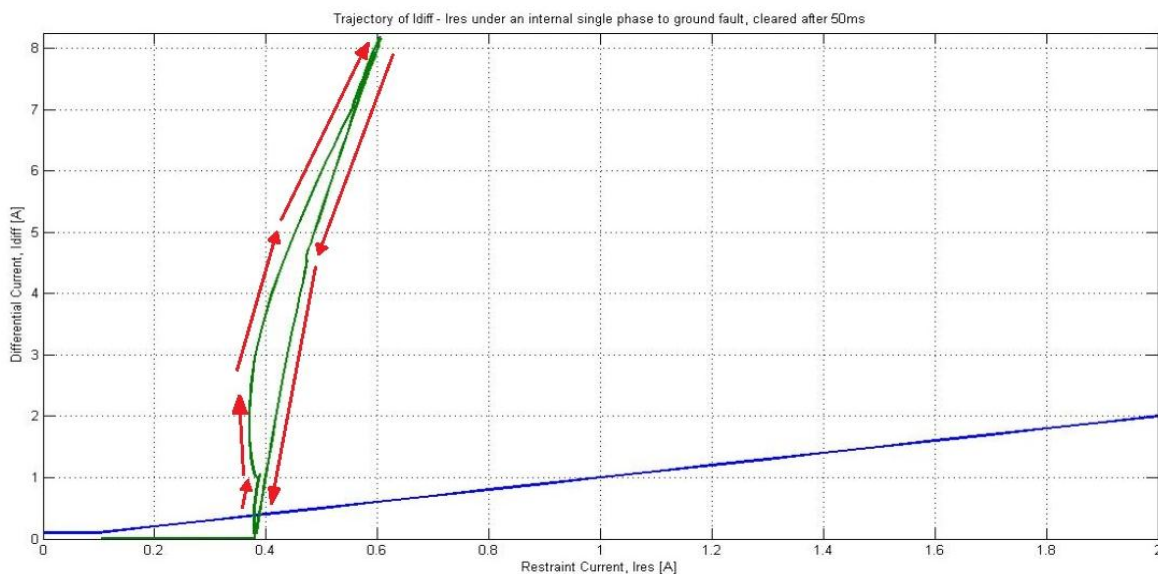


Figure 5-9. $I_{Diff} - I_{Res}$ trajectory and adaptive pick – up characteristic of the differential relay, when the single phase to ground fault is cleared

As it was mentioned above, when the differential protection detects the internal fault conditions, tripping signals are generated and sent to the corresponding circuit breakers, which are responsible for the switching operation. Thus, when the differential current calculated for Phase A exceeds the restraint current, a tripping signal equal to unity is generated for the faulty phase at the output of the relay algorithm. For the two healthy phases, B and C, the value of the corresponding signals remains zero. However, since the single phase fault occurs within the HV cable, a general signal will be generated, which will cause the opening of all the three CB poles and not only of one pole.

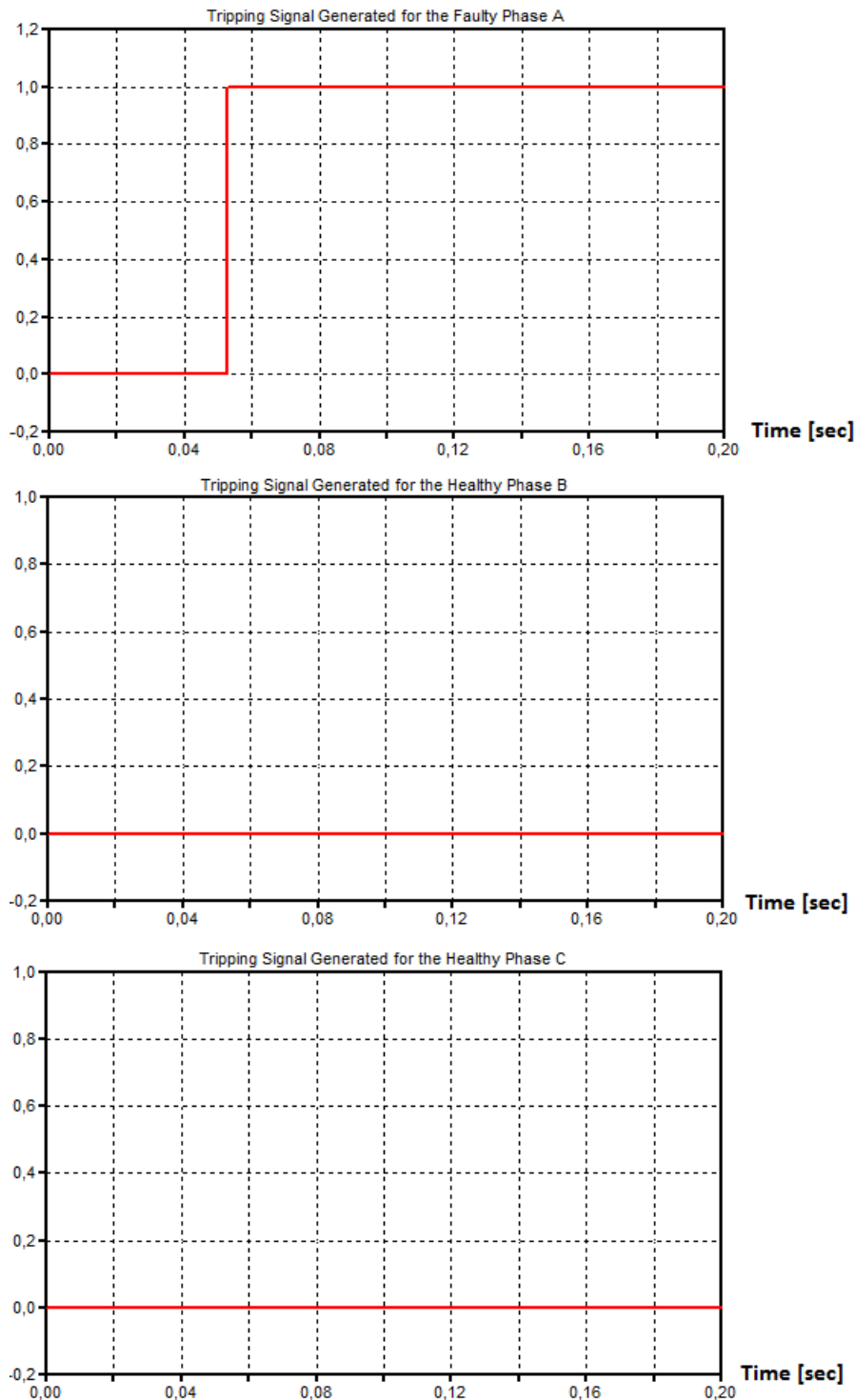


Figure 5-10. Tripping signals generated at the output of the differential relay for each phase separately

5.3.2 Two Phase Fault within the Protected Zone

The second simulation regards an internal fault between the phases A and B of the HV cable. The fault occurs at $t = 0.03$ s and it is cleared after 50 ms. The figure below shows the phase currents flowing at the primary side of the protection CTs and it is clear that unsymmetrical currents flow through the faulty phases.

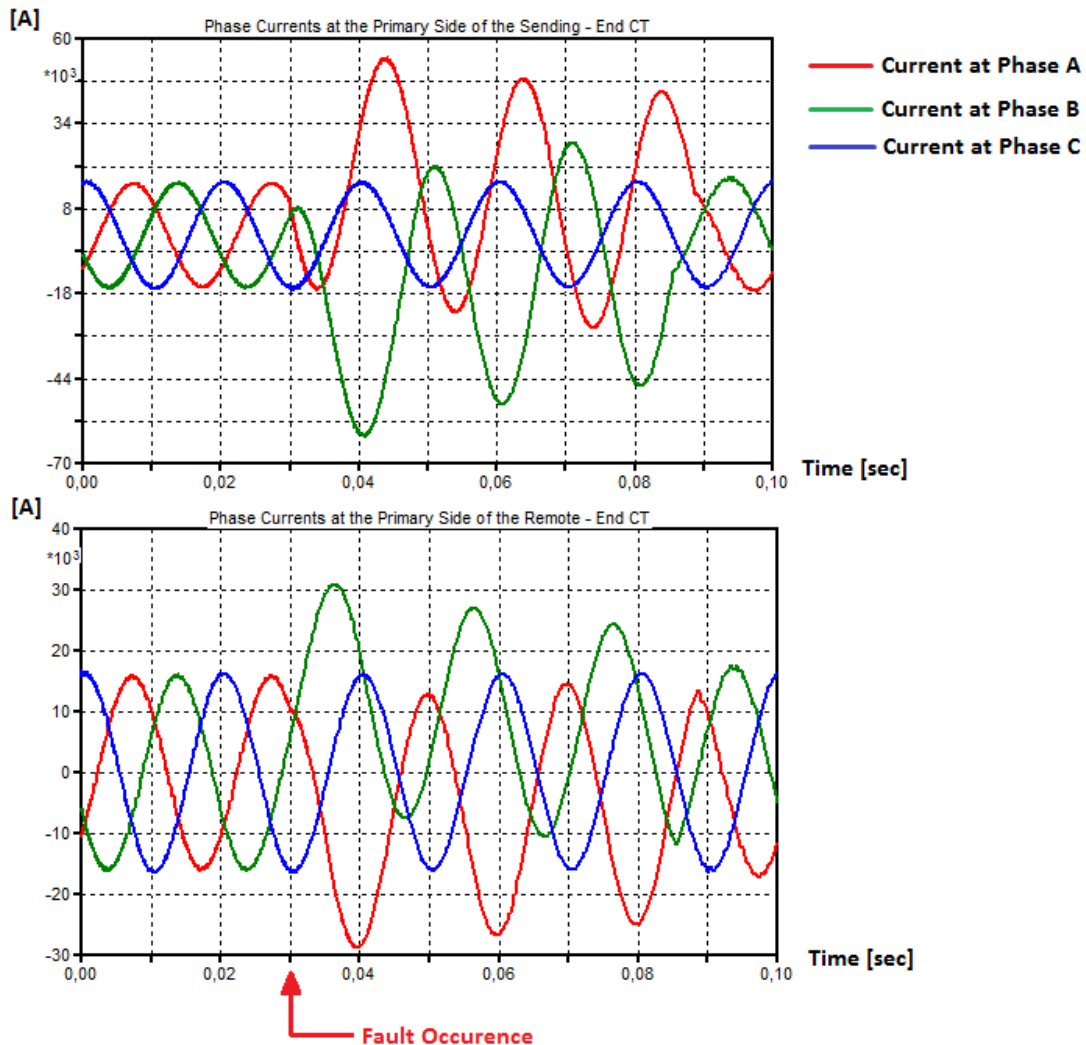


Figure 5-11. Phase currents flowing at the primary side of the protection CTs

Figure 5-12 shows the secondary currents of the protection CTs at both ends of the protected zone. Through the comparison, it can be noticed that the currents of the faulty phases significantly deviate from each other, while the currents of the healthy Phase C are approximately equal. Thus, the differential protection will detect the fault conditions and it will generate the appropriate tripping signals, as it is shown below.

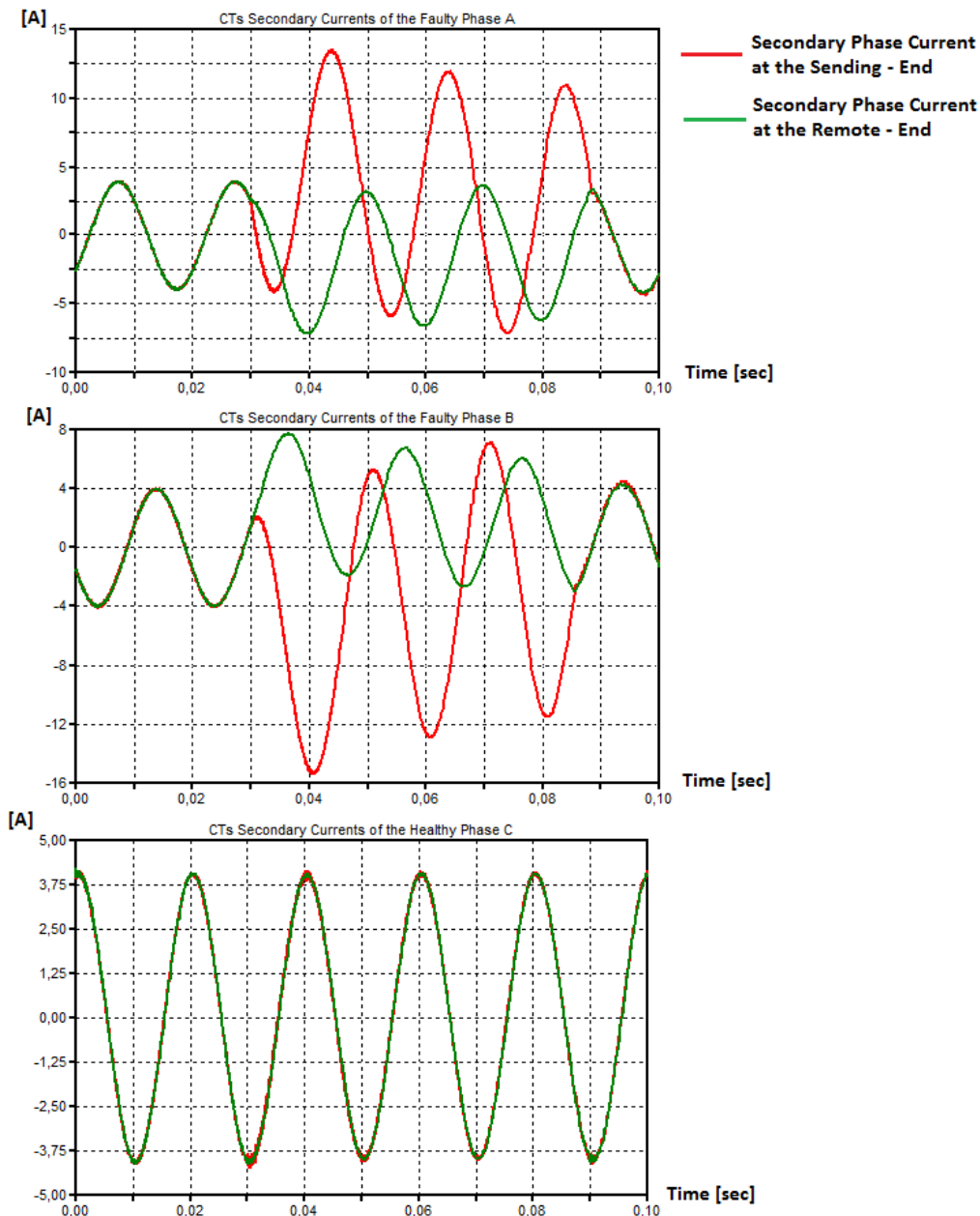


Figure 5-12. Comparison between the CTs secondary phase currents at the sending and remote end of the HV cable respectively

During the fault, the differential currents for Phases A and B will increase in magnitude and at a certain point they will exceed the value of the restraint current. This is when the protection relay detects the fault and operates. After the fault is detected and cleared, the differential currents of the faulty phases will start decreasing in terms of magnitudes, to reach a value lower than the value of the corresponding restraint currents. At that point, the trajectory of the two computed currents, I_{Diff} and I_{Res} , will enter again the restraint zone of the relay's pick – up characteristic. The above are represented in the figures below:

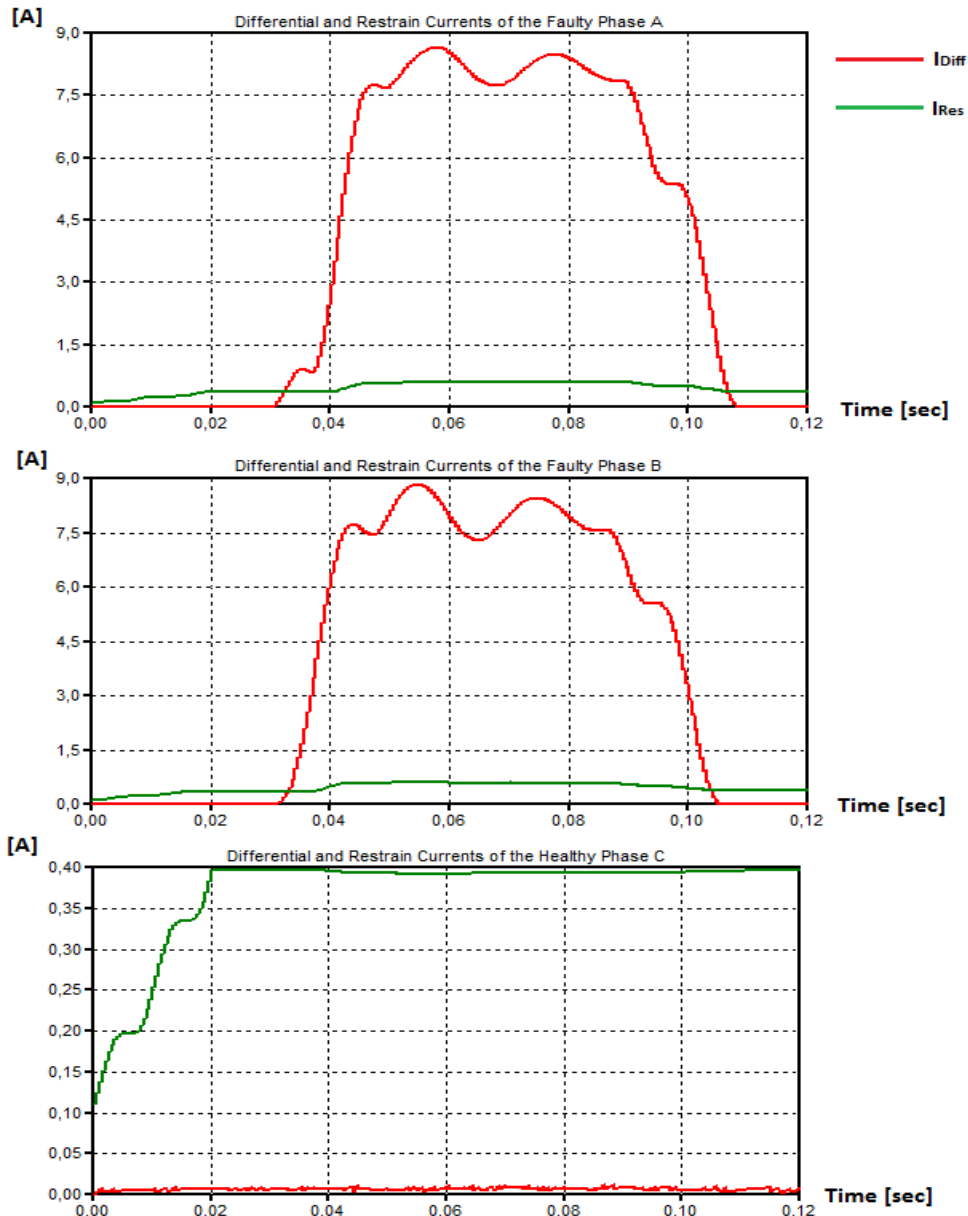


Figure 5-13. I_{Diff} and I_{Res} as calculated for each phase

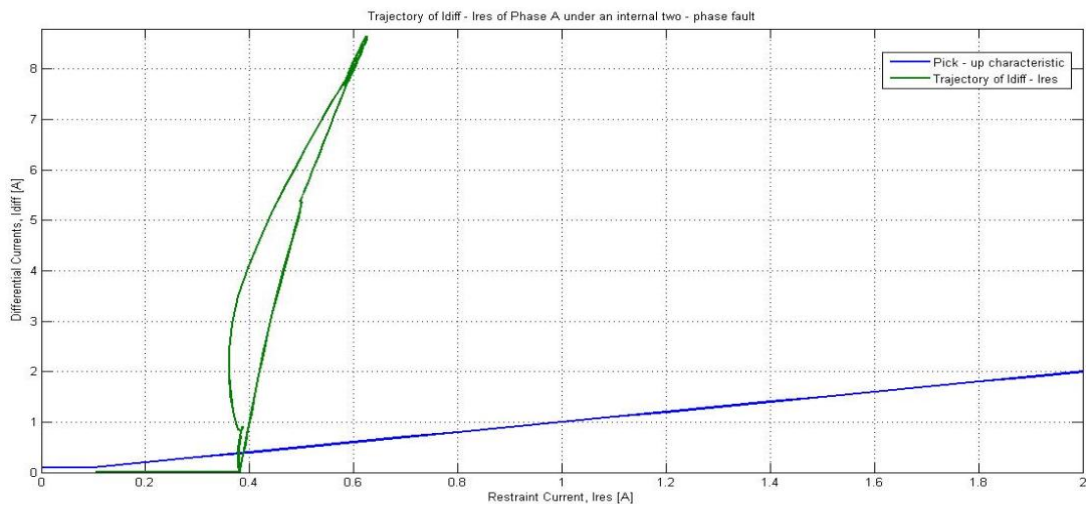


Figure 5-14. I_{Diff} - I_{Res} trajectory of faulty Phase A and adaptive pick – up characteristic of the differential relay

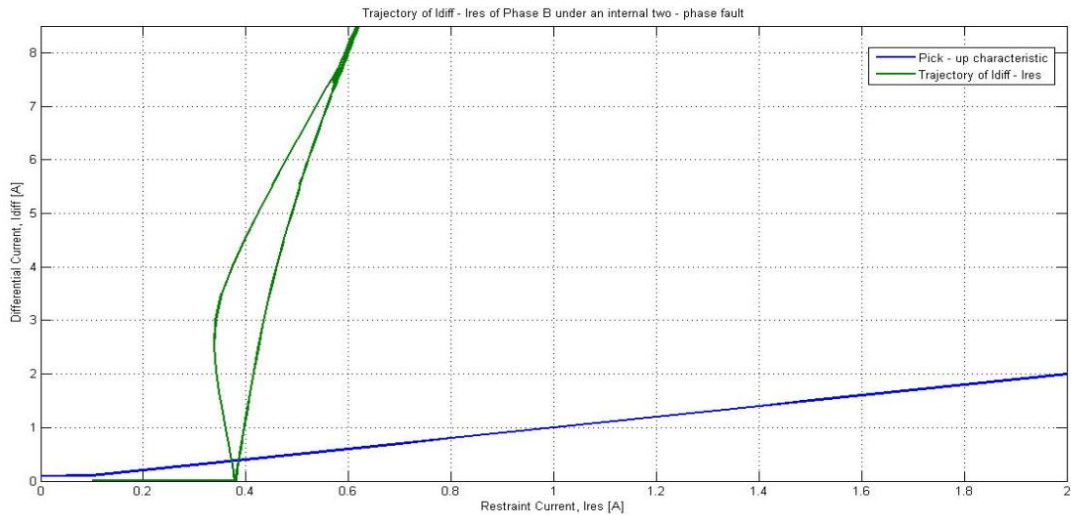


Figure 5-15. $I_{Diff} - I_{Res}$ trajectory of faulty Phase B and adaptive pick – up characteristic of the differential relay

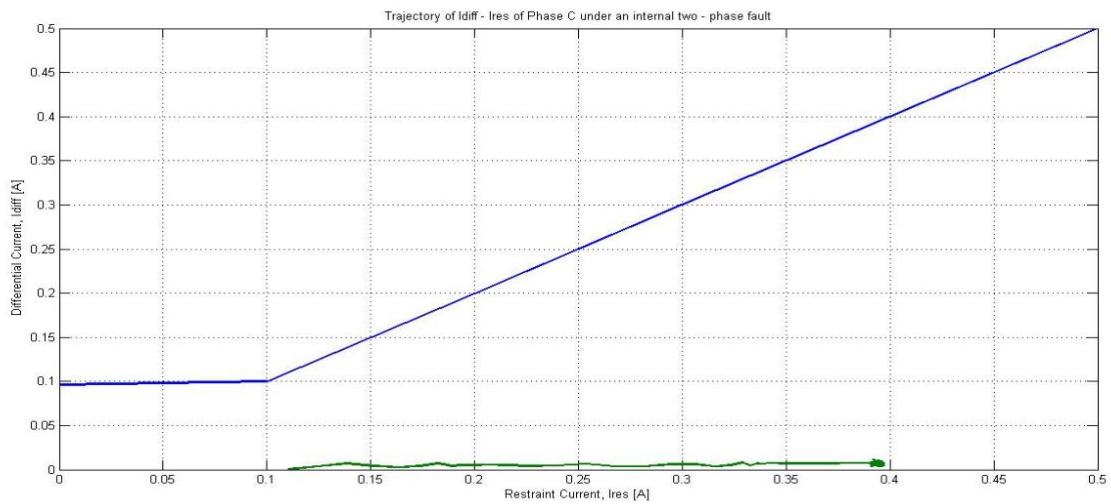


Figure 5-16. $I_{Diff} - I_{Res}$ trajectory of healthy Phase C and adaptive pick – up characteristic of the differential relay

Based on the above, the differential relay will generate and send tripping signals to the circuit breakers to switch off the poles of the faulty phases A and B, as it is shown in Figure 5-17. However, a three – pole switching action will take place, since the fault occurs within the HV cable.

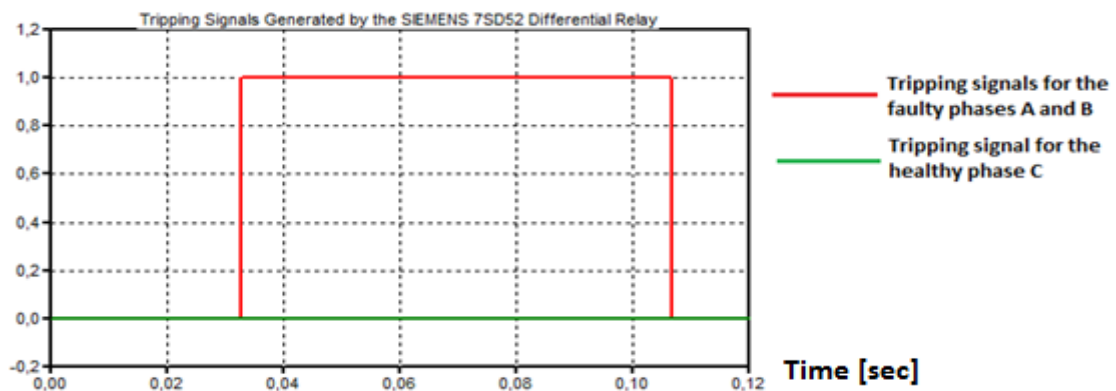


Figure 5-17. Tripping signals generated at the output of the differential relay for each phase separately

5.3.3 Three – Phase to Ground Fault within the Protected Zone

As a next step, an internal three – phase earth fault is simulated, where all the cable phases are connected to ground through resistances with value of $1 \mu\Omega$. The fault occurs at $t = 0.02$ s and it is cleared after 50 ms. The same sequence of figures follows below, where the primary and secondary currents of the two protection CTs, the differential and restraint currents calculated by the relay algorithm, the trajectory of the latter and the generated tripping signals are presented.

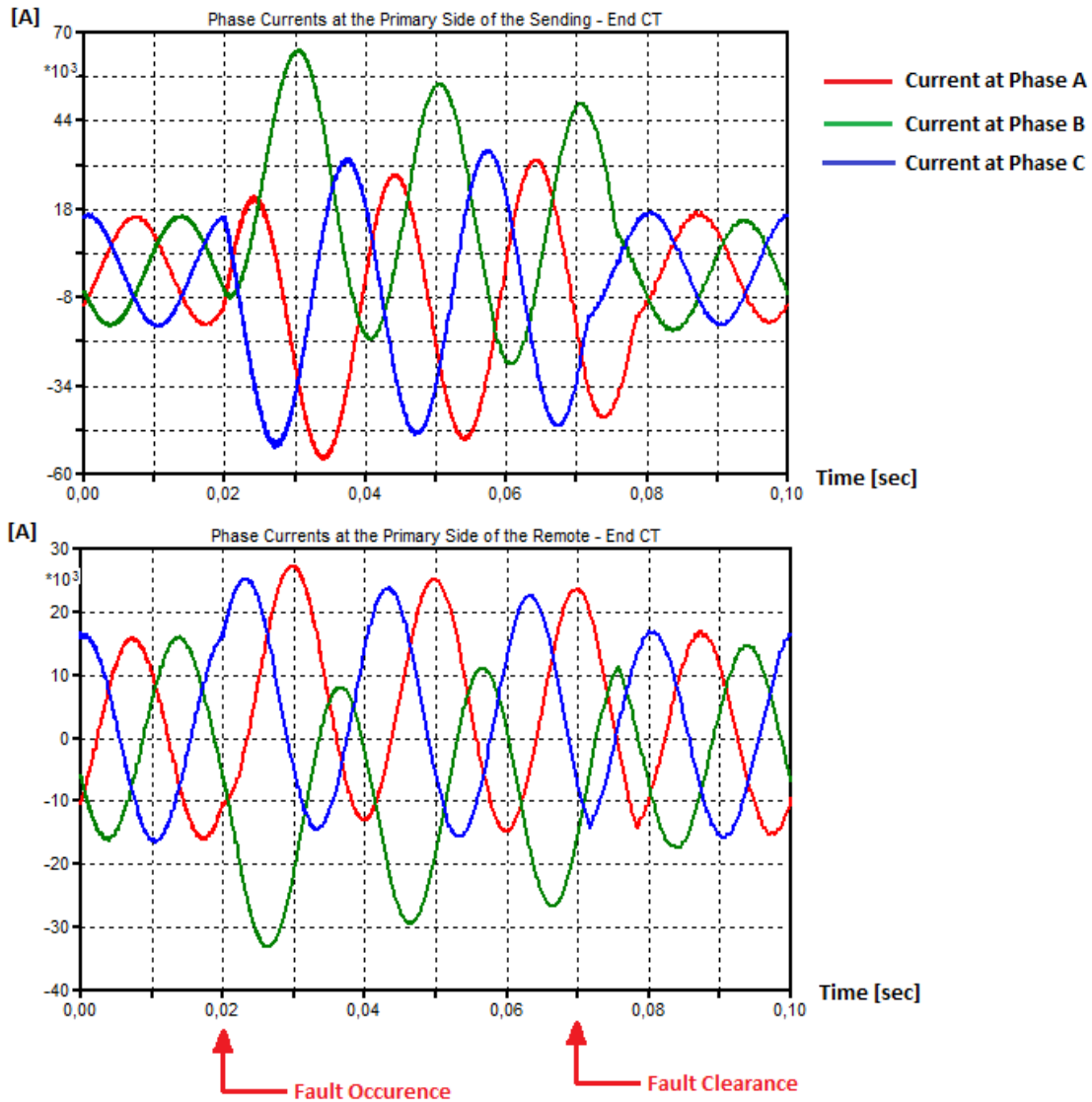


Figure 5-18. Phase currents flowing at the primary side of the protection CTs

It has to be noticed that the initial peak value of the fault current is approximately 65 kA, a value close to the one mentioned in Table 2-8 of Chapter 2. Moreover, as shown in Figure 5-19, the currents flowing at the primary side of the protection CTs are correctly transformed at the secondary winding, since no saturation occurs within the CTs.

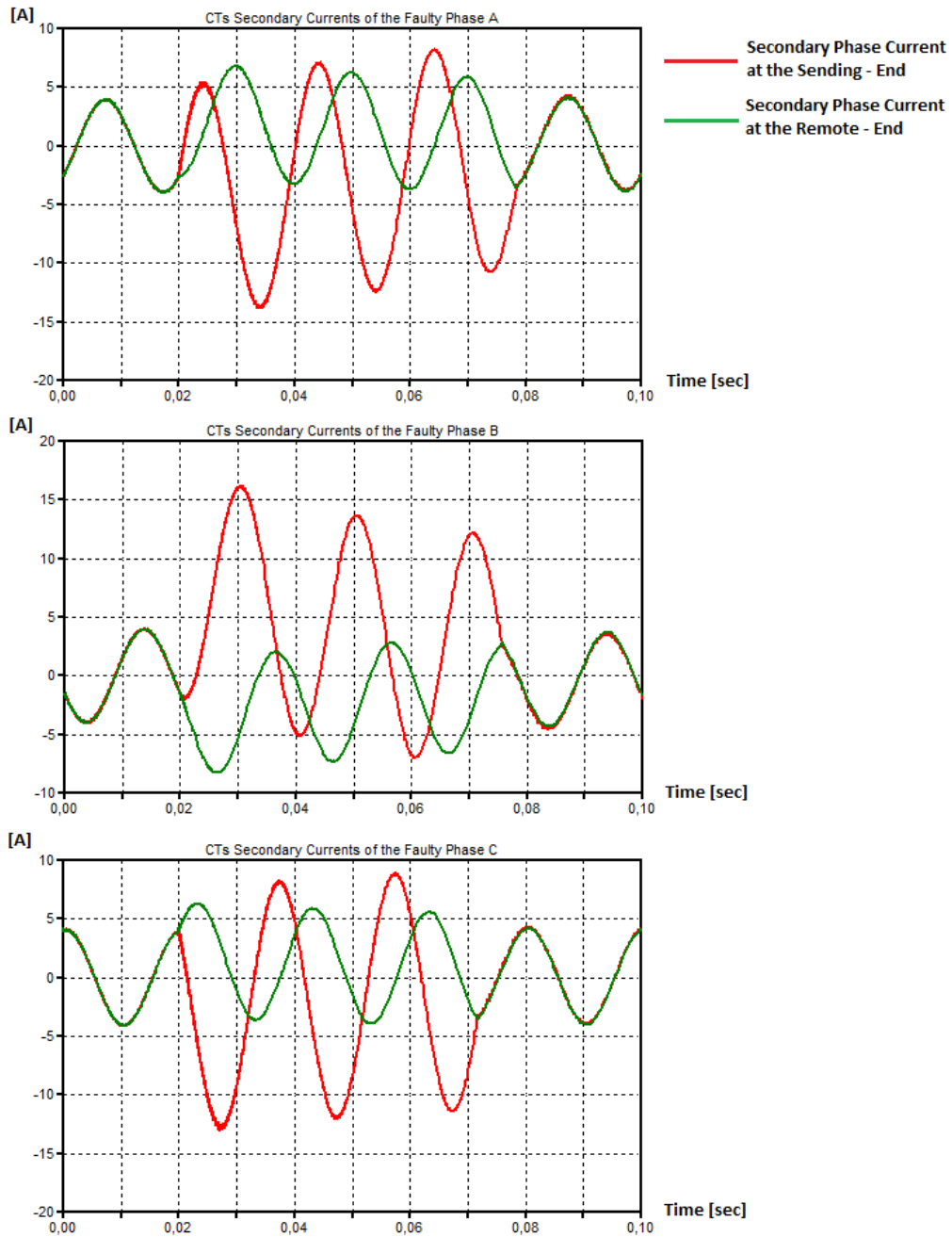
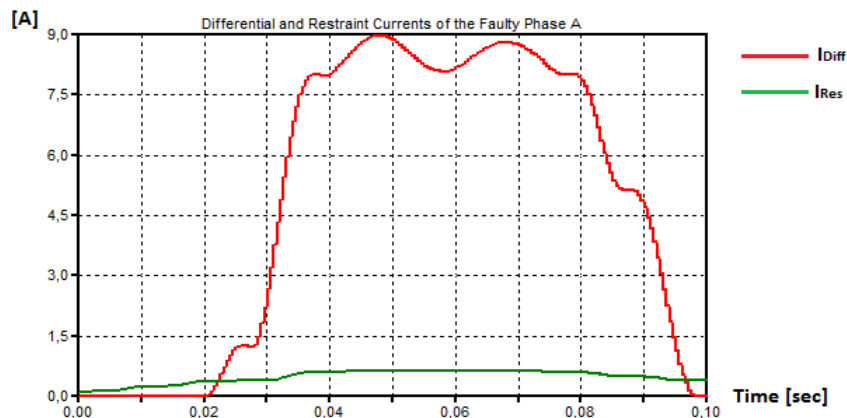


Figure 5-19. Comparison between the CTs secondary phase currents at the sending and remote end of the HV cable respectively



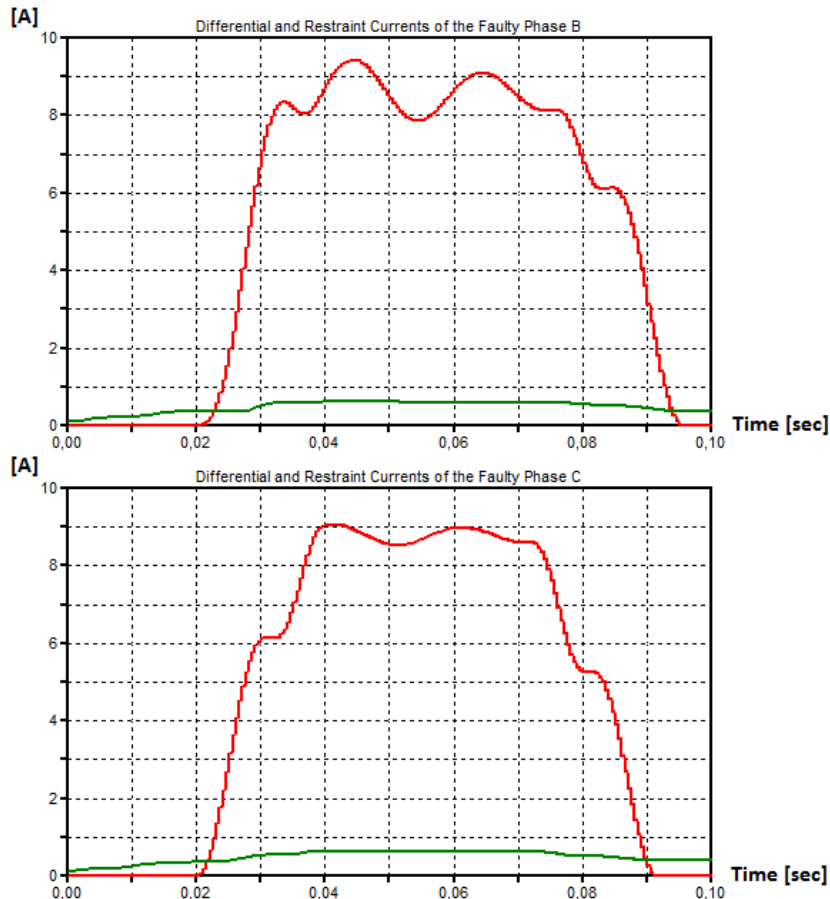


Figure 5-20. I_{Diff} and I_{Res} as calculated for each phase

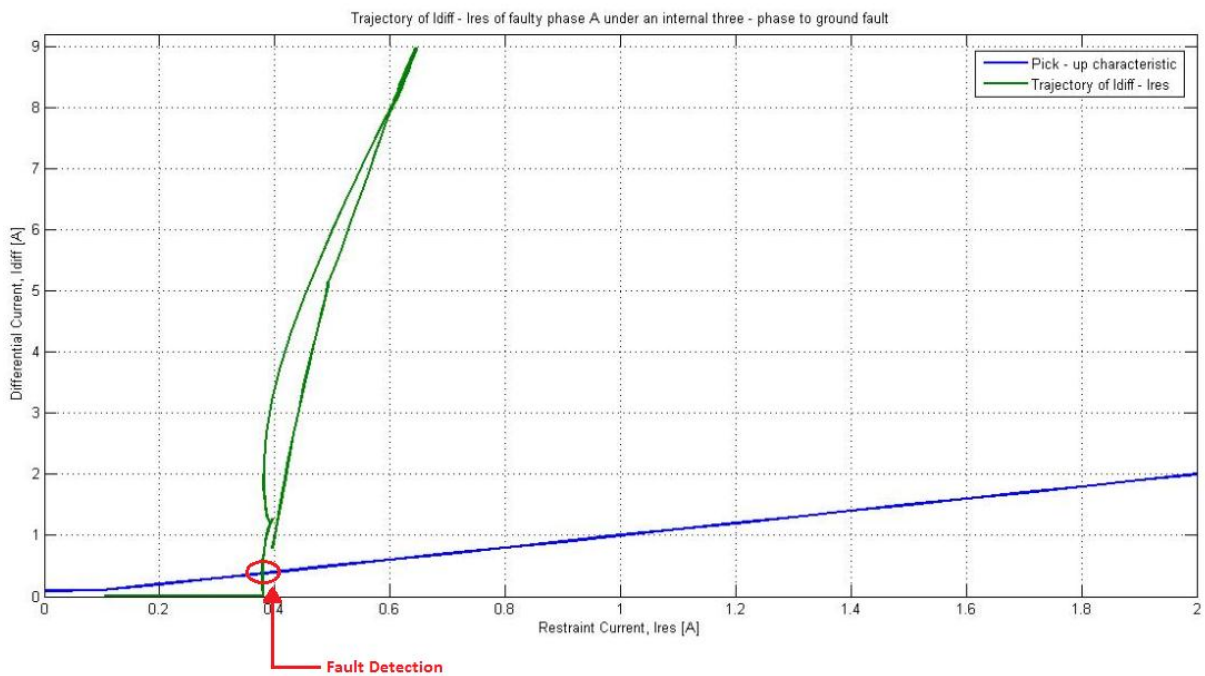


Figure 5-21. I_{Diff} - I_{Res} trajectory of faulty Phase A and adaptive pick – up characteristic of the differential relay

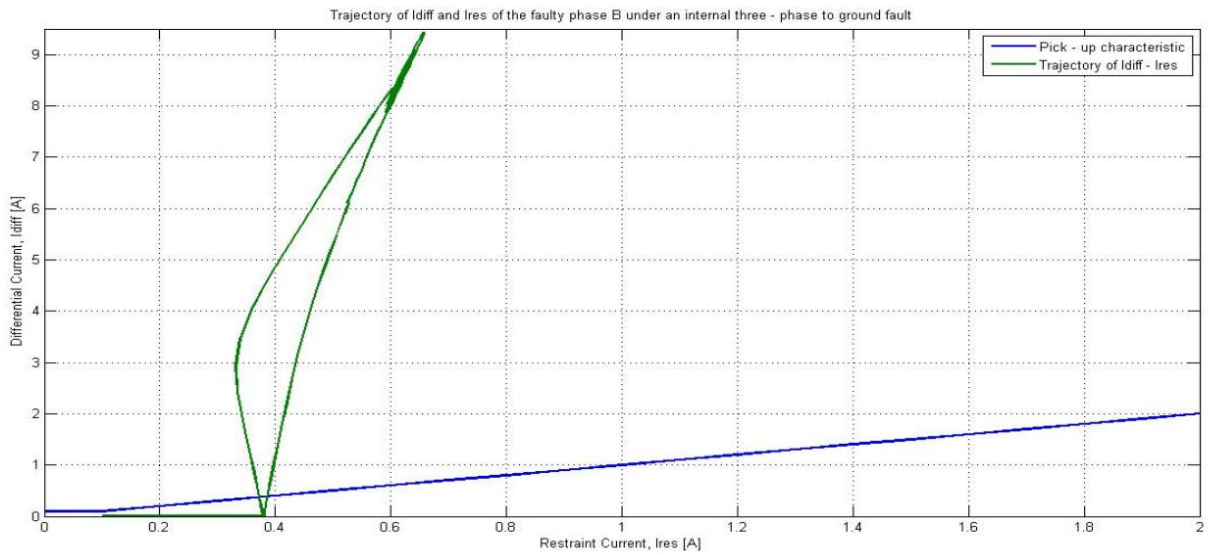


Figure 5-22. $I_{Diff} - I_{Res}$ trajectory of faulty Phase B and adaptive pick – up characteristic of the differential relay

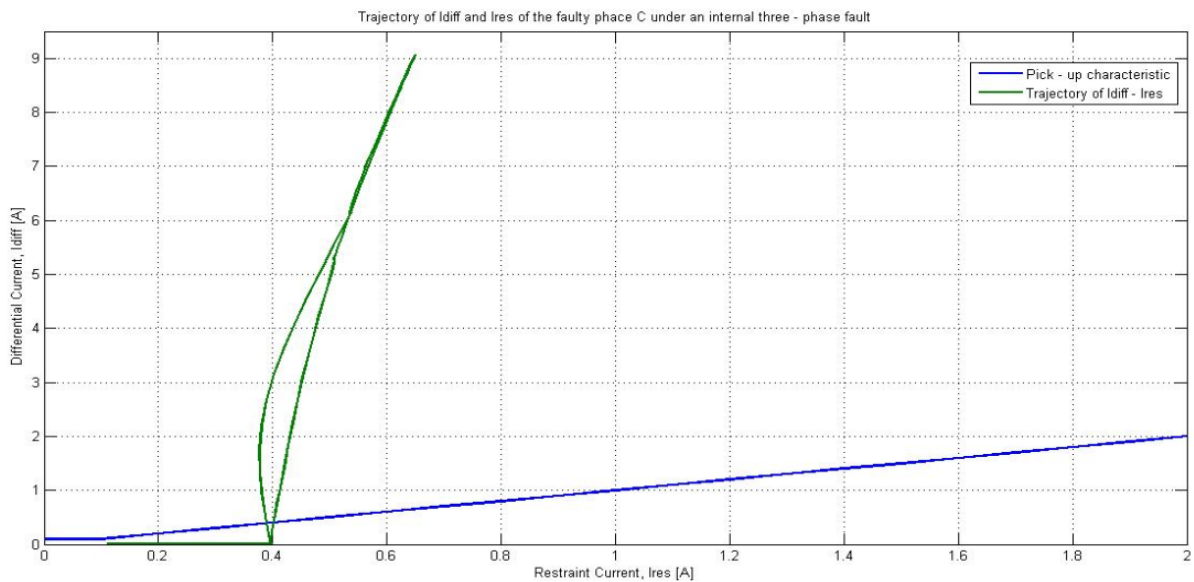


Figure 5-23. $I_{Diff} - I_{Res}$ trajectory of faulty Phase C and adaptive pick – up characteristic of the differential relay

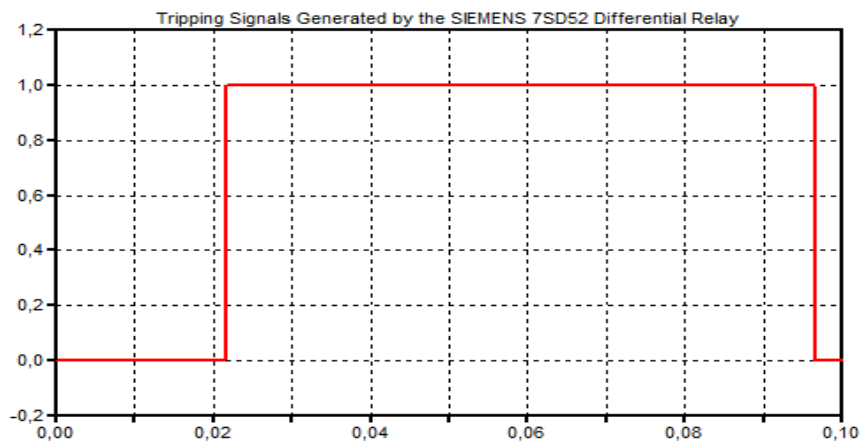


Figure 5-24. Tripping signals generated at the output of the differential relay for each phase separately

5.3.4 Three – Phase to Ground Fault outside the Protected Zone

An external fault is simulated to confirm the correct operation of the differential relay, when a fault occurs outside of its protection zone. More specifically, a three – phase earth fault is simulated at $t = 0.03$ sec, without being cleared. The abnormal condition takes place on the overhead transmission line “MVL – WTL 2”, where all the phases are connected to the ground via resistances of very low value. Figure 5-25 shows the fault currents flowing to the ground, while Figure 5-26 depicts the currents flowing at the primary side of the protection CTs.

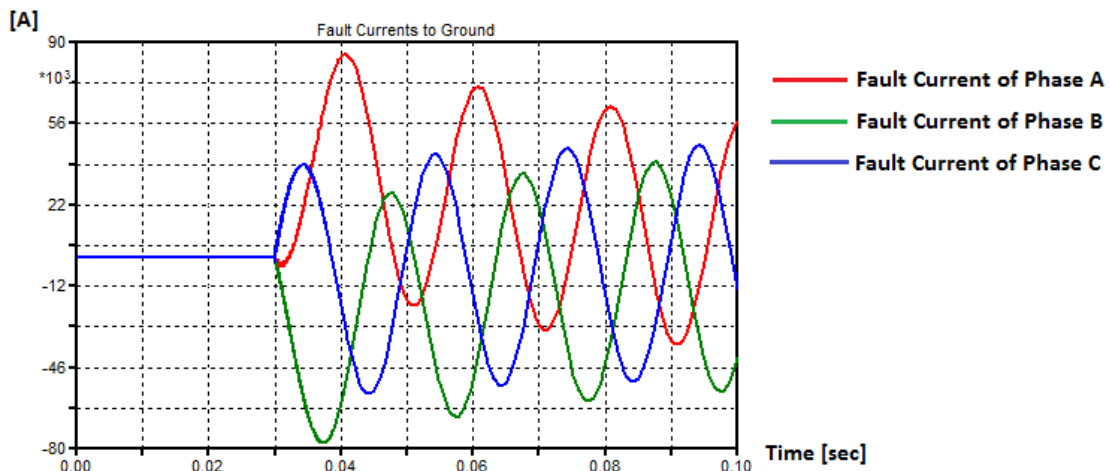


Figure 5-25. Currents to ground of the faulty phases A, B and C

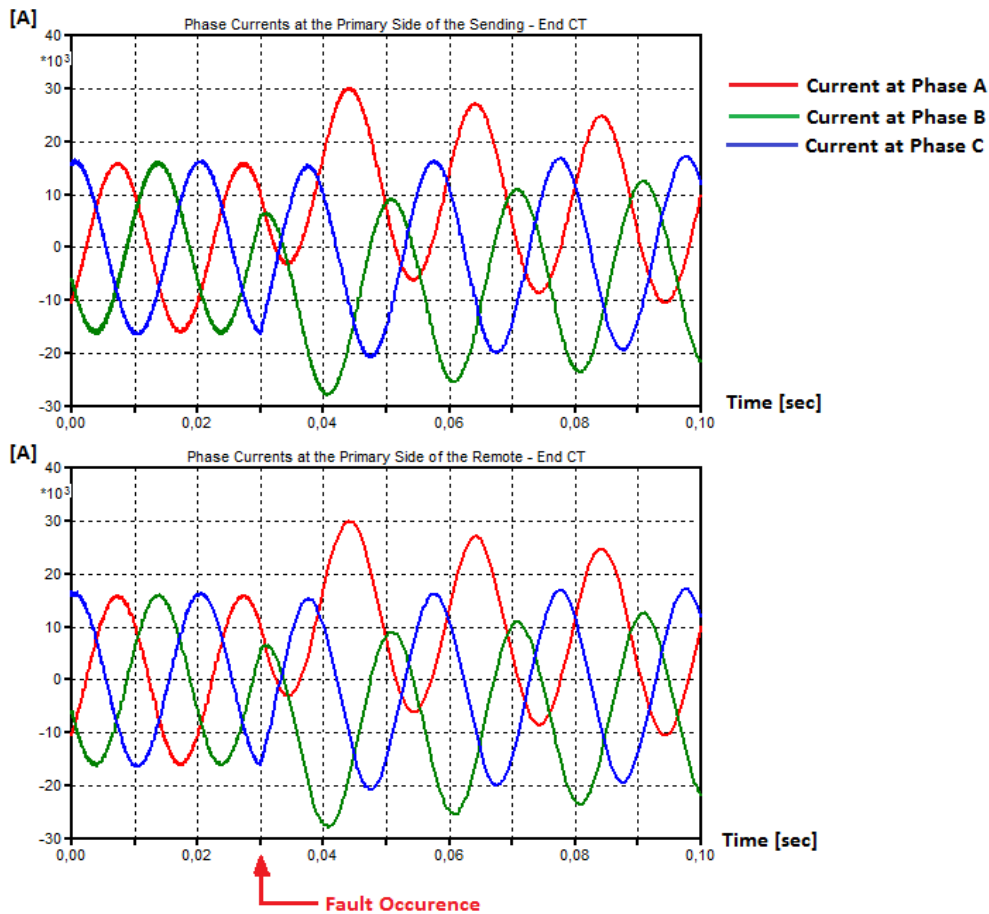


Figure 5-26. Phase currents flowing at the primary side of the protection CTs

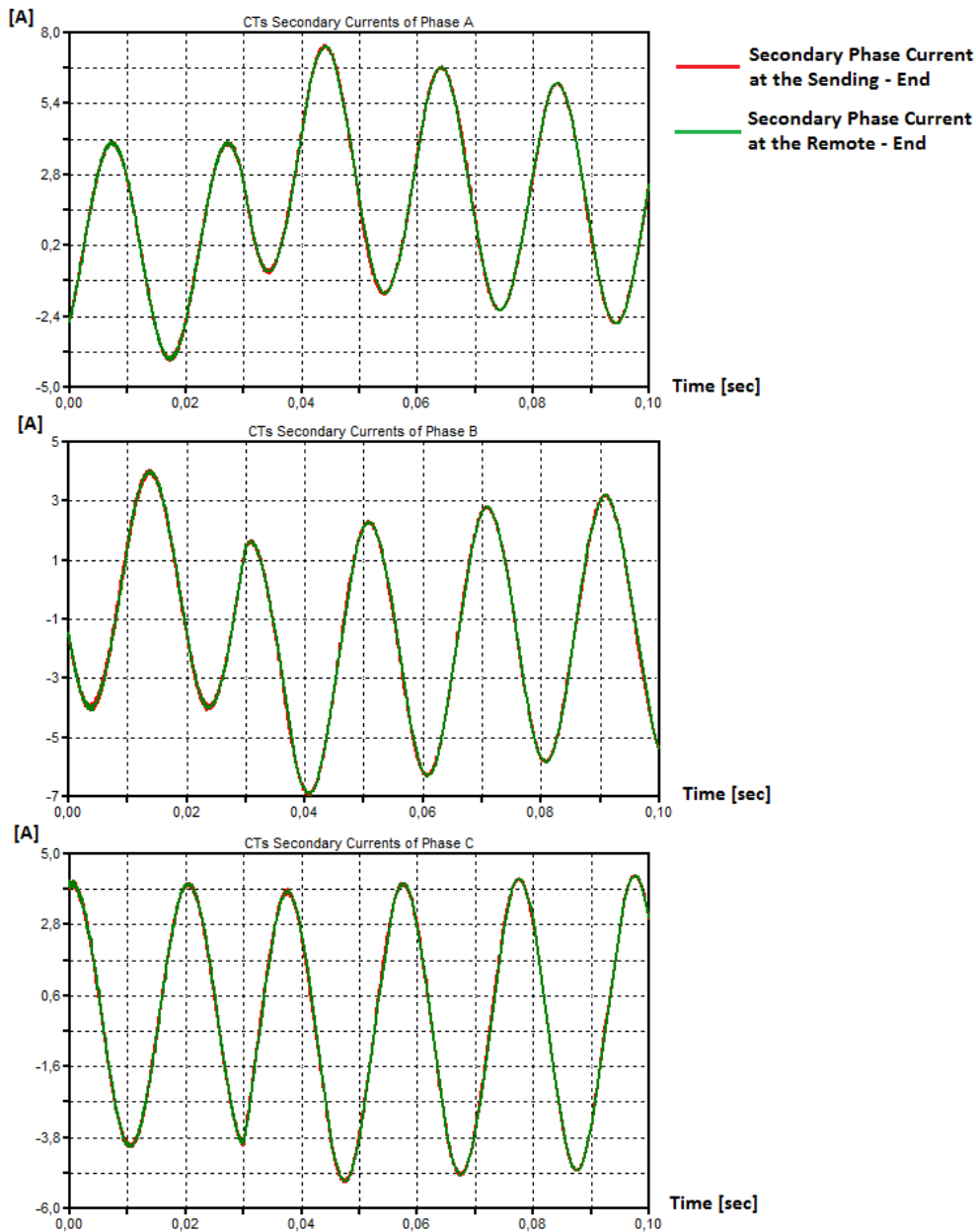


Figure 5-27. Comparison between the CTs secondary phase currents at the sending and remote end of the HV cable respectively

The last figure shows that during the external fault, the currents flowing into the HV cable are equal with these flowing out of the latter. Thus, the differential currents, which are calculated by the relay algorithm, will get values lower than the values of the restraint currents. Consequently, the trajectory of I_{Diff} and I_{Res} will not enter the tripping zone of the pick – up characteristic during the fault and no tripping signals will be generated by the protection relay. The latter is confirmed by the figures below, which show the build – up trajectory of the two computed currents, I_{Diff} and I_{Res} , compared to the pick – up characteristic of the device.

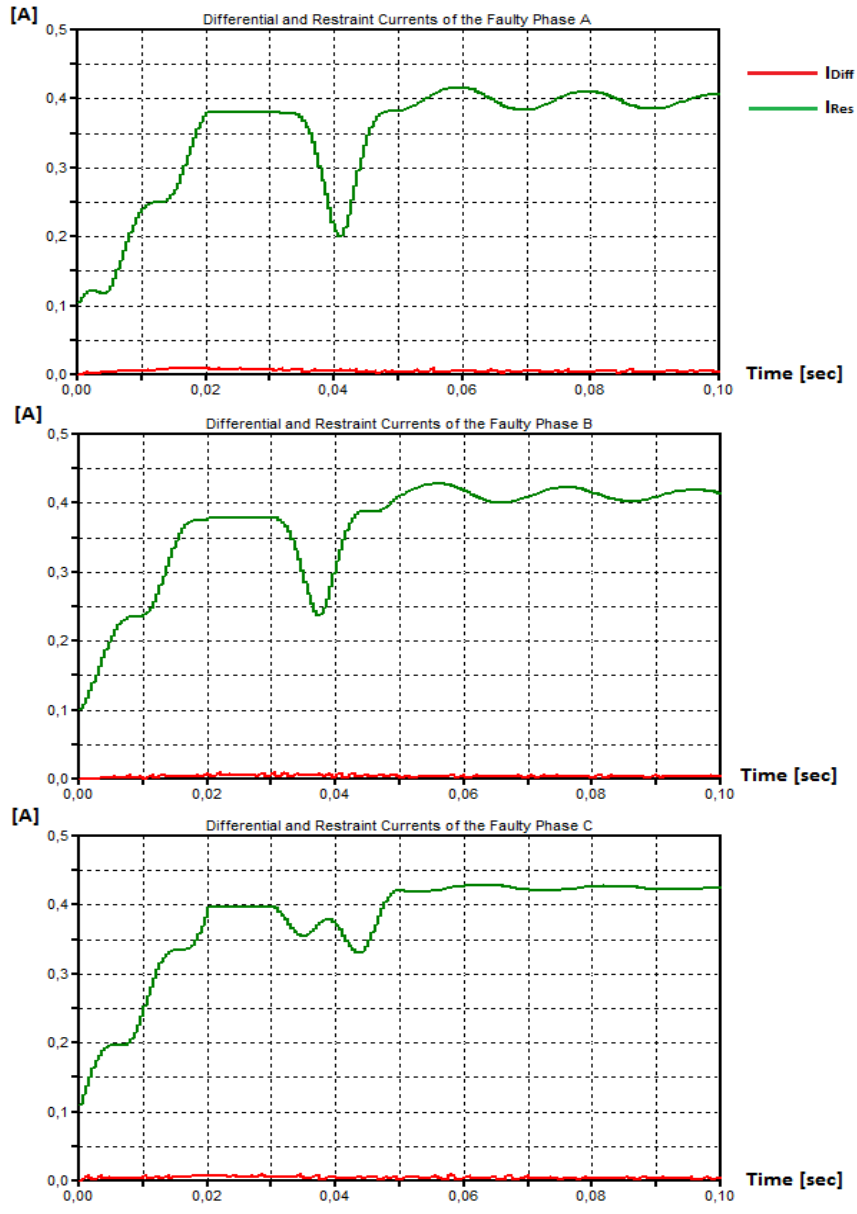


Figure 5-28. I_{Diff} and I_{Res} as calculated for each phase

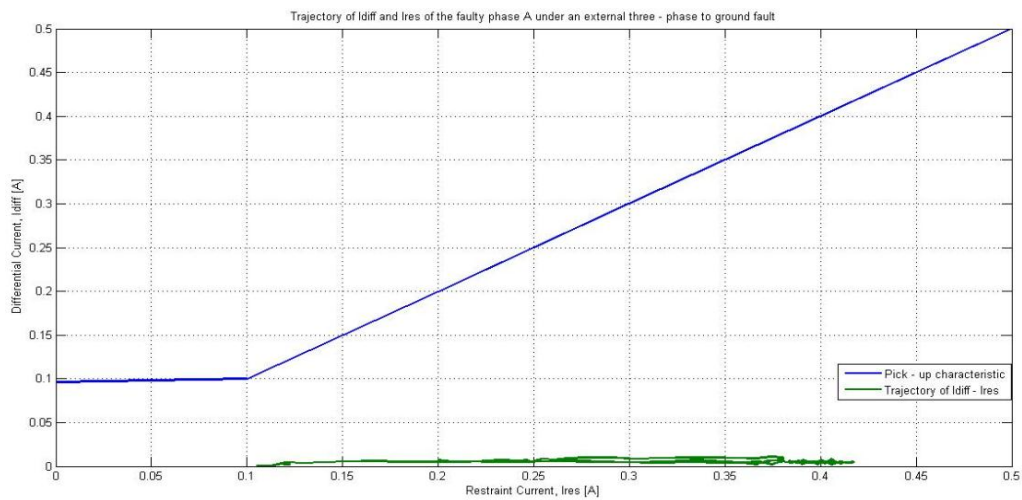


Figure 5-29. $I_{Diff} - I_{Res}$ trajectory of faulty Phase A and adaptive pick-up characteristic of the differential relay

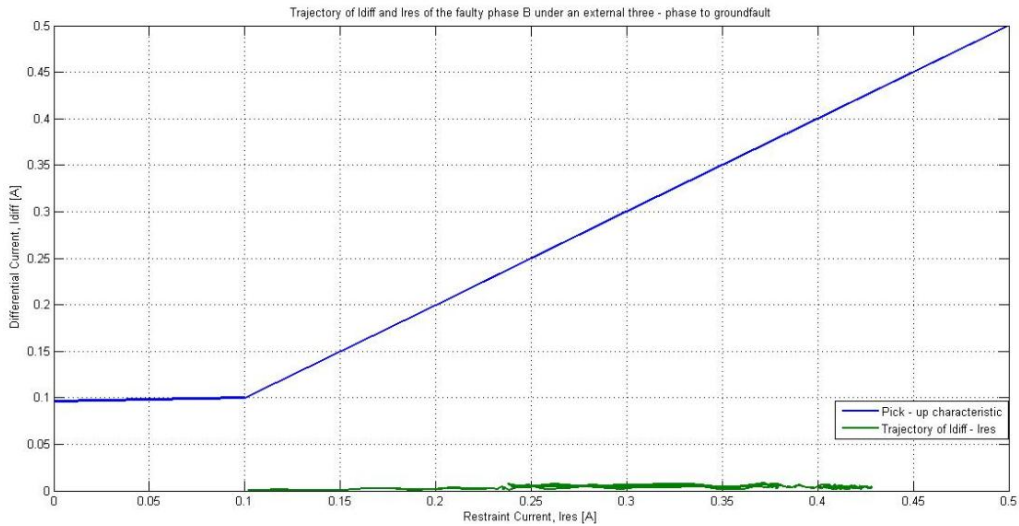


Figure 5-30. $I_{Diff} - I_{Res}$ trajectory of faulty Phase B and adaptive pick – up characteristic of the differential relay

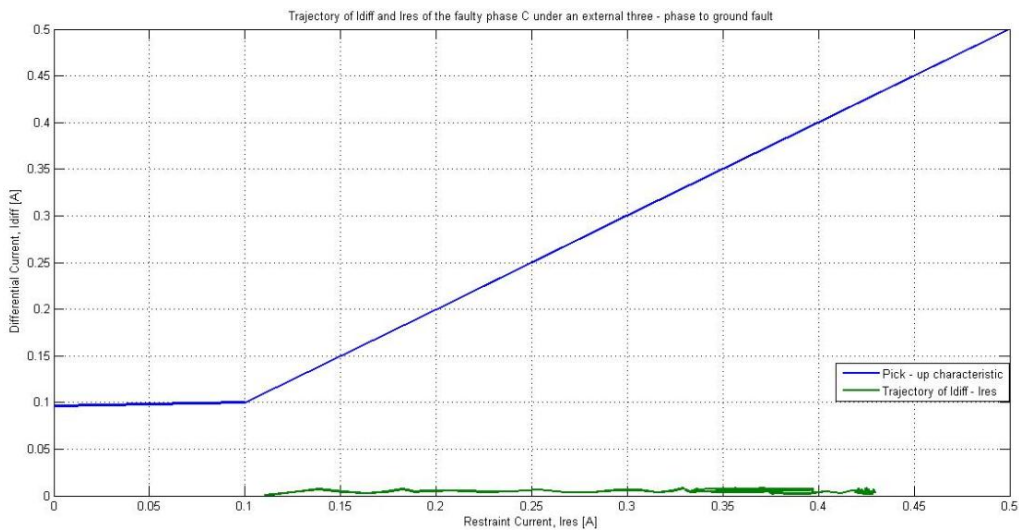


Figure 5-31. $I_{Diff} - I_{Res}$ trajectory of faulty Phase C and adaptive pick – up characteristic of the differential relay

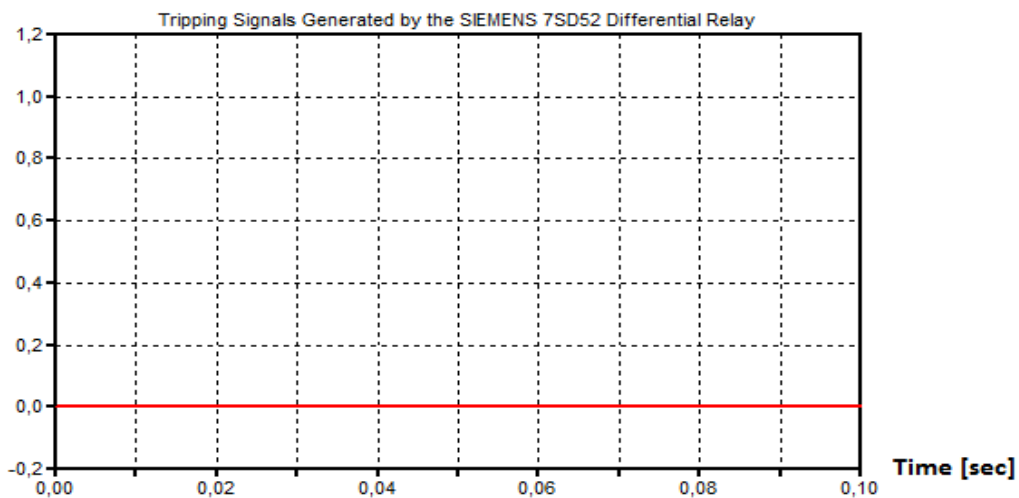


Figure 5-32. Tripping signals generated at the output of the differential relay for each phase separately

5.3.5 Single Phase to Ground Fault Outside the Protected Zone under CTs Heavy Saturation Conditions

As it was mentioned in paragraph 4.4.1 of Chapter 4, the developed algorithm of the differential relay does not take into account any factor for adapting the restraint current under CTs saturation conditions. Thus, in the case the CTs transform the primary currents to the secondary winding with significant errors, the differential relay may cause a false tripping, even if an internal fault does not occur within the protected zone. The latter is shown below, where an external single phase to ground fault is simulated on the “MVL – WTL 2” OHL and the protection CTs are driven into deep saturation. Figure 5-33 shows the secondary currents of the faulty Phase A, which are transformed with significant errors by the CTs.

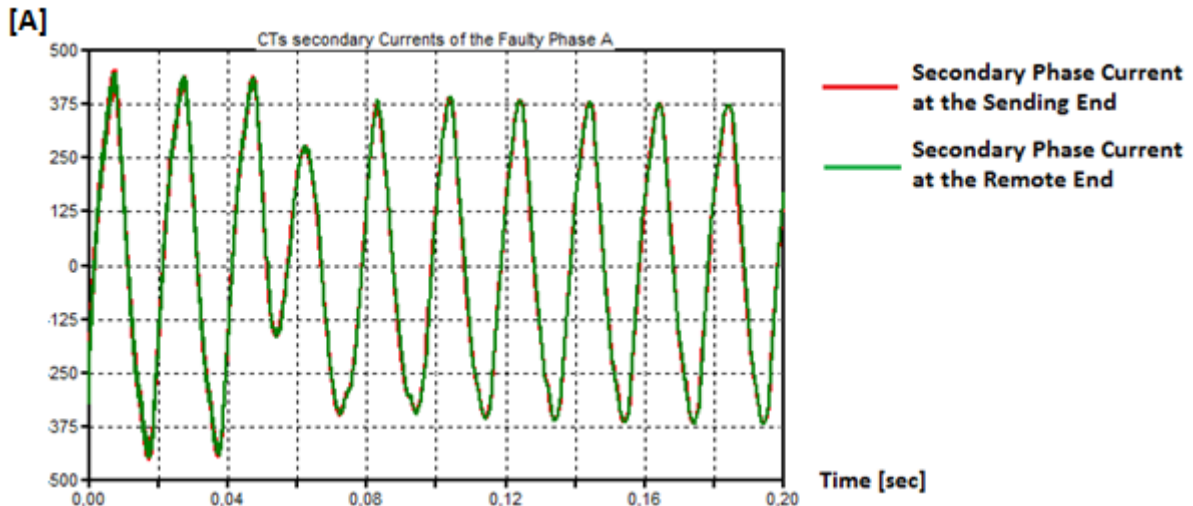


Figure 5-33. Comparison between the CTs secondary currents of Phase A at the sending and remote end of the HV cable respectively

Due to these errors, deviations between currents of the same phase arise at the sending and remote ends of the HV cable. Thus, an increased differential current is computed for each phase separately, compared to the case where no saturation occurs under external fault conditions. The differential current may exceed the value of the restraint current at a certain time step of the computation, leading to a false generated tripping signal by the relay. The latter is confirmed in the figures below, which show the calculated differential and restraint currents of each phase and the trajectory formed by the I_{Diff} and I_{Res} .

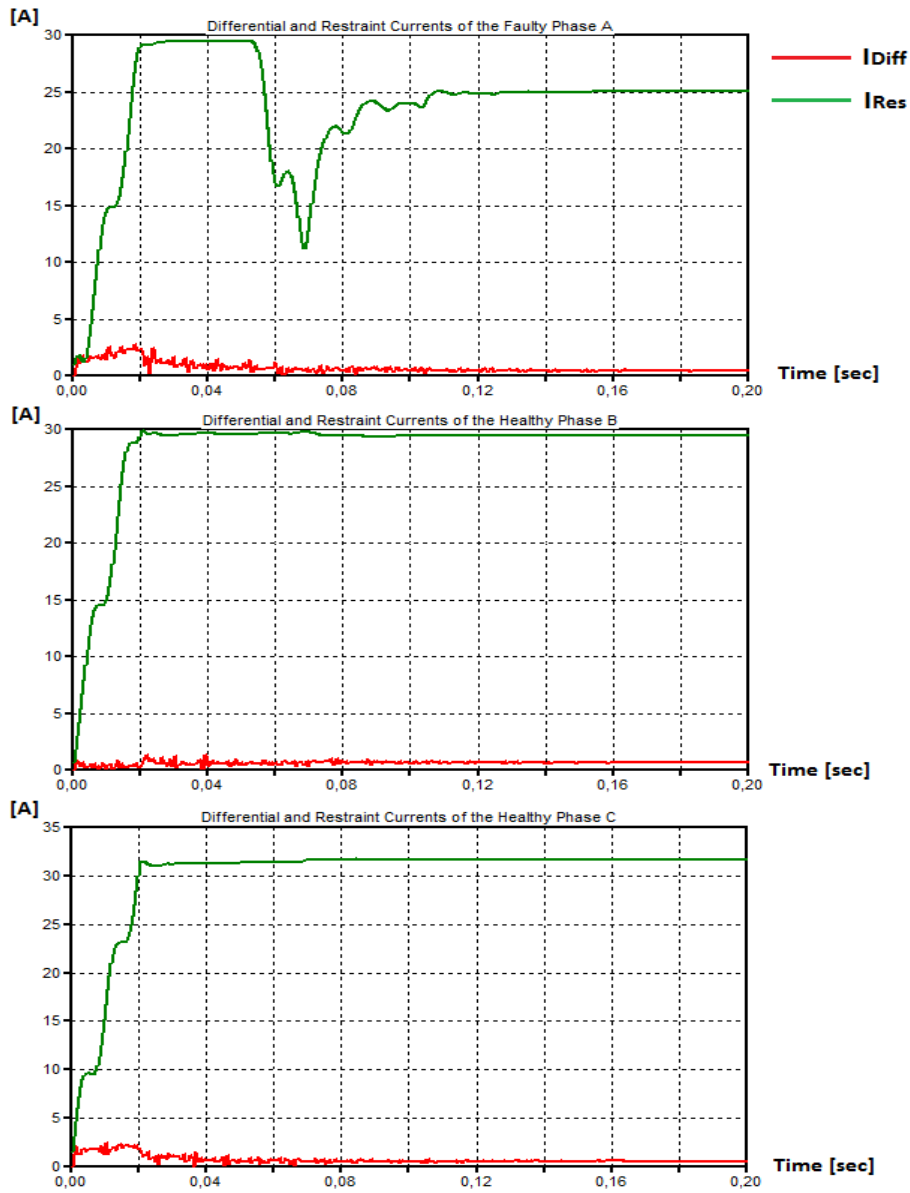


Figure 5-34. I_{Diff} and I_{Res} as calculated for each phase

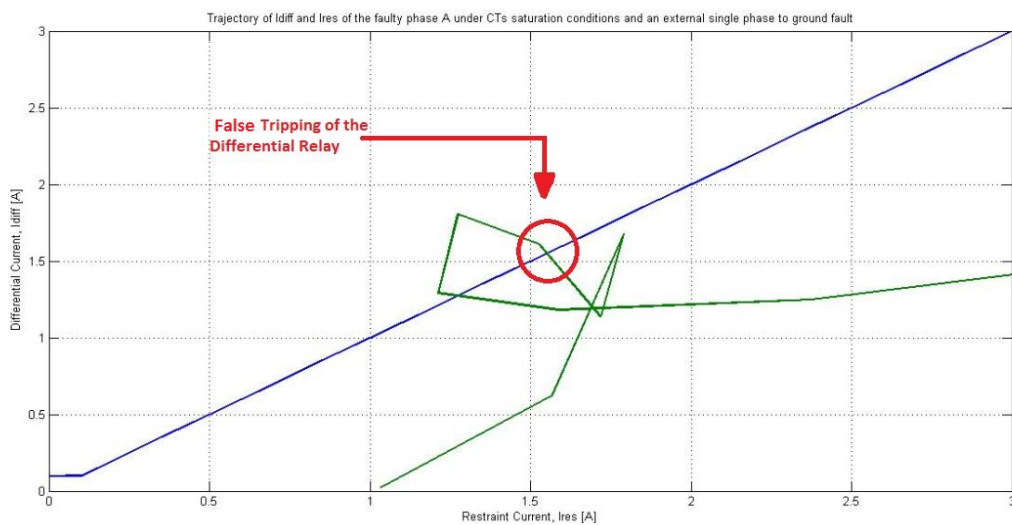


Figure 5-35. I_{Diff} – I_{Res} trajectory of faulty Phase A and adaptive pick – up characteristic of the differential relay

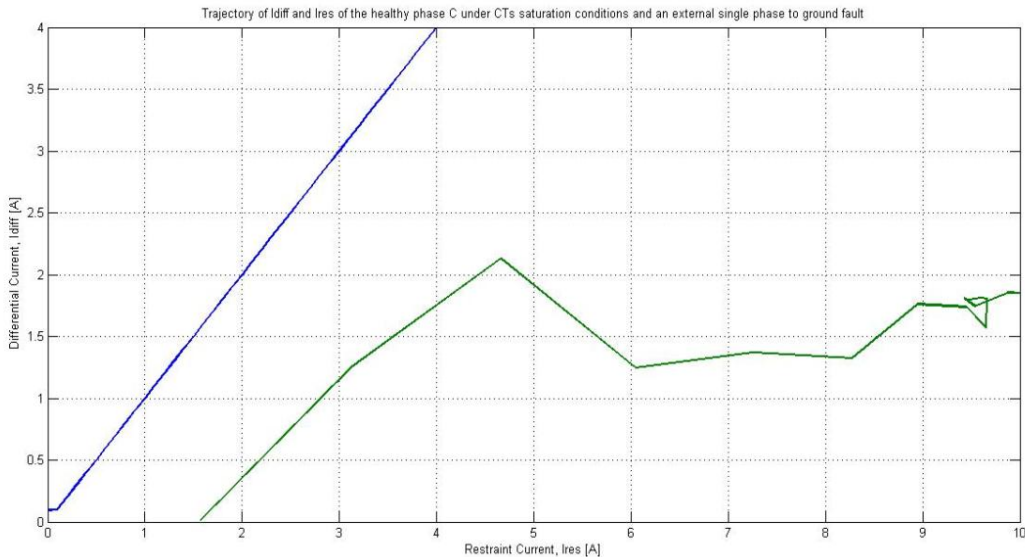


Figure 5-36. $I_{Diff} - I_{Res}$ trajectory of healthy Phase C and adaptive pick – up characteristic of the differential relay

For the faulty Phase A, the trajectory of I_{Diff} and I_{Res} enters the tripping zone of the relay’s pick – up characteristic. Consequently, the protective device will erroneously detect an internal fault and it will generate a false tripping command, as it is shown in Figure 5-37. Also, the trajectory of I_{Diff} and I_{Res} for the healthy Phase C tends to enter the tripping zone of the pick – up characteristic, contrary to the trajectory of Figure 5-31, where the latter lies at values much smaller than these of the operating area. Thus, the saturation of the protection CTs may lead to possible and undesirable maloperation of the differential relay. For that reason, the SIEMENS differential relay 7SD52 makes use of an extra factor, f_{sat} , which is responsible for accordingly adapting the pick – up characteristic. Moreover, fast current comparison methods are implemented for detecting internal and external faults within a 5 ms time window, before saturation errors affect the correct operation of the relay [33].

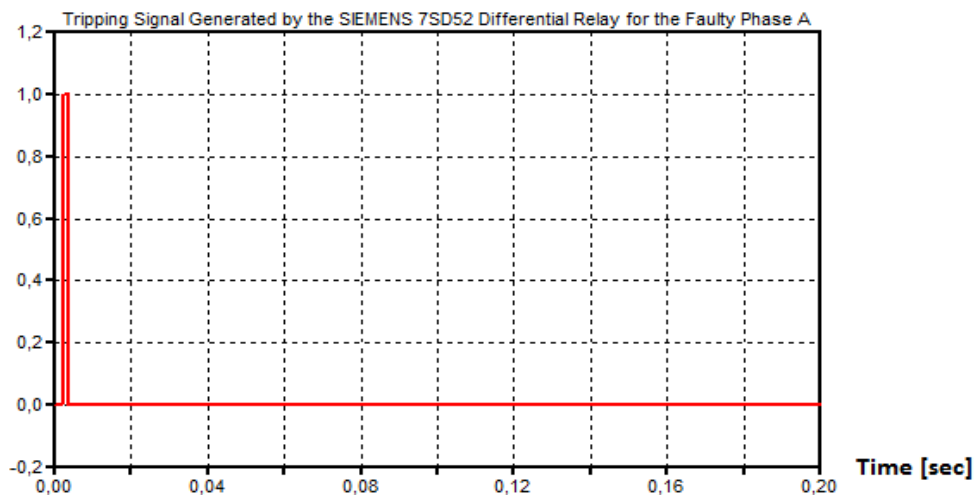


Figure 5-37. Tripping signals generated at the output of the differential relay for the faulty Phase A

5.4 Conclusions

Based on the results presented above, the following conclusions can be reached:

- The protection relay model operates correctly under an internal fault within the protected zone, which is defined by the protection CTs. The relay detects the faulty phase(s), since the algorithm computes the differential and restraint currents for each phase separately. Thus, the appropriate tripping signals are generated and sent to the corresponding CBs that take care of the switching actions.
- The relay algorithm needs a certain time period to build – up the differential currents and detect the abnormal conditions. This time depends on the type of the internal fault and from the results obtained the following are noticed:
 - The relay algorithm needs 2.5 ms to detect a single phase to ground fault
 - 5 ms to detect a two – phase fault
 - 1.5 ms to detect a three – phase to ground fault
- The correct operation of the differential relay under internal fault conditions is also confirmed by the trajectory of the differential and restraint currents, I_{Diff} and I_{res} respectively. More specifically, when a fault occurs within the protected zone, the trajectory enters the operating zone of the pick – up characteristic of the relay. The trajectory will enter the restrain zone again, only when the internal fault is cleared.
- On the other hand, the differential relay does not operate, when a fault occurs outside the protected zone and no CTs saturation takes place. In that case, the phase currents flowing into the HV cable are equal to the phase currents flowing out of the latter, in terms of magnitude and phase. Thus, the differential current, which is calculated for each phase, is smaller than the restraint current during the external fault. Consequently, the trajectory of I_{Diff} and I_{Res} does not enter the operating zone of the pick – up characteristic.
- The protection CTs transform the primary currents to the secondary side, without significant errors. Thus, the correct operation of the differential protection relay is not affected, unless the CTs are driven into deep saturation (extremely high fault currents). In that case, the DP may generate false tripping signals, even when a fault occurs outside the protected zone. This is because of the assumptions and limitations that were taken into account when developing the relay model.

5.5 Recommendations

The results presented in this chapter show that the differential protection scheme model operates correctly for the 380 kV underground cable. However, the latter constitutes only a part of the mixed transmission configuration between the Maasvlakte and Westerlee substations. Thus, the protection scheme model could be extended, in order to simulate the real protection scheme implemented by TenneT TSO in the system studied. More specifically, a future research could include some of the following recommendations:

- The differential protection scheme should be implemented on the series reactors, whereas it should be extended to model the four – point differential

protection scheme at the busbars of the two substations, as it is shown in Figure 5-1.

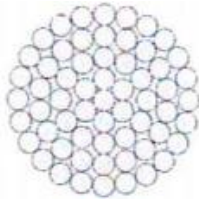
- Moreover, the differential relay model could be verified by using a conventional testing method for the protective relays. More precisely, the data obtained by the simulations through ATP – EMTF could be processed to specific static testing sets, i.e. OMICRON [34]. By this way, the response of the relay model could be compared to that of a real protective device.

- Last but not least, an extensive study should focus on the distance protection scheme, which is implemented on the configuration along with the differential one. The distance scheme protects the whole transmission system extended between the two substations, by adopting three zones of protection with different time grading. At the same time, the distance scheme operates as a back – up protection system, in the case the differential protection fails to operate under fault conditions within its protected zones.

Appendix A

Data of the OHL Phase and Ground Wires

The following tables summarize the basic data for the phase and ground wires of the overhead transmission lines used between the Maasvlakte and Westerlee substations:

Data of the Phase Wires provided by TenneT TSO		
Phase Wires AMS 620 UHC 	Number and Diameter of the aluminum wires	61 x 3.6 /mm
	Number and Diameter of the ACS and ZCS parts	-
	Diameter of aluminum and steel sections	620 mm ² /mm ²
	Outer radius of the conductor	32.4 mm
	Rated weight of the conductor	1806 kg/km
	Rated mechanical strength	161.4 kN
	DC Resistance @20 ⁰	0.0488 Ω/km
	Temperature coefficient of the resistance	0.0036 1/K
	Data of the Ground Wires provided by TenneT TSO	
Ground Wires ACSR Hawk 	Number and Diameter of the aluminum wires	26 x 3.44 /mm
	Number and Diameter of the ACS and ZCS parts	7 x 2.68 /mm
	Diameter of aluminum and steel sections	242/39 mm ²
	Outer radius of the conductor	21.8 mm
	Rated weight of the conductor	979 kg/km
	Rated mechanical strength	130 kN
	DC Resistance @20 ⁰	0.1374 Ω/km
	Temperature coefficient of the resistance	0.0036 1/K

Appendix B

Data of the XLPE HV Cable

The following tables summarize the basic data of the 380 kV XLPE underground cable installed in the Randstad South Ring:

Electrical and Mechanical Data of the 380 kV XLPE Cable provided by TenneT TSO	
Nominal voltage U/U_o/U_m	380/220/420 kV
Conductor's material	Cu
Conductor's cross section	1600 mm ²
Insulating material	XLPE
Rated electric field strength min/max	5.9/11.7 kV/mm
Rated capacitance	0.193 μF/km
Rated AC resistance @90°	0.0154 Ω/km
Rated inductance @50 Hz	0.78 mH/km
Rated weight	35 kg/m
Rated mechanical strength	80 kN
Short – circuit current for 1 sec (symm.)	100 kA
Insulating level BIL/LI/AC	1425/1425/440 kV

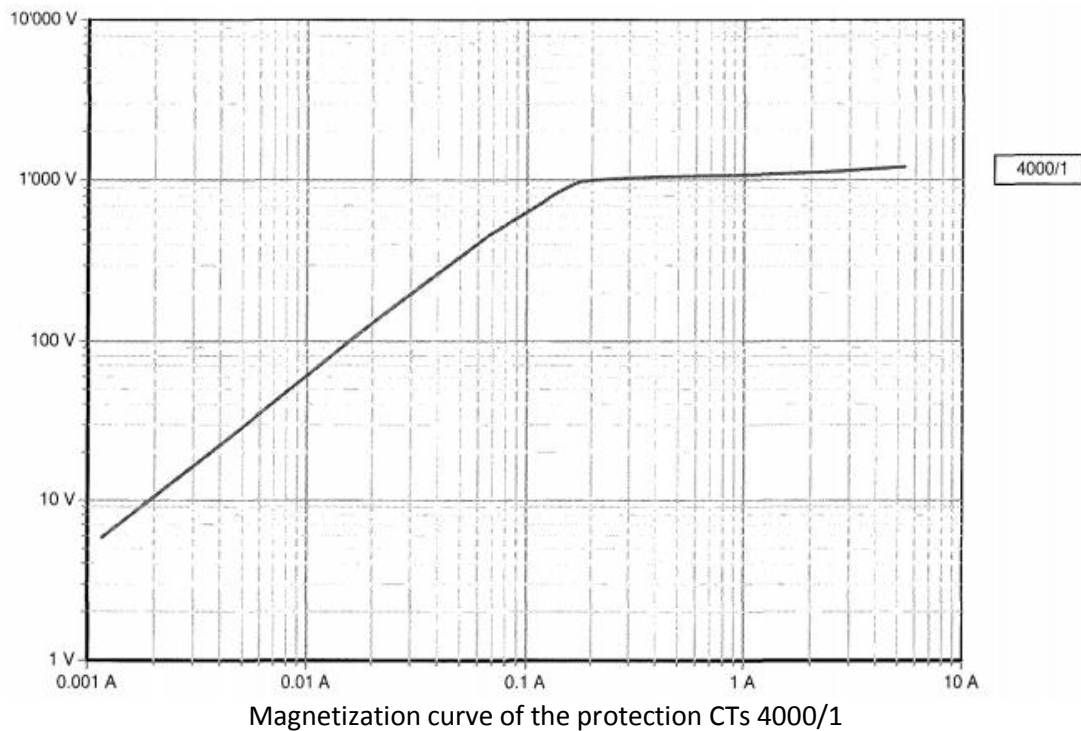
Geometrical Data of the 380 kV XLPE Cable provided by TenneT TSO		
<p>380 kV XLPE Cable</p> 	Diameter over the conductor	49.8 mm
	Semi – conducting layer	2.2 mm
	Insulator thickness	27 mm
	Semi – conducting layer	1.5 mm
	Lead sheath, Alloy Te	2 mm
	Diameter over lead sheath	121 mm
	PE sheath, graphite coated	4.9 mm
	Diameter over complete cable	131 mm

Appendix C

Data of the Protection CTs

The following table summarizes the basic characteristics of the protection current transformers installed in the mixed configuration studied, while the figure shows the magnetization curve of the devices:

Data of the Protection CTs provided by TenneT TSO	
Nominal voltage	460 kV
Nominal frequency	50 Hz
Rated primary current	4000 A
Rated secondary current	1 A
Protection class	5P60



Bibliography

- [1] Canadian/American EMTP User Group, "Alternative Transient Program, Rulebook," Bonneville Power Administration, Portland, Oregon, 1995
- [2] H.W. Dommel, "Electromagnetic Transients Program (EMTP), Theory Book," Bonneville Power Administration, Portland, Oregon, Jul. 1994
- [3] K. Fekete, S. Nikolovski, G. Knezevic, M. Stojkov, Z. Kovac, "Simulation of Lightning Transients on 110 kV Overhead – Cable Transmission Line using ATP – EMTP," in 15th IEEE Mediterranean Electrotechnical Conf. on MELECON, pp. 856-861, Apr. 2010
- [4] C.G. Kaloudas, T.A. Papadopoulos, K.V. Gouramanis, K. Stasinou, G.K. Papagiannis, "Simulation of Switching and Lightning Transients in Parallel Single – Core Underground Cables," in 46th International Universities' Power Engineering Conf., pp. 1-6, Sept. 2011
- [5] U.S. Gudmundsdottir, B. Gustavsen, C.L. Bak, W. Wiechowski, "Field Test and Simulation of a 400 – kV Cross – Bonded Cable System," in IEEE Trans. on Power Delivery, vol.3, pp. 1403-1410, Jul. 2011
- [6] U.S. Gudmundsdottir, J. De Silva, C.L. Bak, W. Wiechowski, "Double Layered Sheath in Accurate HV XLPE Cable Modeling," in Power and Energy Society General Meeting, pp. 1-7, Jul. 2010
- [7] B. Gustavsen, J.A. Martinez, D. Durbak, "Parameter Determination of Modeling System Transients – Part II: Insulated Cables," IEEE PES Task Force on Data for Modeling System Transients of IEEE PES Working Group on Modeling and Analysis of System Transients using Digital Simulation (General Systems Subcommittee), in IEEE Trans. on Power Delivery, vol. 20, pp. 2045-2050, Jul. 2005
- [8] A.I. Chrysochos, T.A. Papadopoulos, G.K. Papagiannis, "Improved Time – Domain Modeling of Underground Cables," in 46th International Universities' Power Engineering Conf., pp. 1-6, Sept. 2011
- [9] R.A.C.T. de Groot, C.S. Engelbrecht, "Transient and Harmonic Study for 380 kV Series Reactors in the Connection Maasvlakte – Westerlee," KEMA Consulting, Arnhem, The Netherlands, Nov. 2008
- [10] ABB, "Calculation of Short – Circuit Currents in Three - Phase Systems," Mannheim, Germany, Aug. 2007
- [11] M. Orhac, "Current Transformers for HV Protection," Schneider Electric, Cahier Technique Merlin Gerin No. 164, Grenoble, France, Mar. 1995
- [12] P. Fonti, "Current Transformers: How to specify them," Schneider Electric, Cahier Technique Merlin Gerin No. 194, Grenoble, France, Febr. 2000
- [13] G. Ziegler, "Numerical Differential Protection, Principles and Applications," SIEMENS, Second Edition, Erlangen: Publicis Publishing, 2012
- [14] D.A. Tziouvaras, Working Group C-5 of the Systems Protection Subcommittee of the IEEE Power System Relaying Committee, "Mathematical Models for Current, Voltage, and Coupling Capacitor Voltage Transformers," in IEEE Trans. on Power Delivery, vol. 15, no. 1, pp. 62-72, Jan. 2000
- [15] IEC 60044-6, "Instrument Transformers, Part 6: Requirements for Protective Current Transformers for Transient Performance," 1992-2003

- [16] R. Luxenburger, P. Schegner, M. Igel, "ATP/EMTP Model of TPX, TPY and TPZ Current Transformers for Realistic Testing of Protection Devices," in 8th IEEE International Conf. on Developments in Power System Protection, vol. 1, pp. 260-263, Apr. 2004
- [17] R. Folkers, "Determine Current Transformer Suitability using EMTP Models," Schweitzer Engineering Laboratories, Pullman, WA, 1999
- [18] A. Nawikavatan, C. Thammart, T. Niyomsat, M. Leelajindakraierk, "The Current Transformer Model with ATP – EMTP for Transient Response Characteristic and its Effect on Differential Relays Performance," in 8th International Conf. on Advances in Power System Control, Operation and Management, pp. 1-6, Nov. 2009
- [19] "Measuring of Protection Cores acc. IEC," PFIFFNER, 8th Edition, Dec. 2004
- [20] K. Solak, W. Rebizant, "Investigation of Transmission Line Differential Protection in ATP – EMTP," unpublished
- [21] D.A. Tziouvaras, Schweitzer Engineering Laboratories, "Protection of High – Voltage AC Cables," in Power Systems Conf. on Advanced Metering, Protection, Control, Communication, and Distributed Resources, pp. 316-328, Mar. 2006
- [22] CIGRE Study Committee, "Protection Applications for Mixed Conductor Circuits," Lausanne, Switzerland, Sep. 2011
- [23] K.A. Tavares, K.M. Silva, "On Modeling and Simulating the Differential Protection of Power Transformers in ATP," in 11th International Conf. on Developments in Power Systems Protection, pp. 1-6, Apr. 2012
- [24] K. Solak, W. Rebizant, "Analysis of Differential Protection Response for Cross – Country Faults in Transmission Lines," in International Symp. on Modern Electric Power Systems, pp. 1-4, Sept. 2010
- [25] I.G. Kulis, A. Marusic, G. Leci, "Protection Relay Software Models in Interaction with Power System Simulators," in 35th International Conv. On MIPRO, pp. 924-929, May 2012
- [26] G. Ziegler, "Numerical Differential Protection, Principles and Applications," SIEMENS, Second Edition, pp. 52-69, Erlangen: Publicis Publishing, 2012
- [27] H. Sherwali, A. Abdrahem, "Simulation of Numerical Distance Relays, MATLAB Modeling, Programming and Simulations," InTech, 2010, [Online: <http://www.intechopen.com/books/matlab-modelling-programming-and-simulations/modelling-of-numerical-distance-relays-using-matlab>]
- [28] K.H. So, J.Y. Heo, C.H. Kim, R.K. Aggarwal, J.C. Kim, G.S. Jang, "An Implementation of Current Differential Relay and Directional Comparison Relay using EMTP Models," in International Journal of Electrical Power & Energy Systems, pp. 261-272, Sept. 2006
- [29] "SIPROTEC, Line Differential Protection with Distance Protection 7SD5, Manual," SIEMENS, v. 4.70, Feb. 2011
- [30] J. Ebberts, A. Cakmak, "Beveiliging Verbinding 380 kV Maasvlakte – Calandkanaal – Hoek van Holland – Westerlee," TenneT TSO, Arnhem, Nov. 2012

- [31] T. Judendorfer, S. Pack, M. Muhr, "Aspects of High Voltage Cable Sections in Modern Overhead Line Transmission Systems," in International Conf. on High Voltage Engineering and Applications, pp. 71-75, Nov. 2008
- [32] A. Cakmak, "Beveiliging Instellingen 380 kV, Station: Maasvlakte 380 kV," TenneT TSO, Arnhem, Jul. 2009
- [33] SIEMENS, "Power Transmission and Distribution, Line Differential Protection 7SD52x/7SD610"
- [34] Y. Liu, H. Gao, X. Wei, P. Wei, M. Xiang, C. Zhou, "Performance Testing of Complete Digital Relays Based on ATP – EMTP and IEC61850-9-2," in 4th International Conf. on Electric Utility Deregulation and Restructuring and Power Technologies, pp. 83-87, Jul. 2011